Oxidative Activation of Light Hydrocarbons in a Perovskite Hollow Fiber Membrane Reactor

Von der Naturwissenschaftlichen Fakultät
der Gottfried Wilhelm Leibniz Universität Hannover
zur Erlangung des Grades

Doktor der Naturwissenschaften
Dr. rer. nat.

genehmigte Dissertation
von
Dipl.-Chem. Oliver Czuprat
geboren am 06.01.1980 in Hannover

2010

Referent: Prof. Dr. Jürgen Caro

Korreferent: Prof. Dr. B. Hitzmann

Tag der Promotion: 29.11.2010

Abstract

The presented thesis contains and condenses six original research articles on the oxidative activation of light hydrocarbons in a catalytic perovskite membrane reactor of the composition $BaCo_xFe_yZr_zO_{3-\delta}$ (BCFZ, x+y+z = 1) and the impact of CO_2 formed during deep oxidation of hydrocarbons on the properties of the membrane, which is used to separate oxygen from oxygen containing gases like air.

The demand for olefins, especially ethene and propene, is expected to increase significantly in the near future due to global economic development. Today, steam cracking is the most important process for the production of light alkenes, although it is a highly endothermic and therefore energy-consuming process. Alternatively, in the oxidative dehydrogenation alkane and oxygen are co-fed giving rise to olefin and water while compensating the endothermic dehydrogenation step without thermodynamic constraint of alkane conversion. However, this mode suffers from consecutive olefin oxidation or thermal cracking decreasing the olefin yield and, therefore, has not been commercialized.

An innovative reactor concept incorporating a multistep oxygen permeating hollow-fiber membrane and a dehydrogenation catalyst is presented in this thesis which allows a controlled oxygen insertion over an extended length in discrete portions. This architecture benefits from high olefin selectivities of a conventional thermal/catalytic dehydrogenation combined with shifting of the chemical equilibrium towards the olefin by burning off selectively the formed hydrogen after each oxygen permeable zone. Comparable ethene yield to those in the steam-cracking process of ca. 50% could be established but at a 100 °C lower temperature using a supported chromia catalyst.

The forementioned concept was successfully transferred onto propene production by using a supported Pt/Sn catalyst. Oxygen separation and propene formation could be established at 625 °C. The highest propene selectivity of 75% was obtained at a propane conversion of 26% and 625 °C whereas the best propene yield of 36% was obtained at 675 °C (48% propene selectivity). From kinetic studies on the role of lattice and adsorbed oxygen, carried out by transient analysis of products, it was found that propane is catalytically dehydrogenated to propene and hydrogen, while lattice oxygen of the perovskite oxidizes primarily hydrogen.

There is a strong economic interest in developing processes that transform methane (as the main constituent of natural gas) to higher-valued products. The oxidative coupling of methane could be demonstrated in a BCFZ hollow fiber membrane reactor filled with a Mn-Na_2WO_4 on silica supported catalyst for the first time in this thesis. Oxygen separation from air and C_2 formation could be established at 800 °C. The highest C_2 selectivity of ca. 75% was observed at a methane conversion of 6% with an ethene to ethane ratio of 2:1.

Since deep oxidation of hydrocarbons is of concern in all reactions mentioned above, the CO_2 stability of BCFZ membranes was investigated. CO_2 in different concentrations was applied as sweep gas while feeding air leading to a decrease and finally stop of oxygen permeation due to $BaCO_3$ formation, which was proven to be fully reversible under CO_2-free conditions. Partial decomposition of BCFZ into high-temperature rhombohedral $BaCO_3$ polymorph was observed under 50 vol% CO_2 in N_2 at 900 °C by *in-situ* X-ray diffraction analysis microscopy. This carbonate structure is not quenchable and cannot be detected by *ex-situ* methods.

Zusammenfassung

Die vorliegende Arbeit umfasst sechs Forschungsarbeiten zur oxidativen Aktivierung von kurzkettigen Kohlenwasserstoffen in einem katalytischen, perowskitischen Membranreaktor der Zusammensetzung $BaCo_xFe_yZr_zO_{3-\delta}$ (BCFZ, $x+y+z = 1$), der zur Abtrennung von Sauerstoff aus Luft verwendet wurde. Darüber hinaus wurde der Einfluss von CO_2, das durch Totaloxidation der Kohlenwasserstoffe entstehen kann, auf die Membraneigenschaften untersucht.

In den kommenden Jahren wird die Nachfrage nach Olefinen, insbesondere Ethen und Propen bedeutsam steigen. Steam Cracking ist derzeit das primäre Darstellungsverfahren für kurzkettige Kohlenwasserstoffe, obgleich dies ein hochgradig endothermer Prozess ist. Bei der oxidativen Dehydrierung hingegen wird das Alkan mit Sauerstoff versetzt wird, so dass neben dem Olefin auch Wasser entsteht. Dessen Bildung kompensiert den endothermen Dehydrierungsschritt und ermöglicht so, die thermodynamische Limitierung der Dehydrierung zu überwinden. Weiteroxidation oder thermisches Cracking der Olefine verringert jedoch deren Ausbeute, so dass bislang keine Kommerzialisierung dieses Verfahrens erfolgt ist.

In dieser Arbeit wird ein innovatives Reaktorkonzept, bestehend aus einem Dehydrierkatalysator sowie einer mehrstufig sauerstofftransportierenden Hohlfasermembran, vorgestellt. Diese ermöglicht einen kontrollierten Sauerstoffeintrag in diskreten Portionen und kombiniert hohe Olefinselektivitäten der thermischen/katalytischen Dehydrierung mit der Verschiebung des chemischen Gleichgewichts zum Olefin durch selektives Verbrennen des durch Dehydrierung gebildeten Wasserstoffs. Es konnten unter Verwendung eines geträgerten Chromoxid-Katalysators vergleichbare Ethenausbeute wie beim Steam Cracking von ca. 50% erreicht werden, jedoch bei einer 100 °C niedrigeren Temperatur.

Das oben genannte Reaktor-Konzept wurde erfolgreich auf die Propendarstellung mittels eines geträgerten Pt/Sn Katalysators bei 625 °C übertragen. Maximale Propenselektivität von 75% konnte bei einem Propanumsatz von 26% und 625 °C erreicht werden, während die höchste Propenausbeute von 36% bei 675 °C beobachtet wurde (48% Propenselektivität). Kinetische Untersuchungen zur Rolle von Gittersauerstoff und adsorbiertem molekularen Sauerstoff mit Transientenmethoden haben ergeben, dass Propan katalytisch zu Propen und Wasserstoff dehydriert wird, während der Gittersauerstoff des Perowskiten hauptsächlich den gebildeten Wasserstoff oxidiert.

Es existiert ein großes wirtschaftliches Interesse an der Veredelung von Methan, dem Hauptbestandteil von Biogas, zu höherwertigen Produkten. Die oxidative Kupplung von Methan wurde in dieser Arbeit erstmals im BCFZ-Hohlfaserreaktor in Kombination mit einem $Mn\text{-}Na_2WO_4$-Katalysator realisiert. Sauerstoffabtrennung aus Luft und Bildung von Ethan und Ethen konnten bei 800 °C gezeigt werden. Die größte C_2-Selektivität von ca. 75% wurde bei einerm Methanumsatz von 6% mit einem Ethen zu Ethan Verhältnis von 2:1 beobachtet.

Luft auf der Feedseite und CO_2-haltige Atmosphären auf der Sweep-Seite führten zu Carbonatbildung auf der Membran und einer Abnahme bzw. Erliegen des Sauerstofftransports. Letzterer ist in CO_2-freien Gasströmen bei hohen Temperaturen vollständig reversibel. Durch *in-situ* Röntgendiffraktometrie konnte bei 900 °C in 50 vol% CO_2 ein rhomboedrischer Polymorph des $BaCO_3$ aufgezeigt werden, der nicht abschreckbar bzw. via *ex-situ* Methoden nachzuweisen ist.

Keywords: membrane reactor, perovskite, hollow fiber, mixed ion electronic conductor, oxygen transporting membrane, oxidative activation, dehydrogenation, oxidative coupling of methane, CO_2, carbonate

Schlagwörter: Membranreaktor, Perowskit, Hohlfaser, gemischt Ionen- und Elektronenleiter, Sauerstofftransportierende Membran, Oxidative Aktivierung, Dehydrierung, Hohlfaser, Oxidative Kupplung von Methan, CO_2, Carbonat

Preface

The presented thesis has been developed since March 2008 during my employment at the Institute of Physical Chemistry and Electrochemistry of the Gottfried Wilhelm Leibniz Universität Hannover under the supervision of Prof. Dr. Jürgen Caro. During this time, I have been a scientific co-worker benefiting from the projects *SynMem* of the German Federal Ministry of Education and Research (BMBF) in cooperation with ThyssenKrupp-Uhde and *NASA-OTM* in cooperation with BASF SE granted by the European Union.

Six research articles are presented within this thesis; in five of them I am the first author. For all articles, I acknowledge helpful discussions as well as support to the manuscript preparation from my co-authors, particularly from Prof. Dr. Jürgen Caro. All dense perovskite hollow fiber membranes used in this work were provided by Dr. Thomas Schiestel from the Fraunhofer Institute of Interfacial Engineering and Biotechnology (IGB) in Stuttgart.

The first three articles are dealing with the concept of repeated dehydrogenation of light hydrocarbons and subsequent selective hydrogen combustion within a BCFZ hollow fiber membrane reactor. All experimental work and data interpretation within the articles *Olefin Production by a Multistep Oxidative Dehydrogenation in a Perovskite Hollow-Fiber Membrane Reactor* and *Oxidative Dehydrogenation of Propane in a Perovskite Membrane Reactor with Multi-Step Oxygen Insertion* were carried out by myself. For the third article in this chapter entitled *Dehydrogenation of propane with selective hydrogen combustion: A mechanistic study by transient analysis of products* I acknowledge the fruitful collaboration with Dres. Evgenii and Vita Kondratenko from the Leibniz Institute for Catalysis at the University of Rostock (LIKAT). The TAP-measurements were carried out together at the LIKAT and the results were elaborated in equal shares. All other experiments and interpretation presented in this article were done by myself.

In the subsequent chapter, studies on the *Oxidative Coupling of Methane in a BCFZ Perovskite Hollow Fiber Membrane Reactor* are summarized. All experiments, data collection and interpretation of the results were done by myself.

The investigations of BCFZ in poisoning CO_2 containing atmospheres and the preparation of the article entitled *Influence of* CO_2 *on the oxygen permeation performance of perovskite-type* $BaCo_xFe_yZr_zO_{3-\delta}$ *hollow fiber membranes*, which can be found in chapter 4 of this thesis, were carried out entirely by myself after beneficial discussion with Dr. Mirko Arnold. The follow-up publication *In-situ X-ray diffraction study of carbonate formation and decomposition in perovskite-type* $BaCo_xFe_yZr_zO_{3-\delta}$, in which Konstantin Efimov is assigned as first author is based on a jointly idea. It contains studies of the microstructure of the BCFZ powder under the influence of CO_2, which were performed by him and me in equal shares. Transmission electron microscopy investigations as well as the major concept and composition of the article were carried out by him.

First of all, I would like to deeply thank Prof. Dr. Jürgen Caro for giving me the chance to work in the both above mentioned projects dealing with such hot topics. It was a period of great pleasure and exciting work for me at the same time. I acknowledge his full support during my employment and his high priority in correcting my manuscripts. I like to extend my gratitude to Prof. Dr. Bernd Hitzmann from the Institut für Technische Chemie of the Gottfried Wilhelm Leibniz Universität Hannover for his kind interest in this work and for the acceptance to conduct the second expertise. Furthermore, I highly appreciate that Priv.-Doz. Dr. Armin Feldhoff is willing to host my thesis defense.

Additional acknowledgments are dedicated to my family and friends, Dr. Katrin Wessels, Jare Lohmeier and Britta Seelandt, Dr. Heqing Jiang, Dr. Mirko Arnold, Dr. Steffen Werth, Dr. Steffen Schirrmeister, Dr. Julia Martynczuk, Konstantin Efimov as well as Dres. Evgenii and Vita Kondratenko for their valuable discussions.

Special thanks are dedicated to Dr. Thomas Schiestel and Marita Zipperle for providing the perovskite hollow fiber membranes. I acknowledge the financial support of the BMBF funded project *SynMem* and the project *NASA-OTM* funded by the European Union. I am very grateful to the industry partners from ThyssenKrupp-Uhde and BASF SE for the permission to publish these results.

Contents

1 INTRODUCTION 11

1.1 General Considerations 11
1.2 Definition of Catalysis 12
1.3 Catalytic Fixed-Bed Reactors 14
1.4 Basic Aspects of Membrane Reactors 16
  1.4.1 Types of Membrane Reactors 17
  1.4.2 Reactors with Oxygen-Selective Membranes 20
1.5 Mixed Oxygen-Ion- and Electron-Conducting Membranes 23
  1.5.1 Structure of perovskite-type oxides 23
  1.5.2 Preparation of Perovskite BCFZ Hollow Fiber Membranes 27
  1.5.3 Oxygen Permeation through MIEC Membranes 29

2 OXIDATIVE DEHYDROGENATION OF LIGHT ALKANES 35

2.1 Summary 35
2.2 Olefin Production by a Multistep Oxidative Dehydrogenation in a Perovskite Hollow-Fiber Membrane Reactor 37
2.3 Oxidative Dehydrogenation of Propane in a Perovskite Membrane Reactor with Multi-Step Oxygen Insertion 45
2.4 Dehydrogenation of propane with selective hydrogen combustion: A mechanistic study by transient analysis of products 59

3 OXIDATIVE COUPLING OF METHANE 65

3.1 Summary 65
3.2 Oxidative Coupling of Methane in a BCFZ Perovskite Hollow Fiber Membrane Reactor 67

4 EFFECT OF CO_2 ON THE BCFZ PEROVSKITE 93

4.1 Summary 93
4.2 Influence of CO_2 on the Oxygen Permeation Performance of Perovskite-type $BaCo_xFe_yZr_zO_{3-\delta}$ Hollow Fiber Membranes 95
4.3 *In-situ* x-ray diffraction study on carbonate formation in perovskite-type $BaCo_xFe_yZr_zO_{3-\delta}$ 115

5 CONCLUSION AND PERSPECTIVES 125

6 BIBLIOGRAPHY 129

7 LIST OF FIGURES 131

APPENDIX A **133**

Oxygen Ion Migration in $Ba_{0.5}Sr_{0.5}Co_{0.8}Fe_{0.2}O_{3-\delta}$ Perovskite - a Molecular Mechanics Study 133

APPENDIX B **143**

Formulas..143

Publications and Contributions to Conferences **145**

Erklärung zur Dissertation **149**

1 Introduction

1.1 General Considerations

All scenarios about the future global energy requirements anticipate an increasing demand for electricity, which in 2030 is predicted to be twice the current demand [1]. Increasing global population and fast growing economies especially in developing countries are identified as main drivers for this trend. These scenarios also indicate that this increase can only be met by considerable use of fossil fuels like coal, natural gas and oil besides nuclear power. Therefore, it is necessary for the chemical industry to create innovative process-engineering technologies for the reduction of energy consumption and the minimization of waste streams.

One way to meet these demands is to invent new *catalysts* or to improve those currently in use. Catalysis, especially heterogeneous catalysis, is of vital importance to the world's economy, allowing us to convert raw materials into valuable chemicals and fuels in an economical, efficient and environmentally benign manner (c.f. chapter 1.2 Definition of Catalysis). For example, heterogeneous catalysts have numerous industrial applications in the chemical, food, pharmaceutical, automobile and petrochemical industries [2] and it has been estimated that 90% of all chemical processes use heterogeneous catalysts [3]. Heterogeneous catalysis is also finding new applications in emerging areas such as fuel cells [4], green chemistry [5], nanotechnology [6] and biotechnology [7].

Another approach can be the intensification of a chemical process, e.g. by incorporating membranes. The *membrane reactor* can improve both the process economics and the efficient use of natural resources as well, especially when used in the two most important and often the most expensive steps in a chemical process: the chemical reaction and the separation of the product stream. Consequently, this leads to potential savings in energy consumption, effective use of raw materials and reduced formation of by-products [8]. Enhancements in the production of pure oxygen or oxygen-enriched air would have immediate beneficial consequences [9,10]. The most common methods for producing pure oxygen or oxygen-enriched air are either by using the liquefaction of ambient air (LINDE Process) or by using the pressure swing adsorption (PSA) [11]. These techniques are both energetically and capitally intensive. Alternative methods, such as those using membrane technologies, are therefore desirable. In view of prospective membrane processes, mixed ionic-electronic conducting (MIEC) membranes, based on a perovskite structure, are under consideration for application in the industrial oxygen separation processes. Such membranes can provide infinite oxygen permselectivities next to remarkable high oxygen fluxes, which meet the economic requirements [12]. Furthermore, the oxygen transported through a membrane can be used *in situ* in a reactor for the oxidative activation of light hydrocarbons (e.g. oxidative dehydrogenation, oxidative coupling etc.) leading to advances in terms of improved selectivities and yields as presented in this thesis.

1.2 Definition of Catalysis

The definition of a catalyst has been discussed thoroughly [13]. A catalyst is a material that converts reactants into products, through a series of elementary steps, in which the catalyst participates while being regenerated to its original form at the end of each cycle during its lifetime. A catalyst changes the kinetics of the reaction, but does not change the thermodynamics [14]. Most catalysts are solids or liquids, but they may also be gases. If the catalyst and reactants or their solution form a common physical phase, then the reaction is called *homogeneous*ly catalyzed. *Heterogeneous* catalysis involves systems in which catalyst and reactants form separate physical phases [15].

The catalyst changes the mechanism of a reaction in order to provide a pathway with a lower activation energy as for the non-catalyzed way. Consequently, the reaction rate constant increases and therefore the reaction rate. The reaction rate at a constant concentration and temperature is characteristic for the activity of a catalyst. The following diagram (Figure 1.1) is showing the potential energy for a typical reaction where A and B are the reactants and C equals the product.

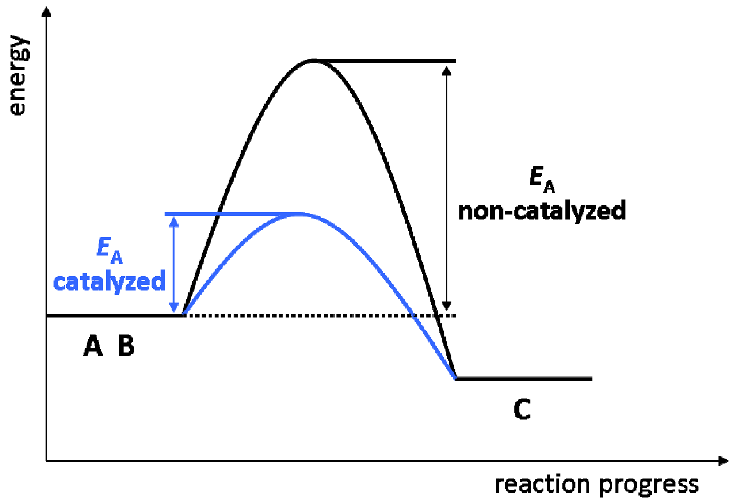

Figure 1.1: Energy diagram comparing a catalyzed and non-catalyzed reaction (E_A: activation energy).

According to the SABATIER principle, the existence of an unstable intermediate compound formed between the catalyst surface and at least one of the reactants is proposed [16]. This intermediate must be stable enough to be formed in sufficient quantities and labile enough to decompose to yield the final product or products.

As emphasized by BOUDART [17], the conditions under which catalytic processes occur on solid materials vary drastically. The reaction temperature can be as low as 78 K and as high as 1500 K, and pressures can vary between 10^{-9} and 100 MPa. The reactions can occur thermally or with the assistance of photons, radiation, or electron transfer at electrodes. Pure metals and multicomponent and multiphase inorganic compounds can act as catalysts.

The main advantage of using a heterogeneous catalyst is that, being a solid material, it is easy to separate from the gas and/or liquid reactants and products of the overall catalytic reaction. The heart of a heterogeneous catalyst involves the active sites (or active centers) at the surface of the solid. The catalyst is typically a high-surface area material (10-1000 m^2 g^{-1}) and it is usually desirable to maximize the number of active sites per reactor volume. Moreover, the surface of the catalytic particles contains sites associated with terraces, edges, kinks and vacancies [18]. If the catalyst contains more than one component (as it is generally the case), the surface composition may be different from that of the bulk. Finally, the surface atomic structure and composition may change with time-on-stream as the catalytic reaction proceeds.

1.3 Catalytic Fixed-Bed Reactors

The easiest and by far the most common way to carry out a heterogeneously catalyzed gas phase reaction is by passing the gas mixture over a fixed catalyst. The arrangement of the fixed catalyst is generally called a fixed-bed, and the respective reactor a fixed-bed reactor. The simplest type of fixed catalyst bed is a random packing of catalyst particles in a tube (Figure 1.2). The minimum diameter for the particles is limited primarily by pressure drop considerations, and the maximum diameter by the specific outer surface area for mass and heat transfer.

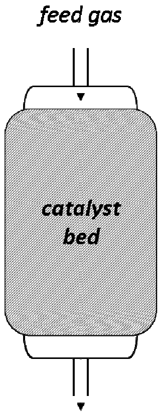

Figure 1.2: Basic type of a catalytic fixed-bed reactor.

In the chemical industry, fixed-bed reactors are used as standard in heterogeneously catalyzed gas phase reactions and are also used in the present thesis. Only if special conditions such as rapid catalyst deactivation or operation in the explosive regime have been taken into account, the alternative of fluidized-bed operation is considered. In this type of reactor, a fluid (gas or liquid) is passed through a granular solid material (usually a catalyst possibly shaped as tiny spheres) at high enough velocities to suspend the solid and cause it to behave as though it were a fluid.

Within a production plant the reactor may justifiably be regarded as the central item of apparatus with the catalyst as the essential part of the reactor. Seen from the flowing gas in heterogeneous catalyzed process, the following steps of the overall reaction can be distinguished (Figure 1.3). As most reactions take place with a considerable heat of reaction, a corresponding heat transport is superimposed on the mass transport.

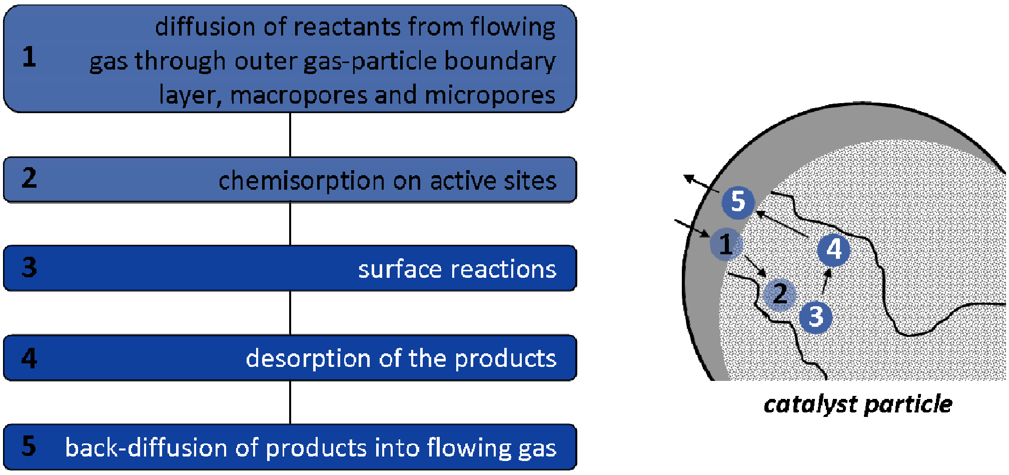
1 diffusion of reactants from flowing gas through outer gas-particle boundary layer, macropores and micropores
2 chemisorption on active sites
3 surface reactions
4 desorption of the products
5 back-diffusion of products into flowing gas
5
1
4
2
3
catalyst particle

Figure 1.3: Simplified scheme for diffusion, sorption and reaction in heterogeneous catalysis.

The control of the microkinetics (micropore diffusion, chemisorption, surface reaction and desorption) is the specific task of the catalyst developer. Once the catalyst is specified, reaction conditions (feed concentrations, pressure, temperature and residence time) must be found by the reaction engineer that lead to optimal yield. This is not a simple straightforward procedure, but requires multiple iteration loops. In the case of selectivity-sensitive multistep reactions, any deviation from the optimum reaction conditions may be the result of a non-uniform residence time distribution due to flow dispersion and flow bypass phenomena in the fixed bed, as well as of deviations from uniform reaction conditions in the catalyst as a result of mass-transport resistance in the particles and the outer boundary layer [19].

The influence of mass-transport resistance in the particles can only be excluded if the reaction rate is substantially lower than the mass transfer velocity. This leads to a need for good external mass transfer (i.e. a sufficiently rapid flow rate in the packed bed) as well as for short diffusion paths and large transport pores in catalyst particles.

In the case of exothermic or endothermic reactions, the local reaction rate must be controlled by the packed-bed temperature. Thus, temperature control plays a predominant role in selective reaction control.

A further requirement placed on the catalyst is a low pressure loss. This applies particularly if the conversion in a single pass through the reactor is low, so that a large amount of gas has to be recirculated.

In a more recent development *integrated* or *multifunctional reactor* concepts are to provide optimal reaction conditions in the reaction unit by incorporating optimal heat and reaction component addition or extraction at the reaction site, e.g. by using membrane-based reactors (c.f. chapter 1.4 Basic Aspects of Membrane Reactors). Since catalytic fixed-bed reactors are often operated with flammable or potentially explosive gas mixtures at high temperatures and elevated pressures, issues of operational safety are of major concern. Once again, the use of membranes inside the reactor can help to ensure a safe process.

1.4 Basic Aspects of Membrane Reactors

Catalytic membrane reactors have received increased attention over the past decades, initially due to progress made in the field of inorganic membranes. In contrast to organic membranes, inorganic membranes can withstand high temperatures, they are chemically much more stable under the often harsh environments of industrial reactions and they are more robust.

From an engineering point of view, the vision of process intensification through *multifunctional reactors* first conceived during the early 1990s [20], has intensified research on catalytic membrane reactors permitting the elimination of process steps and hence lead to more compact and cost-efficient plants which was also the aim of the work in hand.

1.4.1 Types of Membrane Reactors

According to the IUPAC definition, a membrane reactor is *a device for simultaneously carrying out a reaction and membrane-based separation in the same physical enclosure* [21]. Separation, in this case, means that the membrane shows a preferred permeation for one or several constituents of the reaction mixture. There are numerous concepts to classify membrane reactors [22,23], for example the reactor design such as extractors, distributors or contactors, the division into inorganic and organic based materials as well as porous or dense ones.

The most common concept is the selective removal of products from the reaction zone (Figure 1.4a), known as the *extractor membrane reactor*, which is mainly applied to equilibrium-restricted reactions to increase the yield of desired products beyond the equilibrium value. On the basis of the intention to overcome the equilibrium restriction the conversion must not be limited by the reaction kinetics; that is, the reaction must be sufficiently fast compared to the mass transport through the membrane, a feature summarized by the term *kinetic compatibility*. In order to drive the reaction to completion, the products not removed from the membrane must not inhibit the reaction kinetically, e.g. by competing with the reactants for adsorption sites. An especially favorable situation is found if the desired product is removed through the membrane selectively enough for the target application. Then, the membrane reactor not only benefits from overriding the equilibrium constraint but also provides an integrated product purification.

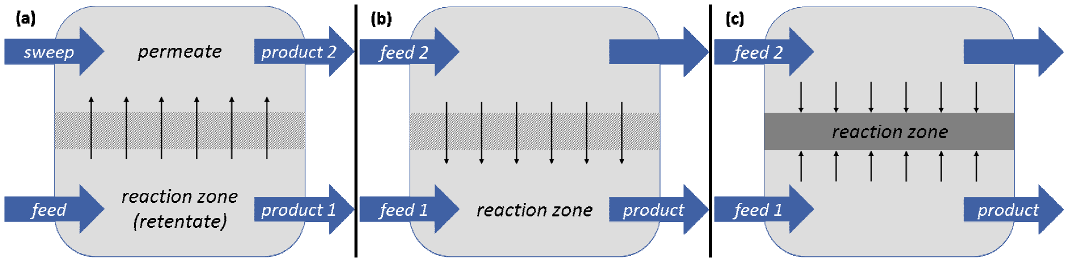

Figure 1.4: Selective removal of products (a) and selective supply of reactants (b) via a permselective membrane. The reaction defines the reaction zone in a non-permselective membrane (c).

In a different approach, one or several of the reactants are fed through a membrane to the reaction zone (Figure 1.4b). This so-called *distributor* membrane reactor does not necessarily require a selective membrane, provided that the trans-membrane flux can be properly controlled by the differential pressure. It allows establishing a more uniform concentration of the dosed species along the reactor, if this provides a higher selectivity or yield, or an improved safety. The total amount of reactants that can be supplied without exceeding the concentration limit in the feed for safe operation can also be increased. If suitable membranes are available or a design in sections is feasible, a specific shape of the concentration profile could be established, if this pays back in terms of improved reactor performance due to kinetic reasons. One additional effect observed when applying a distributed feed along the reactor is an increased flow rate downstream of the reactor. Together with the fact that fluid elements entering the reactor futher downstream have a reduced residence time compared to reactants supplied at the entrance, this alters the residence time distribution and may improve the selectivity or yield of intermediate products in multiple reactions. An addional benefit on the process level results also in the distributor membrane reactor from a membrane being able to extract the desired reactants *selectively* from a mixture with undesired components (e.g. oxygen from air); then again, one process unit may be eliminated. Oxygen ion-selective ceramic membranes for catalytic partial oxidation fall into this category (cf. 1.5 Mixed Oxygen-Ion- and Electron-Conducting Membranes).

Finally, a third concept refers to the case where the membrane is used to set the reaction zone (Figure 1.4c). For reactions relying on a catalyst, an active material could be incorporated into the membrane. Two reactant streams could then be passed along the different sides and would mix in the catalytic zone by diffusion. One consideration for this type of configuration might be a porous membrane and a solid active material coated to the pore walls, due to the higher trans-membrane fluxes that such systems allow compared to dense membranes. Even if no catalyst is required, the same principle can be applied if the reaction is fast enough to reach complete conversion within the membrane.

As mentioned above, the mass transport across a membrane can be either *permselective*, if only some components of a mixed-feed permeate through it (e.g. oxygen from air, Figure 1.4a,b), or *non-permselective,* if all species pass through at comparable rates (Figure 1.4c). Permselective transport, which is found in dense membranes, is governed by a solution-diffusion mechanism (c.f. chapter 1.5 Mixed Oxygen-Ion- and Electron-Conducting Membranes). Non-permselective transport normally occurs in macroporous and mesoporous membranes; in the latter, KNUDSEN diffusion is often the dominating transport mechanism. Microporous membranes show both activities, with both permselective and non-permselective transport being possible depending on the size of the permeating molecules compared to the pore size, and on their interaction with the membrane material.

When the membrane reactor is used for carrying out a catalyzed reaction, the question arises if the membrane itself has a catalytic function. If it does act as a catalyst, this is referred to as a *catalytic membrane reactor* (CMR), but if not it is known as an *inert membrane catalytic reactor* (IMCR, Figure 1.5a). The CMR case is further subdivided into two categories: (i) when the membrane acts as the *only* catalyst (b) or (ii) when a conventional catalyst is present in addition (c) [24].

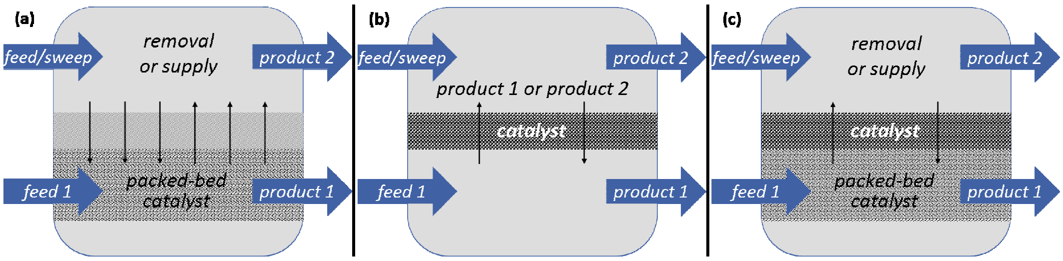
(a)
removal
or supply
feed/sweep
product 2
packed-bed
catalyst
feed 1
product 1
(b)
feed/sweep
product 2
product 1 or product 2
catalyst
feed 1
product 1
(c)
removal
or supply
feed/sweep
product 2
catalyst
packed-bed
catalyst
feed 1
product 1

Figure 1.5: Packed-bed catalytic reactor incorporating an inert membrane (a) in comparison to catalytic membrane reactor (b) and a packed-bed catalytic membrane reactor (c).

Besides the elimination of process units and the utilization of synergy effects from the integration of reaction and mass transport into one unit, a third level exists where membranes may offer advantages for catalyzed reactions. It requires that the catalyst is an integral part of the membrane. With dense membranes employed in a distributor membrane reactor it is possible that the membrane, due to its chemical nature, supplies one of the reactants in a special form, perhaps more active and/or selective in the reaction that one wishes to catalyze than in its usual form. An example is a ceramic oxygen ion-conducting membrane, which can provide reactive lattice oxygen (e.g. for the selective combustion of hydrogen, c.f. chapter 2 Oxidative

Dehydrogenation of Light Alkanes) or pass oxygen ions to a solid catalyst attached to it; thus in both cases the use of molecular oxygen from the reactant gas phase is avoided or at least suppressed.

1.4.2 Reactors with Oxygen-Selective Membranes

In equilibrium-limited reactions such as dehydrogenations (e.g. in the case of propane)

$$C_3H_8 \leftrightarrows C_3H_6 + H_2 \qquad \Delta G_r = +124 \text{ kJ mol}^{-1} \qquad (1.1)$$

the achievable conversion can be increased by using extractor membrane reactors (extraction of H_2) or by supplying oxygen in terms of a distributor membrane (combustion of H_2). In the latter case, hydrogen is then consumed by oxygen delivered through the membrane according to

$$H_2 + \tfrac{1}{2}\, O_2 \rightarrow H_2O \qquad \Delta G_r = -229 \text{ kJ mol}^{-1} \qquad (1.2)$$

shifting the reaction equilibrium towards the desired olefin and supplying heat of reaction as well as steam to suppress coke formation inside the reactor (c.f. chapter 2 Oxidative Dehydrogenation of Light Alkanes).

Numerous oxidation reactions have been performed successfully in the laboratory scale in membrane-supported catalytic reactors. Today, the challenges for technical application lie in membrane development and increased module reliability under extreme temperature cycling. Until now, no important industrial applications of inorganic membrane reactors in the process industry, including partial oxidation reactions, have been realized. Figure 1.6 gives an overview on ceramic membranes for oxygen transport.

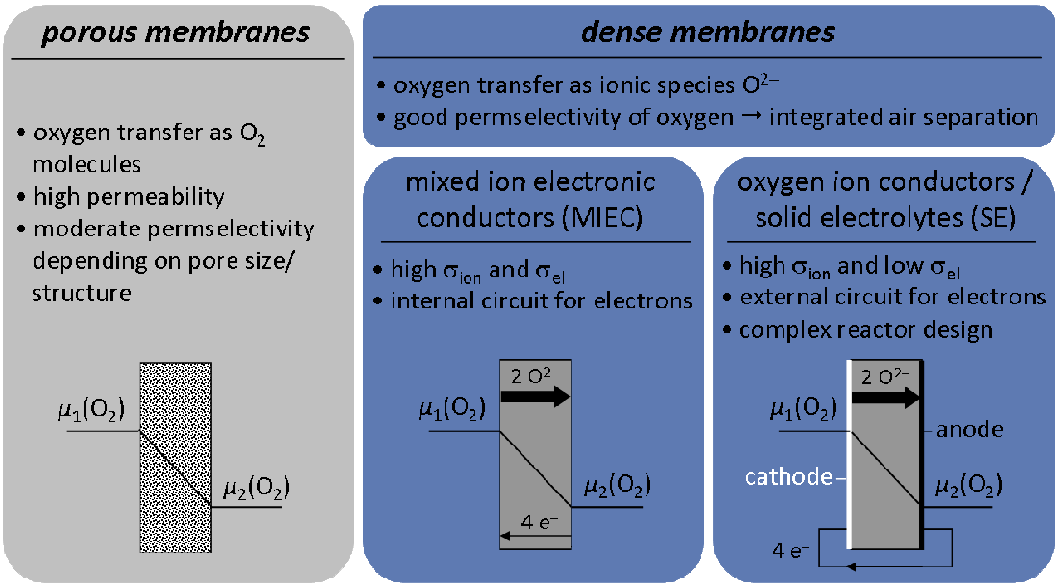
porous membranes
• oxygen transfer as O2 molecules
• high permeability
• moderate permselectivity depending on pore size/ structure
μ1(O2)
μ2(O2)
dense membranes
• oxygen transfer as ionic species O2−
• good permselectivity of oxygen → integrated air separation
mixed ion electronic conductors (MIEC)
• high σion and σel
• internal circuit for electrons
2 O2−
μ1(O2)
μ2(O2)
4 e−
oxygen ion conductors / solid electrolytes (SE)
• high σion and low σel
• external circuit for electrons
• complex reactor design
2 O2−
μ1(O2)
anode
cathode
μ2(O2)
4 e−

Figure 1.6: Classification of ceramic membranes for oxygen transport. σ denotes the conductivity (ionic or electronic); μ is the chemical potential.

Air or oxygen is delivered through a non-selective porous membrane into the reactor. The benefit is a uniform and lower oxygen partial pressure over the reactor length, whereas in conventional oxygen co-feed mode a decreasing oxygen partial pressure profile exists. A reduced oxygen partial pressure kinetically favors partial oxidation over total oxidation, because the rate of total oxidation is influenced more strongly by the oxygen partial pressure than that of the partial oxidation. There are no specific requirements toward the membrane material, and almost every porous Al_2O_3, TiO_2 or ZrO_2 can be used.

Porous inorganic membranes are classified by their pore diameter (*d*p) and can be divided into macroporous (*d*p > 50 nm), mesoporous (50 nm > *d*p > 2 nm) and microporous (*d*p < 2 nm) [8]. Macroporous materials, such as α-alumina membranes, are normally used to support layers of smaller pore size to form composite membranes or as catalyst support in applications where a well-defined reactive interface is required. Mesoporous materials for membranes have general pore sizes in the range of 4-5 nm, so that permeation is governed by KNUDSEN diffusion. Microporous membranes offer the potential for molecular sieving effects, with very high separation factors, and materials such as carbon molecular sieves, porous silicas, zeolites and most recently MOFs (metal-organic frameworks) have been studied [25].

If membranes show oxygen ion transport but no electronic conductivity, they are referred to as *solid electrolytes*. Two operation modes are possible: (i) the partial oxidation is combined with the generation of electricity; (ii) an external electric source supports the transport of oxygen ions through the membrane (oxygen pumping) [26]. In the latter case, the electrochemical cell consists of the oxygen-ion conducting membrane and two attached porous electrodes (Figure 1.6). Typical high temperature ion-conductors are the classical yttria-stabilized and scandia-stabilized zirconias (YSZ, ScSZ) as well as perovskite compositions without electronic conductivity such as Sr/Mg-doped lanthanium gallate. A driving force for oxygen transport through the membrane is generated if the chemical potential of oxygen at the two electrodes is different.

Membranes with high oxygen ion and electron transport are referred to as *mixed ionic and electronic conductors* (MIEC), and can be used to separate oxygen from air (c.f. chapter 1.5 Mixed Oxygen-Ion- and Electron-Conducting Membranes).

Supplying oxygen for hydrocarbon activation through a solid oxide membrane has technical, economic and environmental advantages over the direct use of air as oxidant. Membranes can be used to distribute oxygen to a reactor, thereby providing a low and uniform oxygen partial pressure along the reactor. This avoids large differences of the reaction rate and selectivity along the reactor which are typical of conventional co-feed reactors (Figure 1.7).

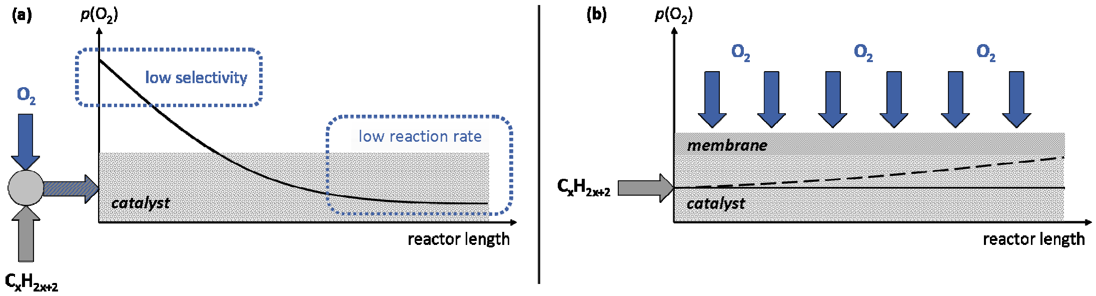

Figure 1.7: Oxygen concentration in axial direction in the catalyst bed. (a) Co-Feed reactor with strongly decreasing oxygen concentration. (b) Membrane as oxygen distributor with constant or even increasing oxygen concentration.

Safety benefits from the separation of hydrocarbon and oxygen and restrictions posed on the feed composition by the explosion limits are less severe. As the membrane is impermeable to nitrogen, NO_x formation is avoided. For industrial use, an oxygen flux of more than 1 $mL_N\ min^{-1}\ cm^{-2}$ for oxygen-conducting MIEC membranes has been estimated [27].

1.5 Mixed Oxygen-Ion- and Electron-Conducting Membranes

1.5.1 Structure of Perovskite-Type Oxides

Compounds with ABO_3 stoichiometry (A = alkaline earth, rare earth; B = transition metal; O = oxygen) tend to form perovskiste-type oxides. A convenient way to describe their structures is by using the closest spheres packing. The cubic and the hexagonal perovskite structure can be regarded as hexagonally packed layers of A-site cations with oxygen ions (AO_3) as illustrated in Figure 1.8. The stacking sequence of these layers is *ABC**ABC**ABC* in cubic perovskites, whereas the stacking sequence for hexagonal perovskites is *AB**AB**AB**AB***.

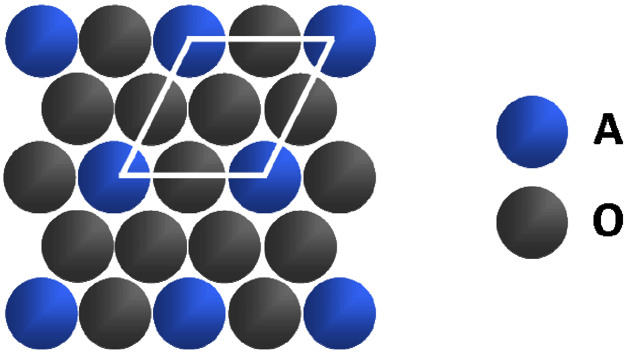

Figure 1.8: Layered AO_3 structure with hexagonal arrangement of the A site cations (blue). Oxygen ions are colored gray.

These layers form a cubic closed packing (ccp) of the A and oxygen ions with the B ions in the octahedron vacancies, shown in Figure 1.9. The A site cations are twelvefold and B site cations sixfold coordinated by oxygen, respectively.

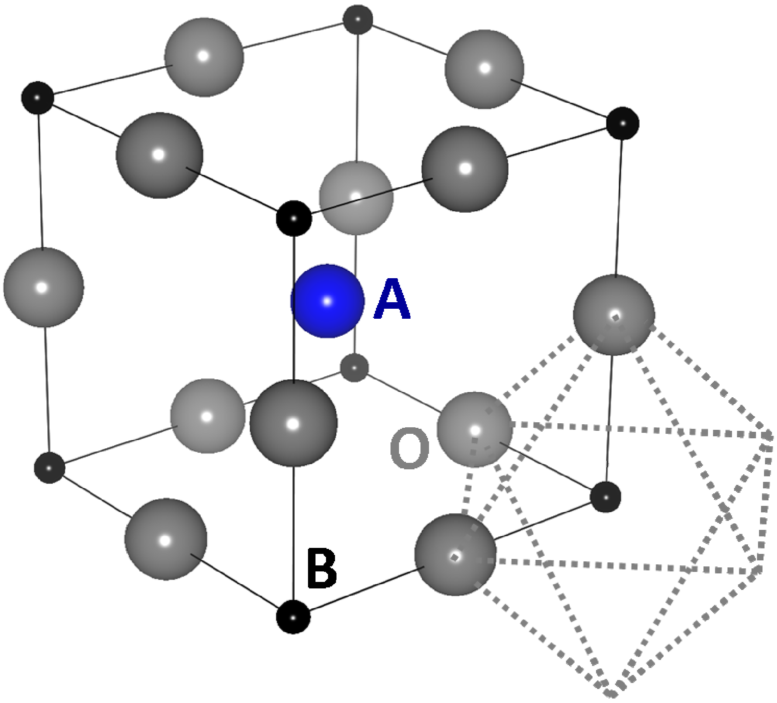

Figure 1.9: Structure of perovskite-type oxide.

The perovskite-type oxide crystal structure can be approximated by using GOLDSCHMIDT's tolerance factor t (eqn. 1.4). This factor is defined as the sum of the radii of the A-site cation (r_A) and oxygen (r_O) divided by the sum of the B-site cation (r_B) and oxygen radii multiplied by $\sqrt{2}$ (according to the PYTHAGOREAN Theorem as illustrated in Figure 1.10).

$$2 \times (r_A + r_O) = 2 \times \sqrt{2}\,(r_B + r_O) \tag{1.3}$$

$$\Rightarrow t \equiv \frac{r_A + r_O}{\sqrt{2}\,(r_B + r_O)} \tag{1.4}$$

If $t = 1$, the ideal cubic perovskite is realized as shown in Figure 1.10. An ideal undistorted cubic perovskite structure is relatively rare and can be found in $SrFeO_3$ and $SrTiO_3$.

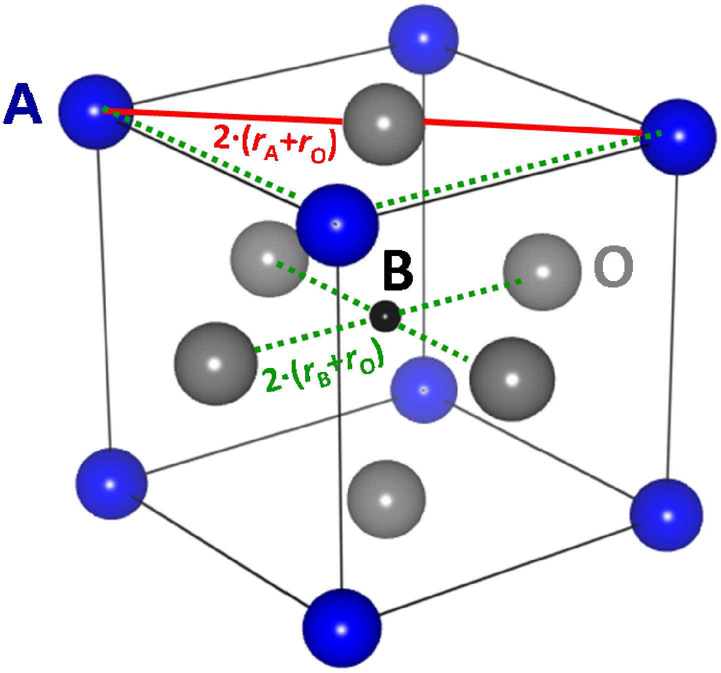

Figure 1.10: Geometric construction of GOLDSCHMIDT's tolerance factor in the ideal cubic perovskite structure.

In case that the A-site cation has a small ionic radius, the tolerance factor decreases ($t < 1$) resulting in rhombohedral or orthorhombic distortions of the formerly cubic structure. If the alkaline earth or rare earth is replaced by a transition metal yielding to a value $t < 0.8$, the ilmenite structure will be realized as it is in the case of the mineral ilmenite $FeTiO_3$. For $t > 1$, the hexagonal perovskite structure is found.

Consequently, the ideal cubic perovskite is based only on corner-sharing BO_6 octahedra, in contrast to chains of face-sharing BO_6 octahedra for the hexagonal perovskite. The ilmenite structure differs significantly from this architectural principle since only the oxygen ions form a hexagonally close-packed structure, in which two thirds of the octahedral sites are occupied by both iron and titanium. Therefore, A-site and B-site are equivalent in the ilmenite structure, which directly reflects the similarity of the A- and B-site cations in the ilmenite structure. Face- and edge-sharing $A(B)O_6$ ocahedra result from this building principle [28]. Figure 1.11 illustrates the forementioned three different perovskite structures, simplified as connected BO_6 octahedra for the cubic and hexagonal type as well as connected

A(B)O_6 octahedra for ilmenite. Cubic structure with $Pm\bar{3}m$ symmetry was found for $BaCo_xFe_yZr_zO_{3-\delta}$ (BCFZ, x+y+z = 1), the membrane material studied in this work [29].

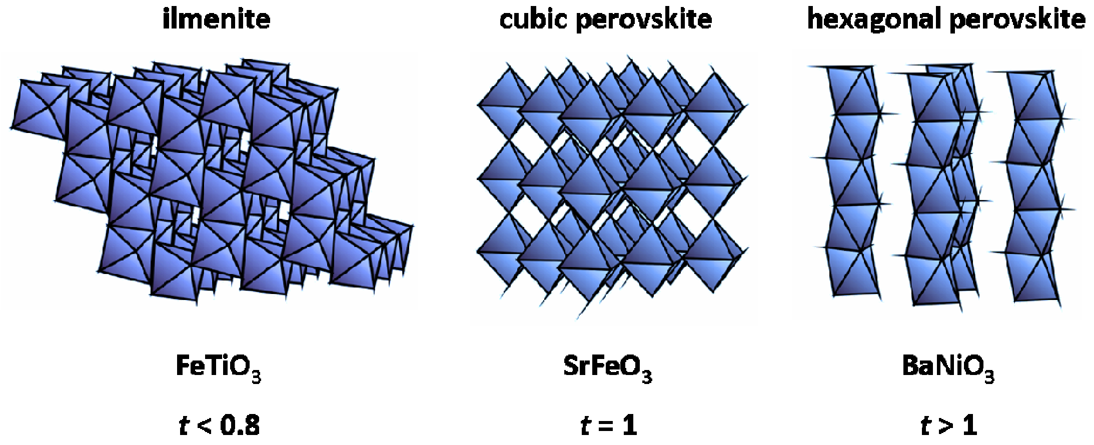

Figure 1.11: Overview of various ABO_3 perovskite-type structures. Displayed are the BO_6 and A(B)O_6 octahedra in the case of ilmenite, respectively. Differently distorted perovskite-type structures have been reported.

By applying GOLDSCHMIDT's tolerance factor, only ionic bonding is considered important in these structures, which is generally not the case. Strong contributions of covalent bonding also have to be considered [30]. Another issue which has to be addressed in regards to deviations from the ideal perovskite structure is oxygen non-stoichiometry. It is well known that perovskite-type oxides tend to form oxygen vacancies in their crystal lattice.

The aim of the material synthesis is to substitute, for example, the lattice position A and/or B of the basic ABO_3 perovskite structure by cations of similar size but lower charge in order to create an oxygen-transporting material with both ionic and electronic conductivity and sufficient chemical and mechanical stability. Whereas most oxygen-transporting MIEC membrane materials presently studied are of perovskite-type structure (ABO_3), fluorite (AO_2), brownmillerite ($A_2B_2O_5$) and pyrochlore ($A_2B_2O_7$) structures have also been evaluated. The latter two have even demonstrated oxygen transport in the undoped formulation [31].

The above mentioned ideal cubic perovskite structure $SrFeO_3$ should actually be written as $SrFeO_{3-\delta}$ to emphasize this non-stoichiometry, e.g. with $\delta = 0.03$ after synthesis under oxygen pressures of 500 atm [32]. For $Ba_{0.5}Sr_{0.5}Co_{0.8}Fe_{0.2}O_{3-\delta}$ an oxygen stoichiometry of 2.48 at room temperature was reported after synthesis under ambient air [33], where the non-stoichiometry is balanced through the valence of the B-site cations. At this high degree of vacant oxygen positions, the assumed octahedral coordination of the B-site cations by oxygen is only a rough estimation. In BCFZ with stoichiometric oxygen, cobalt as well as iron should be in the +4 oxidation state. However, in order to compensate the oxygen deficiency, Co is in the +2 and +3 and Fe in the +2, +3 and +4 oxidation states, respectively.

1.5.2 Preparation of Perovskite BCFZ Hollow Fiber Membranes

To prepare perovskite-type oxygen separating membranes, the desired perovskite is first synthesized as a powder, which can be prepared by a range of methods, e.g. chemical vapor deposition, combustion synthesis and sol-gel method. The latter process benefits from an excellent chemical homogeneity in the product. Moreover, the fine mixing as well as the partially hydrolyzed species forming extended networks allows lower calcination and sintering temperatures.

The perovskite hollow fiber membranes presented in this thesis were manufactured at the Fraunhofer Institute for Interfacial Engineering and Biotechnology (IGB) in Stuttgart by a phase inversion spinning followed by sintering [34]. The homogeneous slurry of a polymer solution and the BCFZ powder was obtained by ball milling up to 24 hours with a solid content of 50-60 mass%. The slurry was spun through a spinneret and the obtained infinite green hollow fiber was cut into 0.5 m long pieces before sintering the fiber in a hanging position. After sintering at 1295 °C for 15 h, the length of the green fiber reduced from 50 cm to ~32 cm and the sintered fiber had a wall thickness of ca. 150 µm with an outer diameter of 1.15 mm and an inner diameter of 0.85 mm (Figure 1.12). The transverse rupture stress was evaluated experimentally to be approximately 150 MPa.

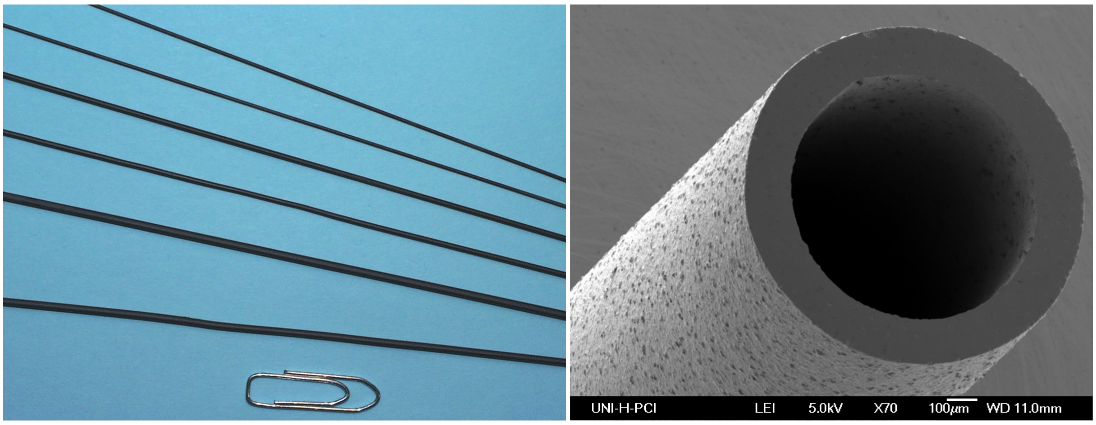

Figure 1.12: Photograph (left) and SEM micrograph (right) of sintered BCFZ hollow fiber membranes.

The driving force for the sintering process is the reduction of the free energy of the system, which can be accomplished by reducing the surface free energy of the consolidated particles. Generally, the sintering process can be divided into three stages: *initial*, *intermediate* and *final stage*.

During the *initial stage*, particles can rearrange and the coordination number can increase. Grain boundaries are formed and large discrepancies between the surface curvatures are removed. Up to 65% of the maximum density is achieved at this stage. In the *intermediate stage*, a reduction in the pore cross section is accomplished. Continuous porosity is replaced by isolated pores and the intermediate stage is taken to have ended when a density of 90% is reached. The *final stage* is characterized by the elimination of isolated pores which leads to a further increase of the density up to 95-98%. High density ceramics are prepared starting with small particles and with relatively low heating rates during the sintering process in order to remove pores from the solid.

After sintering, these membranes consist of well-separated but closely intergrown grains with a size of several micrometers, as shown by scanning electron microscopy (SEM) analysis of the outer surface of the hollow fibers [35]. Because of their relatively thin walls, the BCFZ hollow fibers show an extremely high oxygen flux. For example, at 850 °C, for a wall thickness of 175 µm, an O_2 flux of 6 mL_N min^{-1} cm^{-2} was measured using sweep gases [35]. If the oxygen partial pressure on the permeate side is decreased further by the presence of CH_4 under reaction conditions the driving force for O_2 transport is increased and the O_2 fluxes become even higher.

When arranged in bundles, hollow-fiber membranes reach a high membrane area of 400 to 5000 $m^2\ m^{-3}$ of the reactor/permeator volume. Economic goals of a price well below 1000 € m^{-2} are met by the perovskite hollow fibers. The good perspectives of perovskite hollow fibers are expected to trigger a similar development, as it has been observed in the field of organic polymer hollow-fiber membranes [36].

1.5.3 Oxygen Permeation through MIEC Membranes

As described in section 1.4.2 membranes with a perovskite structure and MIEC are useful as oxygen separating membranes due to the high oxygen permeation fluxes accessible through these membranes as well as their infinite permselectivity. In order to achieve an oxygen permeation flux through the membrane, a gradient $\nabla\mu_{O_2}$ of the oxygen chemical potential has to be produced. This gradient forces oxygen to migrate towards a lower oxygen chemical potential. The basic principle of this mechanism is illustrated in Figure 1.13.

The permeation process can be divided into three steps. First, oxygen ions are inserted into the perovskite lattice by reduction of oxygen molecules. Second, oxygen ions migrate through the perovskite membrane. Finally, oxygen is released from the perovskite membrane into the gas phase.

For charge balance, oxygen ions/oxygen vacancies and electrons/electron holes are transported simultaneously in opposite directions. As a consequence, the separated oxygen can be used for partial oxidations such as the oxidative dehydrogenation of hydrocarbons to the corresponding olefins (c.f. chapter 2 Oxidative Dehydrogenation of Light Alkanes) or the oxidative coupling of methane to C_2 hydrocarbons (c.f. chapter 3 Oxidative Coupling of Methane).

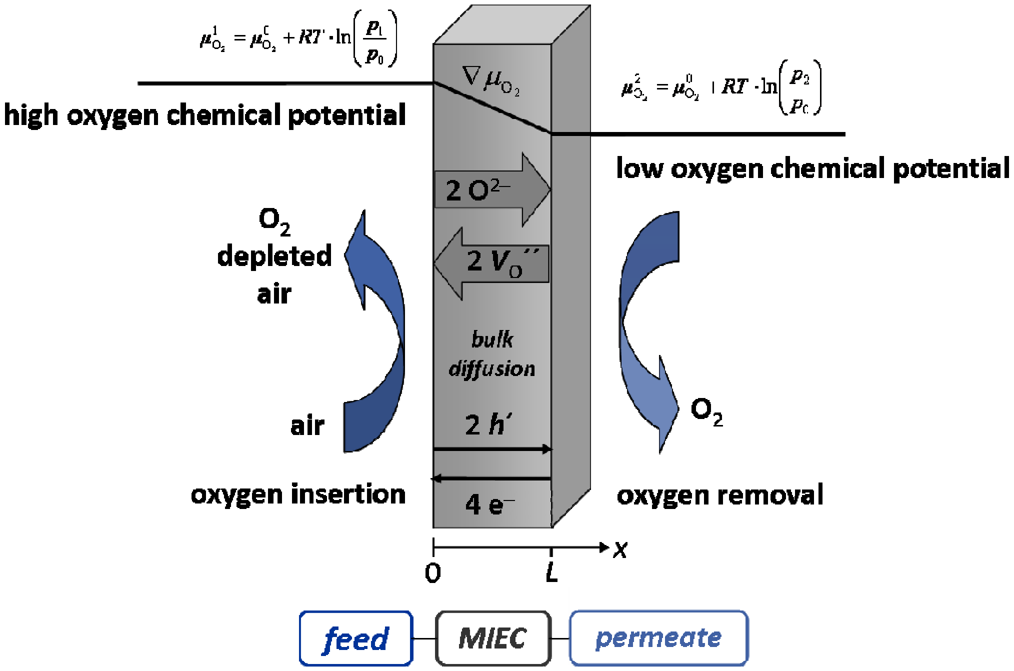
$\mu_{O_2}^1 = \mu_{O_2}^0 + RT \cdot \ln\left(\frac{p_1}{p_0}\right)$
high oxygen chemical potential
$\nabla \mu_{O_2}$
$\mu_{O_2}^2 = \mu_{O_2}^0 + RT \cdot \ln\left(\frac{p_2}{p_0}\right)$
low oxygen chemical potential
$2\,O^{2-}$
$2\,V_O^{''}$
O_2 depleted air
air
bulk diffusion
$2\,h'$
$4\,e^-$
O_2
oxygen insertion
oxygen removal
0
L
x
feed
MIEC
permeate

Figure 1.13: The principle of oxygen permeation through dense perovskite membranes resulting from the gradient $\nabla\mu_{O_2}$ between the oxygen chemical potentials of the feed side ($\mu_{O_2}^1$) and the permeate side ($\mu_{O_2}^2$). $\mu_{O_2}^0$ denotes the standard potential, p_1 the oxygen partial pressure on the feed side, p_2 the oxygen partial pressure on the permeate side, p_0 the standard pressure, $h´$ the electron holes and $V_O´´$ the oxygen ion vacancies.

Two types of kinetics, *bulk transport* and *surface exchange* contribute to the whole process and are discussed separately (c.f. 1.5.3.1 Bulk Transport and Surface Exchange).

1.5.3.1. Bulk Transport and Surface Exchange

In order to describe the oxygen transport through the bulk of mixed conducting perovskites, a counteracting transport of oxygen ions and electrons is assumed [12], where oxygen vacancies provide a pathway for oxygen ions as shown in Figure 1.14.

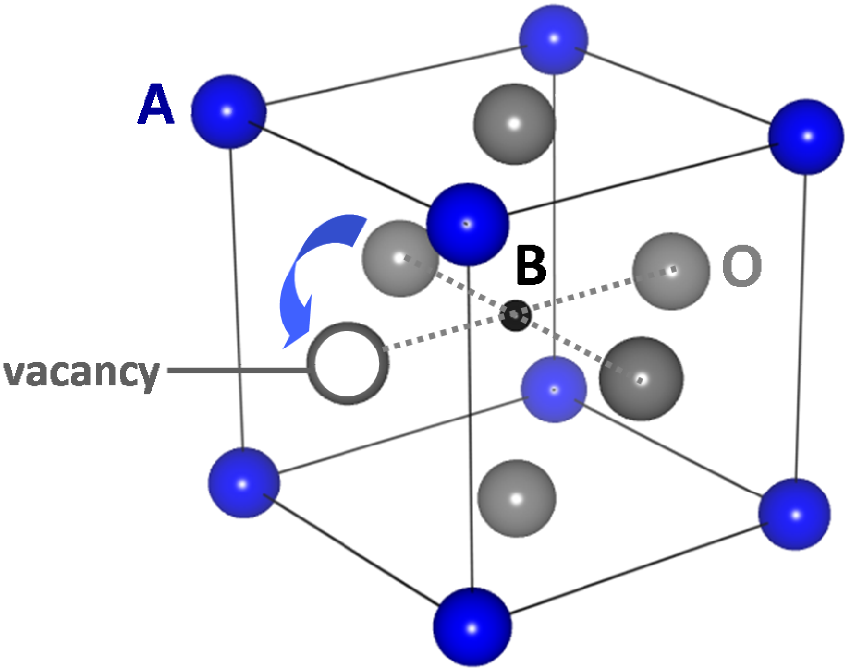

Figure 1.14: Oxygen diffusion along oxygen vacancies in the perovskite crystal lattice.

Defect simulations using computer modeling techniques have evaluated the lowest energy interstitial site as well as a trend for the oxygen migration pathway which can be found in Appendix A. The perovskite-type $Ba_{0.5}Sr_{0.5}Co_{0.8}Fe_{0.2}O_{3-\delta}$ (BSCF) was selected as a model system. The interstitial oxygen migration has been predicted via a non-linear pathway.

According to WAGNER, the single particle flux of the charge carrier is proportional to the conductivity of each charge carrier as well as to the gradient of the electrochemical potential [37]. Accordingly, the oxygen flux j_{O_2} is dependent on both, the single particle flux of oxygen ions (ionic conductivity, σ_{ion}) and on the single particle flux of the electrons (electronic conductivity, σ_{el}):

$$j_{\mathrm{O}_2} \propto -\frac{\sigma_{\mathrm{el}}\sigma_{\mathrm{ion}}}{\sigma_{\mathrm{el}}+\sigma_{\mathrm{ion}}}\nabla\mu_{\mathrm{O}_2} \tag{1.5}$$

For membrane applications, it is convenient to describe the oxygen chemical potential in terms of the oxygen partial pressure gradient across the membrane. Eqn. 1.5 then becomes the usual WAGNER-Equation (1.6), where $p_{\mathrm{O}_2}^2$ denotes the oxygen partial pressure of the low chemical potential side and $p_{\mathrm{O}_2}^1$ of the high chemical potential side and *L* is the membrane thickness.

$$j_{\mathrm{O}_2} \propto -\frac{1}{L}\int_{\ln p_{\mathrm{O}_2}^1}^{\ln p_{\mathrm{O}_2}^2}\frac{\sigma_{\mathrm{el}}\sigma_{\mathrm{ion}}}{\sigma_{\mathrm{el}}+\sigma_{\mathrm{ion}}}\,d\ln p_{\mathrm{O}_2} \tag{1.6}$$

The oxygen ionic conductivity is much lower compared to the electronic conductivity in perovskite-type oxides [12]. Therefore, the oxygen ionic electronic conduction is rate limiting and eqn. 1.6 can be simplified as follows:

$$j_{\mathrm{O}_2} \propto -\frac{1}{L}\int_{\ln p_{\mathrm{O}_2}^1}^{\ln p_{\mathrm{O}_2}^2}\sigma_{\mathrm{ion}}\,d\ln p_{\mathrm{O}_2} \tag{1.7}$$

The oxygen surface exchange demands to be considered as a multi-step process which includes adsorption, oxygen reduction, surface diffusion and the incorporation of oxygen into the perovskite lattice [12,38]. Consequently, two different processes, bulk transport and surface exchange, contribute to the oxygen permeation. Usually, the oxygen permeation flux is mainly dominated by the bulk transport, as long as the membrane thickness does not drop below a critical value, which is referred to the critical membrane thickness L_{C}. Depending on the perovskite material and on the temperature (surface exchange and bulk diffusion have different activation energies), L_{C} may be of the order of 0.01 to 10 mm. That means that for membranes thinner than L_{C} there is no linear relationship between the oxygen flux j_{O_2} and the reciprocal membrane thickness L^{-1}. Consequently, extremely thin supported perovskite layers often do not show the expected high oxygen flux as it is the surface exchange reaction that becomes rate-limiting rather than the oxygen bulk diffusion.

Further general considerations and corresponding theoretical background is given in the introduction section of each subsequent publication.

2 Oxidative Dehydrogenation of Light Alkanes

2.1 Summary

This chapter comprehends two original research articles dealing with a novel concept for hydrocarbon dehydrogenation to the corresponding olefins and a third publication giving mechanistic insights into this reaction.

Conventional catalytic or thermal dehydrogenation of light alkanes suffers from low alkane conversions due to thermodynamic limitation, even though high olefin selectivities can be achieved. In contrast, oxidative dehydrogenation can overcome constraints in conversion and benefits from the formation of steam. However, consecutive reaction of olefin combustion because of high oxygen concentrations, especially at the entrance of the reactor, decreases its yield. Furthermore, the production of pure oxygen leads to extensive costs for the process.

The novel concept for olefin production from light alkanes presented in this chapter combines the positive aspects of both methods, the catalytic/thermal and the oxidative dehydrogenation. Oxygen is separated from air via a membrane and fed to the reaction mixture in the fixed bed of a catalyst to reach conversions above the equilibrium. The membrane ensures a constant low average oxygen partial pressure over the axial length of the reactor which increases the selectivity. Intitial experiments for ethane dehydrogenation have shown that feeding the equal amount of oxygen in five successive portions into the reactor increases both, alkane conversion and olefin selectivity resulting in a higher olefin yield compared to an insertion at once (Table 1).

Table 1: Effect of feeding the equal amount of oxygen in five separate portions compared to the addition at once on ethane conversion, product selectivites and ethene yield (*shell*: 1.2 mL_N min^{-1} ethane, 2.4 mL_N min^{-1} steam, 50 mL_N min^{-1} helium; *core*: F_{total} = 50 mL_N min^{-1} air; 1.0 g of catalyst, *WHSV* = 0.1 h^{-1}, T = 725 °C).

membrane surface / cm^2	$X(C_2H_6)$	$S(C_2H_4)$	$S(CH_4)$	$S(CO)$	$S(CO_2)$	$Y(C_2H_4)$
1 x 2.20 = 2.20	0.78	0.35	0.14	0.04	0.47	0.27
5 x 0.44 = 2.20	0.99	0.48	0.19	0.02	0.32	0.48

Therefore, a BCFZ hollow fiber membrane was partly passivated with gold paste forming alternating oxygen permeable and non-permeable zones, which allows a sequenced thermal and/or catalytic dehydrogenation and selected combustion of the abstracted hydrogen helping to overcome thermodynamic limitations. The use of the membrane enables a precise control of a low average oxygen concentration inside the reactor compared to the conventional co-feed mode of operation and it also reduces the risk of explosive mixtures of hydrocarbons and oxygen.

Oxygen separation from air and an ethylene yield of 50% could be established at 725 °C, which is comparable to those for industrial steam-cracking process but at an approximately 100 °C lower temperature. Combining the hollow fiber membrane with a commercial alumina supported chromia catalyst as a packed bed around the fiber, the presented membrane reactor can compete with the best catalysts used in the co-feed mode in the range of low and moderate ethane conversions.

The propylene yield in the BCFZ membrane reactor with a Pt/Sn catalyst on an alumina support shows a maximum of 36% at 725 °C at a propane conversion of 75%, whereas the total olefin yield (C_2 + C_3) amounts 69%. The propene yield in the presented catalytic membrane reactor was twice the yield in the catalytic dehydrogenation without oxygen supply.

Moreover, the role of lattice and adsorbed oxygen species in propane dehydrogenation in the above mentioned catalytic membrane reactor was elucidated by transient analysis of products (TAP) with a sub-millisecond time resolution. Propane is mainly dehydrogenated non-oxidatively to propene and hydrogen over the catalyst, while lattice oxygen of the perovskite oxidizes preferentially H_2.

2.2 Olefin Production by a Multistep Oxidative Dehydrogenation in a Perovskite Hollow-Fiber Membrane Reactor

OLIVER CZUPRAT, STEFFEN WERTH, STEFFEN SCHIRRMEISTER, THOMAS SCHIESTEL, JÜRGEN CARO

ChemCatChem **2009**, *1*, 401-405.

This is the pre-peer reviewed version of the published article.

FULL PAPER

DOI: 10.1002/cctc.200((will be filled in by the editorial staff))

Olefin production by a multi-step oxidative dehydrogenation in a novel perovskite hollow fiber membrane reactor

Oliver Czuprat,*[a] Steffen Werth,*[a] Steffen Schirrmeister,[b] Thomas Schiestel,[c] Jürgen Caro[a]

Light alkenes are among the most important intermediate products in the chemical industry. In 2003, the worldwide production of ethene was 100 x 10^6 t.[1] The demand for ethene is expected to increase significantly in the near future. It is primarily used for the production of polymers like polyethylenes or polyvinylchlorides. At the present time, the main sources of olefins are steam cracking, fluid-catalytic-cracking and catalytic dehydrogenation.

Steam cracking of hydrocarbons is the most important process for the production of light alkenes although it is a highly endothermic process with extensive coke formation. World-scale steam crackers have the capacity to produce more than 10^6 t per annum of ethene. Selectivity to ethene from ethane in steam cracking is reported to be about 84 % at 54 % ethane conversion (800 ℃) and 78 % at 69 % ethane conversion (833 ℃).[2]

The use of chromium-based catalysts for catalytic dehydrogenation was first described by Frey and Huppke[3] in the 1930s and has repeatedly been investigated since then. In the 1940s the first plants for the catalytic dehydrogenation of butanes were built, where chromia/alumina catalysts were used.[4] In the following years, different commercial alkane dehydrogenation processes (Uhde's Star-process[5], UOP, Houdry etc.) based on different catalyst technologies where developed. Today, catalytic dehydrogenation is an established commercial route for example in the production of propene.

However, the technical realization of catalytic dehydrogenation of ethane to ethene (ODE) remains difficult due to its strongly endothermic character and the high temperature necessary to achive economic relevant equilibrium conversions (>750℃ for conversions >50%).

One way to shift the reaction equlibria is the addition of oxygen to partially convert the produced hydrogen. Addition of oxygen further leads to decreased coke formation and helps to introduce the energy required for the dehydrogenation step. Nevertheless, oxydehydrogenation is not without its own set of challenges that, in the case of ethane, have kept it from being practiced on a commercial scale. Technological challenges include especially the handling of hydrocarbon/oxygen mixtures and olefin selectivities, commercial challenges are mostly oriented on the cost of the required pure oxygen.

In the last years, large efforts have been devoted to the preparation of ODE catalysts showing commercial attractive selectivities when used in co-feed reactors. However, results often remained disappointing due to high oxygen concentration at the reactor inlet leading to low ethene yields even with very good catalysts.

One way to retain a high selectivity at high conversions even with simple catalysts is a repeated dehydrogenation and hydrogen combustion in a reactor. In this case, the initial alkane dehydrogenation occurs in a first reaction zone. The product is then fed to a second reaction zone in which a part of the produced hydrogen is burned with oxygen. An additional non-oxidative dehydrogenation of the remaining alkane occurs in a subsequent reaction zone, and then a repeated addition of oxygen burns off the hydrogen and so on. Comprehensive investigations of this concept were carried out for example by Grasselli et al. using a solid oxygen carrier.[6, 7]

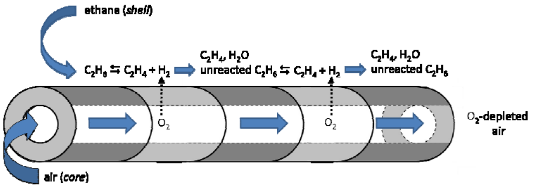
ethane (*shell*)
$C_2H_6 \leftrightarrows C_2H_4 + H_2$
C_2H_4, H_2O unreacted $C_2H_6 \leftrightarrows C_2H_4 + H_2$
C_2H_4, H_2O unreacted C_2H_6
O_2
O_2
O_2-depleted air
air (*core*)

Figure 1. Scheme of the membrane reactor for the ODE.

---

[a] *Oliver Czuprat, Dr. Steffen Werth, Prof. Dr. Jürgen Caro*
Institute for Physical Chemistry and Electrochemistry
Leibniz Universität Hannover
Callinstr. 3A, 30167 Hannover (Germany)
Fax: (+49) 511-762 - 19121
E-mail: steffen@werthnetz.de
[b] *Dr. S. Schirrmeister*
Uhde GmbH
Friedrich-Uhde-Straße 15, 44141 Dortmund (Germany)
[c] *Dr. T. Schiestel*
Uhde GmbH
IGB, Nobelstraße 12, 70569 Stuttgart (Germany)

A very interesting alternative to the use of solid oxygen carriers or multiple oxygen dosing systems within the reactor are membranes to achive a continuous addition of oxygen to the reaction zone. Using a membrane, the oxygen is only introduced in small portions, which reduces the average oxygen concentration and therefore helps to avoid local hot spots and to increase selectivity.

Besides the use of non-selective distributor-type membranes, the oxygen may also be fed by using mixed ionic electronic conductor materials (MIEC) like perovskites, capable of separating oxygen from oxygen containing gases like air at infinite selectivities[8] and therefore avoiding cost intensive oxygen separation plants. Such systems were investigated in the oxidative dehydrogenation of ethane (ODE) for example by Akin and Lin[9] who obtained an ethene yield of 56 % with a selectivity of 80 % at 875 °C using a dense tubular membrane reactor made of $Bi_{1.5}Y_{0.3}SmO_3$ and no catalyst.

An alternative membrane geometry is the use of hollow-fiber membranes which allows for a significantly increased ratio of membrane area per reactor volume. Such systems have previously been described by our group for example in the production of oxygen-enriched air[10], the direct decomposition of nitrous oxide to nitrogen by in situ oxygen removal[11] and the simultaneous production of hydrogen and synthesis gas by combining water splitting with partial oxidation of methane.[12]

In this work we present the use of a dense mixed oxygen ion and electron conducting (MIEC) perovskite hollow fiber membrane for the oxidative dehydrogenation of ethane. In contrast to earlier membrane based investigations, in our concept the catalytic dehydrogenation of ethane takes place in a first zone without addition of oxygen followed by the selective oxidation of hydrogen with oxygen delivered through the membrane (see Figure 1). These steps can be repeated several times. By assuring a signifcant hydrogen concentration at the entry of each oxidation zone, very high selectivities and conversions beyond the thermodynamic equilibrium can be obtained even with non sophisticated catalysts.

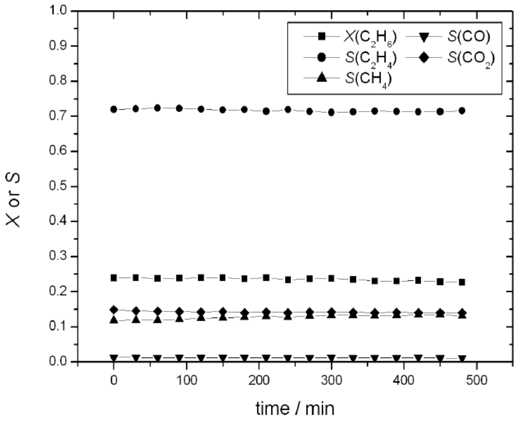

Figure 2. Fixed bed reactor performance for the conventional catalytic ethane dehydrogenation (without oxygen supply) using a commercial Cr-catalyst. Ethane conversion and product selectivities as a function of time (1.2 mL_N min^{-1} ethane, 2.4 mL_N min^{-1} steam; 50 mL_N min^{-1} helium; 1.0 g of catalyst, WHSV = 0.09 h^{-1}, T = 725 °C)..

Figure 2 shows the ethane conversion and product selectivities of the catalytic ethane dehydrogenation in a fixed bed without additional oxygen supply using a commercial Cr-based dehydrogenation catalyst. In this case of conventional dehydrogenation the conversion is roughly 25 % whereas the ethene selectivitiy is approximately 70 %. A signficant amount of by-products like methane, CO and CO_2 are produced.

In contrast, by supplying oxygen through a $BaCo_xFe_yZr_zO_{3-\delta}$ membrane the ethane conversion can be significantly improved while retaining high ethene selectivities (see Figure 3).

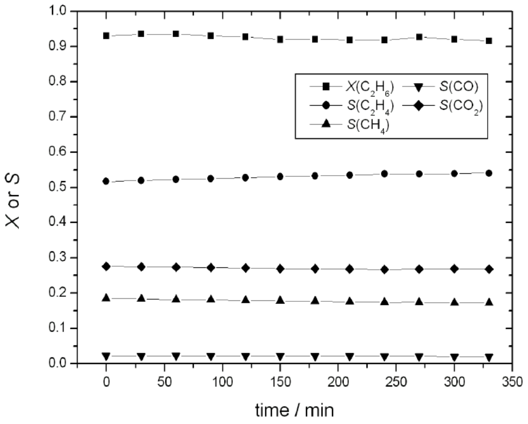

Figure 3. Oxidative dehydrogenation using a multi-step oxygen permeating hollow fiber membrane (*shell*: 1.2 mL_N min^{-1} ethane, 2.4 mL_N min^{-1} steam, 41 mL_N min^{-1} helium; *core*: 40 mL_N min^{-1} air, 40 mL_N min^{-1} helium; 5 x 0.44 cm² effective membrane surface, 0.9 g of catalyst, WHSV = 0.1 h^{-1}, T = 725 °C).

The most relevant factor for achieving good selectivities in our system is the kinetic compatibility between the reaction velocity of the hydrogen forming dehydrogenation step and the amount of permeated oxygen. The amount of permeated oxygen can be influenced by either the ratio of active membrane surface to passivate membrane surface or by reducing the oxygen partial pressure on the feed side of the membrane as shown in Table 1. For example when reducing the oxygen feed concentration from 16 % to 8 % while leaving the conditions on the permeate side untouched, the ethene selectivity can be increased from 51 % to 58 % while retaining the conversion at roughly 90 %.

Table 1. Interplay of oxygen partial pressure on the core side on ethane conversion and product selectivities on the shell side (*shell*: 1.2 mL_N min^{-1} ethane, 2.4 mL_N min^{-1} steam, 50 mL_N min^{-1} helium; *core*: F_{total} = 50 mL_N min^{-1} air diluted by helium; 5 x 0.44 cm² effective membrane surface, 0.9 g of catalyst, *WHSV* = 0.1 h^{-1}, *T* = 725 ℃).

O2 conc. / %	X(C2H6)	S(C2H4)	S(CH4)	S(CO)	S(CO2)
20	1.00	0.50	0.18	0.02	0.31
18	0.98	0.50	0.17	0.01	0.32
16	0.92	0.51	0.17	0.01	0.32
14	0.90	0.52	0.17	0.01	0.31
12	0.87	0.54	0.17	0.00	0.30
10	0.84	0.55	0.17	0.00	0.29
8	0.89	0.58	0.16	0.00	0.27
6	0.84	0.59	0.16	0.01	0.24
4	0.79	0.62	0.16	0.00	0.22
2	0.75	0.64	0.15	0.00	0.20
1	0.64	0.67	0.14	0.02	0.17
0	0.23	0.72	0.13	0.01	0.14

To further clarify these results, Figure 4 shows the ethane conversion and product selectivities as a function of the molar ratio between permeated oxygen and hydrogen formed by dehydrogenation.

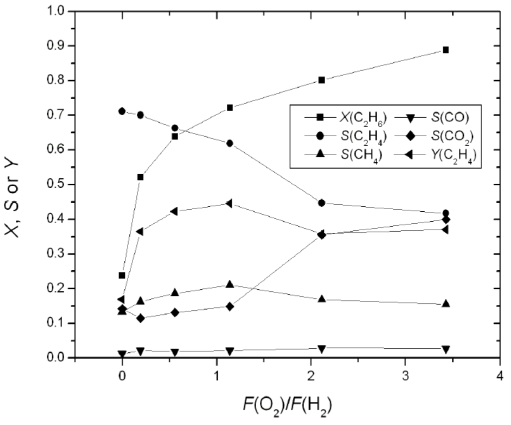

Figure 4. Ethane conversion and product selectivities for different ratios of permeated oxygen $F(O_2)$ to hydrogen produced by dehydrogenation $F(H_2)$ (*shell*: 1.2 mL_N min^{-1} ethane, 2.4 mL_N min^{-1} steam, 40 mL_N min^{-1} helium; *core*: F_{total} = 50 mL_N min^{-1}; 5 x 0.44 cm² effective membrane surface, 1.0 g of catalyst, *WHSV* = 0.09 h^{-1}, *T* = 725 ℃).

As expected, lowering the ratio between oxygen and hydrogen increases the ethene selectivity and lowers the ethane conversion. The optimum in ethane yield is found close to a ratio of oxygen and hydrogen of 0.5 according to the formation of water out of its elements. Further increase of the oxygen/hydrogen-ratio leads to increased oxidation of the hydrocarbon compounds therefore lowering the ethene selectivity.

Most notably, the increase of the oxygen/hydrogen-ratio from 0 to 0.5 significantly increases the ethane conversion from 23 % to 63 % while the ethene selectivity remains nearly constant. In this oxygen deficiency regime (based on the available molecular hydrogen) the attainable selectivity is mostly determined by the catalyst while the addition of oxygen only influences the attainable conversion.

For a commercial relevant technology, high concentrations of the ethane/steam feed are required. Table 2 shows the results of experiments with increased hydrocarbon concentration in helium. As expected, the conversion decreases when increasing the *WHSV*, while the selectivities remain nearly constant. This once again supports the idea, that the attainable selectivities in our system are mostly determined by the intrinsic catalytic selectivity of the dehydrogenation step and not by the addition of oxygen to the reaction system.

Table 2. Increase of ethane conversion by diluting the feed with helium and oxygen supply through a multi-step oxygen permeating hollow fiber (shell: Ftotal = 40 mLN min-1, steam/carbon = 1 diluted by helium; core: 50 mLN min-1 air; 5 x 0.44 cm² effective membrane surface, 0.9 g of catalyst, WHSV 0.08-0.65 h-1, T = 725 ℃).

C2H6/ steam in He / %	X(C2H6)	S(C2H4)	S(CH4)	S(CO)	S(CO2)	WHSV / h-1
20	0.65	0.46	0.28	0.14	0.12	0.08
30	0.51	0.48	0.25	0.08	0.18	0.32
30	0.64	0.67	0.15	0.06	0.11	0.40
40	0.54	0.48	0.25	0.09	0.18	0.40
50	0.41	0.44	0.25	0.05	0.26	0.48
60	0.35	0.41	0.24	0.04	0.31	0.65

Further addition of hydrogen to the hydrocarbon stream at a steady state increases the ethene selectivity, e.g. from 60 to approximately 70 %, while decreasing the total ethane conversion from 60 to approximately 50 % (see Figure 5). Schmidt et al. investigated the effect of hydrogen addition on the ODE using Pt catalyst at 1000 ℃ and very short contact times. [13] In their case, the ethylene selectivity increases from 65 to 72 %, while ethane conversion drops from 70 to 52 %. Schmidt et al. proposed that the oxygen exclusively oxidizes the hydrogen on the Pt/Sn-surface. The heat of reaction promotes a conventional catalytic dehydrogenation, in which the same amount of hydrogen is formed as fed originally on the ethane side. In our case, the mechanism of the oxidation of hydrogen was not studied in detail. However, recently published TAP-studies of the interaction of ethane with the perovskite seem to favor a Mars-Van Krevelen mechanism.[14]

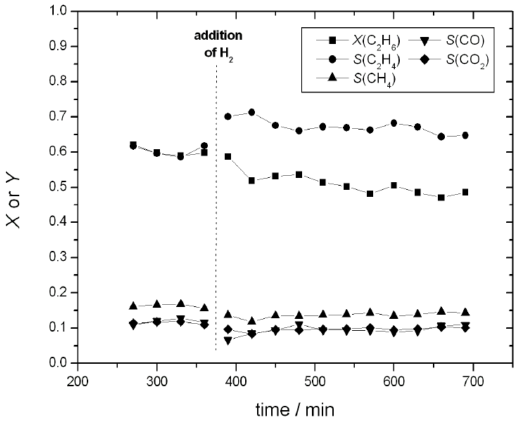

Figure 5. Effect of hydrogen addition to the feed on ethane conversion and product selectivities with oxygen supply through a multi-step oxygen permeating BCFZ hollow fiber membrane (*shell*: 1.2 mL_N min^{-1} ethane, 1.2 mL_N min^{-1} hydrogen, 2.4 mL_N min^{-1} steam, 40 mL_N min^{-1} helium; *core*: 2.5 mL_N min^{-1} air, 47.5 mL_N min^{-1} helium, 5 x 0.44 cm² effective membrane surface, 1.0 g of catalyst, *WHSV* = 0.09 h^{-1}, *T* = 725 ℃).

A novel concept for hydrocarbon dehydrogenation to the corresponding olefins in a multi-zone hollow fiber membrane reactor with successive dehydrogenation- and oxidation-zones is proposed. The use of an oxygen permeating membrane can increase the ethane conversion significantly compared to a conventional catalytic dehydrogenation and allows a precise control of the oxygen insertion. It also reduces the risks of explosive mixtures during an ODE by having a dense membrane that separates the hydrocarbon and oxygen feeds from each other. Furthermore it avoids the significant costs associated with the production of pure oxygen required in the conventional oxydehydrogenation. At the same time it provides a low average oxygen concentration which gives a high ethene selectivity by selectively burning off *in situ* the hydrogen from conventional catalytic dehydrogenation. The novel hollow fiber membrane reactor for the production of ethene possesses a good long-term stability (see Figure 3).

For an industrial implementation of such a system, one could think about a multitude of hollow fibre bundels in a catalytic fixed bed and operated in cross-flow to avoid the need for gold-sealing of the different membrane-zones.

Reaction conditions could be established that have a comparable ethylene yield (~50 %, see Figure 3 and Table 1) to those in the industrial steam cracking process, but at a temperature that is approximately 100 ℃ lower. For an ethane conversion of around 95 % an ethylene selectivity of approximately 55 % was found (see Figure 3). The highest ethylene selectivity at 725 ℃ was 70 % at an ethane conversion of around 52 % (see Figure 4).

Summarizing, in the range of low and moderate ethane conversions, our membrane reactor using a standard commercial catalyst can compete with the best catalysts used in the co-feed mode of the ODE (see Figure 6). The effect of using a more sophisticated catalyst in conjunction with the multi-zone membrane reactor remains to be investigated.

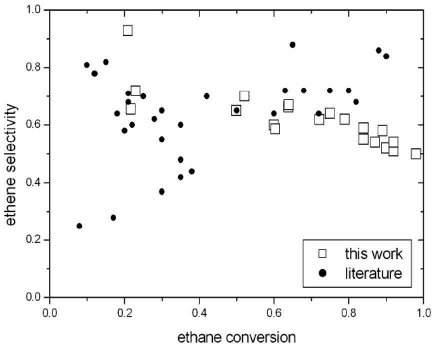

Figure 6. Ethylene selectivity as a function of ethane conversion. The data for various catalytic systems reported in the literature between 2000 and 2006 and giving alkane conversion higher than 10 % were taken from [15]. Systems operating in millisecond-contact-time reactors have not been taken into consideration.

Experimental Section

The manufacture of the hollow fiber membrane of the composition $BaCo_xFe_yZr_zO_{3-\delta}$ (BCFZ, x+y+z=1) is described elsewhere.[16] The fibers were coated with gold paste (C 5754 B, Hereaus) and sintered at 950 ℃ for 5 hours to obtain 5 permeation zones (2 cm each) alternating with passivated areas (2 cm each, see Figure 7). This procedure was repeated three times to ensure a leak-proof gold layer. The coated membranes were inserted into a porous alumina tube with an outer diameter of ~2 mm and a wall thickness of ~0.7 mm. The dehydrogenation catalyst (Actisorb 410, Südchemie, Cr_2O_3 on Ca aluminate) was milled in a mortar, a sieve fraction between 10 and 500 µm was sieved out and dispersed between the inner porous alumina tube and an outer dense alumina tube.

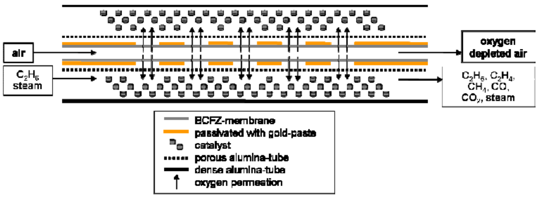

Figure 7. Schematic drawing of a multi-step hollow fiber with five active zones for catalytic ODE. At both ends 6 cm of the 30 cm long fiber were coated with gold. The inner 18 cm of the fiber were alternately passivated over 2 cm with and without gold thus forming 5 active zones for oxygen permeation, each 2 cm long. The active surface area for the multi-step oxygen permeating BCFZ hollow fiber is 2.2 cm² with a total oxygen permeable length of 10 cm.

For the ODE, ethane (99.95 %) diluted with steam and helium (99.996 %) was fed to the shell side, while synthetic air was fed to the core side. All gas flows were controlled by mass flow controllers (Bronkhorst Hi-Tech). The gases at the exit of the reactor were analyzed by a gas chromatograph (Agilent Technologies, HP 6890 with two auto valves, Carboxen 1000 column from Supelco). Concentrations of C_2H_6, C_2H_4, CH_4, CO, CO_2, H_2, N_2 and O_2 were determined by calibration against standard gases. The absolute flow of the effluents was determined by using neon (99.995 %) as an internal standard. The catalyst was activated under a stream of 10 % hydrogen in helium (F_{total} = 20 mL_N min^{-1}) at 725 °C for 30 minutes. The ODE was performed at a temperature of 725 °C.

Acknowledgements

The authors acknowledge the financial support of the project SynMem by the German BMBF and Uhde GmbH and Borsig GmbH for the permit of publication as well as Südchemie AG for providing the catalyst.

Keywords: membrane reactor • oxidative dehydrogenation • ethane dehydrogenation • perovskites • ethylene

[1] *Chemiewirtschaft in Zahlen*, Verband der Chemischen Industrie e.V. VCI, Frankfurt, **2005**, p. 120.

[2] H.-J. Arpe in *Ullmann's Encyclopedia of Industrial Chemistry*, 5th Edition, Vol. A10, VCH, Weinheim, **1987**, p. 54.

[3] F. E. Frey, W.F. Huppke, *Ind. Eng. Chem. Res.* **1933**, *25*, 54.

[4] M.M. Bhasin, J.H. McCain, B.V. Vora, T. Imai, P.R. Pujadó, *Appl. Catal. A: General* **2001**, *221*, 397.

[5] K.J. Caspary, H. Gehrke, M. Heinritz-Adrian, M. Schwefer in *Handbook of Heterogeneous Catalysis*, 2nd Edition, Vol. 7, Wiley-VCH, Weinheim, **2008**, p. 3206.

[6] R.K. Grasselli, D.L. Stern, J.G. Tsikoyiannis, *Appl. Catal., A* **1999**, *189*, 1.

[7] R.K. Grasselli, D.L. Stern, J.G. Tsikoyiannis, *Appl. Catal., A* **1999**, *189*, 9.

[8] P.J. Gellings, H.J.M. Bouwmeester, *Catal. Today* **1992**, *12*, 1.

[9] F.T. Akin, Y.S. Lin, *J. Membr. Sci.* **2002**, *209*, 457.

[10] H. Wang, S. Werth, T. Schiestel, J. Caro, *Angew. Chem. Int. Ed.* **2005**, *44*, 6906.

[11] H. Jiang, H. Wang, F. Liang, S. Werth, T. Schiestel, J. Caro, *Angew. Chem. Int. Ed.* **2009**, *121*, 3027.

[12] H. Jiang, H. Wang, S. Werth, T. Schiestel, J. Caro *Angew. Chem. Int. Ed.* **2008**, *47*, 9341.

[13] A.S. Bodke, D. Henning, L.D. Schmidt, S.S. Bharadwaj, J.J. Maj, J. Siddall, J. Catal. **2000**, *191*, 62.

[14] E. Kondratenko, V. Kondratenko, H. Wang, J. Caro, *J. Mol. Cat. A* **2009**, *297*, 142.

[15] F. Cavani, N. Ballarini, A. Cericola, *Catal. Today* **2007**, *127*, 113.

[16] T. Schiestel, M. Kilgus, S. Peter, K.J. Caspary, H. Wang, J. Caro, *J. Membr. Sci.* **2005**, *258*, 1.

Received: ((will be filled in by the editorial staff))
Published online: ((will be filled in by the editorial staff))

2.3 Oxidative Dehydrogenation of Propane in a Perovskite Membrane Reactor with Multi-Step Oxygen Insertion

OLIVER CZUPRAT, STEFFEN WERTH, JÜRGEN CARO, THOMAS SCHIESTEL

American Institute of Chemical Engineers Journal **2010**, *56*, 2390-2396.

This is the pre-peer reviewed version of the published article.

Oxidative dehydrogenation of propane in a perovskite membrane reactor with multi-step oxygen insertion

Oliver Czuprat[a,*] Steffen Werth[a], Thomas Schiestel[b] and Jürgen Caro[a,*]

[a]Institute for Physical Chemistry and Electrochemistry, Leibniz Universität Hannover, 30167 Hannover, Germany
[b]Fraunhofer Institute for Interfacial Engineering and Biotechnology, 70569 Stuttgart, Germany

A membrane reactor incorporating a hollow fiber with successive parts of oxygen permeable and passivated surface segments has been developed and was used for the oxidative dehydrogenation of propane. This membrane geometry allows a controlled oxygen feeding into the reactor over its axial length. In the oxidative dehydrogenation, the thermodynamic limitation of propane dehydrogenation can be overcome. By using this novel hollow fiber membrane reactor with a Pt/Sn/K dehydrogenation catalyst, oxygen separation and propene formation could be established even at temperatures as low as 625 °C with long-term stability. Combining the hollow fiber membrane and the dehydrogenation catalyst, the highest propene selectivity of 75% was observed at a propane conversion of 26% and 625 °C whereas the best propene yield of 36% was obtained at 675 °C (48% propene selectivity). The performance of this reactor is evaluated by applying various reaction conditions.

Topical heading: Reactors Kinetics and Catalysis

Keywords: membrane reactor, oxidative dehydrogenation, propane dehydrogenation, oxygen transporting membrane, perovskites

Introduction

The demand for olefins, especially propene, is expected to increase significantly in the near future. Propene was the first petrochemical raw material to be employed on an industrial scale and is important for the production of polymers, mainly for the production of polypropylene (PP), but also in the production of cumene, acrylonitrile, and acrylic acid/acrolein or propylene oxide.[1] In 2002, approximately 61% of propene production was via steam cracking and 34% was obtained by catalytic cracking. To cover the continuously increasing demand for propene, it was also necessary to generate about another 3% by catalytic dehydrogenation.[2] An increase in the share of the catalytic dehydrogenation of propane in the overall production of propene can be expected.

A number of technologies are available commercially for the dehydrogenation of propane to propene: these include *Oleflex* developed by UOP, Des Plaines, Illinois; *Catofin* developed by Air Products and Chemicals, Allentown, Pennsylvania; and Uhde's *STAR* developed by Phillips Petroleum, Bartlesville,[3] Oklahoma. These processes differ in their modes of operation, the dehydrogenation catalyst, and the methods of catalyst regeneration.[1] The Uhde *STAR* process achieves a propene yield of 35.6% per pass at a propane selectivity of 89%. The temperature range inside the reactor which is operated discontinuously (7 h operation, 1 h regeneration) is between 570-590 °C at 5 bar.[2]

One concept to overcome the thermodynamic limitation of propane conversion is the oxidative dehydrogenation of hydrocarbons (ODH), where alkane and oxygen are co-fed and give rise to the olefin and water. The Gibbs free energy of the formation of water (-228.7 kJ mol^{-1} at room temperature) compensates the Gibbs free energy of the endothermic dehydrogenation of propane ($+124.3$ kJ mol^{-1}). Pioneering work was done by Imai and Jan on the dehydrogenation of low alkanes.[4]

The main problem encountered in propane ODH is the presence of the consecutive reaction of olefin combustion, e.g. deep oxidation into carbon dioxide and water as well as partial oxidations or thermal cracking at higher reaction temperature that rapidly decreases the propylene yield when the conversion of the alkane is increased. The best yields reported in the co-feed method are lower than 30% with propane conversions lower than 40% which is still insufficient for technical applications. The best performance (24% propene yield) has been obtained with non-reducible alkali earth metal oxides at 650 °C whereas the addition of lithium increased selectivity from 40 to 70 % at low conversion.[5]

One way to retain a high selectivity at high conversions is a repeated dehydrogenation and hydrogen combustion in a reactor. In this case, the initial catalytic alkane dehydrogenation occurs in a first reaction zone. The product is then fed to a second reaction zone in which the major part of the produced hydrogen is burnt with oxygen. A repeated non-oxidative conventional dehydrogenation of the remaining alkane occurs in a subsequent reaction zone, and then a repeated addition of oxygen burns off the hydrogen and so on. Comprehensive investigations of this concept were carried out, e.g. by Grasselli et al. using a solid oxygen carrier.[6]

The use of membranes is an interesting alternative to solid oxygen carriers in order to dose oxygen at a reduced average concentration to the reaction zone avoiding local hot spots and increasing selectivity. Additionally, high temperature oxygen-permselective membranes feed activated oxygen species leading to a different catalytic behaviour than under conventional hydrocarbon/oxygen co-fed operations. Wang et al. investigated the oxidative dehydrogenation of propane in a dense tubular $Ba_{0.5}Sr_{0.5}Co_{0.8}Fe_{0.2}O_{3-\delta}$ membrane reactor. The propene selectivity was 4% at 23% conversion compared to 15% propene selectivity achieved under identical conditions in the fixed-bed reactor.[7]

In contrast, the geometry of a hollow-fiber membrane offers a significantly higher ratio of membrane surface area per reactor volume and provides continuously active lattice oxygen. Recently, Wu et al. reported the use of an asymmetric alumina hollow fiber with an outer Pd/Ag catalytic layer as an extractor membrane for hydrogen in the catalytic dehydrogenation of propane. An initial propane conversion of 42% was achieved, but serious coke deposition on the catalytic surface led to a decrease in activity soon.[8] Systems using dense perovskite hollow fiber membranes have been presented by our group, e.g. for the direct decomposition of nitrous oxide to nitrogen by in situ oxygen removal,[9] the simultaneous production of hydrogen and synthesis gas by combining water splitting with partial oxidation of methane[10] and recently the multi-step oxidative dehydrogenation of ethane (ODE).[11,12]

In this publication we present the use of a dense mixed oxygen ion and electron conducting (MIEC) perovskite hollow fiber membrane of the composition $BaCo_xFe_yZr_zO_{3-\delta}$ (BCFZ, x+y+z=1) for the oxidative dehydrogenation of propane with and without employing a dehydrogenation catalyst. To the best of our knowledge, it is the first time that the oxidative dehydrogenation of propane (ODP) has been investigated with a perovskite hollow fiber membrane. It is an advantage of our BCFZ hollow fiber that it shows sufficient oxygen flux and stability at temperatures << 800 °C.[12] Addionally, steam is fed on the hydrocarbon side of the membrane in order to lower the partial pressure of propane as well as reducing coke deposition.

Most probably, two mechanisms occur simultaneously. As presented for the ODE, in our concept the dehydrogenation (DH) of propane

$$C_3H_8 \leftrightarrows C_3H_6 + H_2 \qquad (1)$$

occurs in a first reaction zone without addition of oxygen followed by the selective combustion (SC) of hydrogen

$$H_2 + \tfrac{1}{2}\, O_2 \rightarrow H_2O \qquad (2)$$

with oxygen delivered through the membrane (Figure 1).

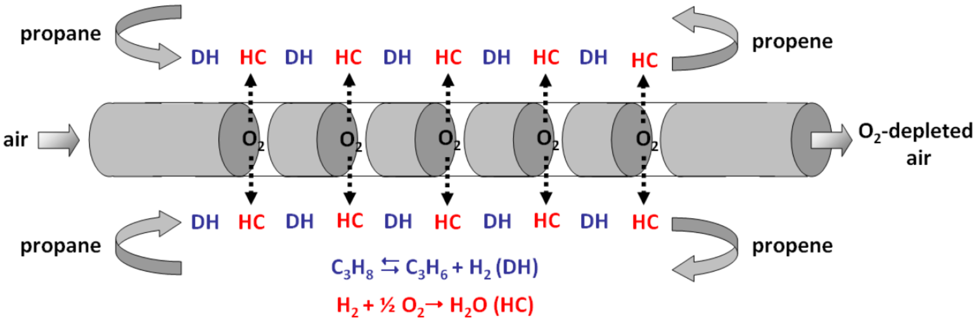
propane
DH HC DH HC DH HC DH HC DH HC
propene
air
O_2
O_2-depleted air
DH HC DH HC DH HC DH HC DH HC
propane
propene
$C_3H_8 \leftrightarrows C_3H_6 + H_2$ (DH)
$H_2 + ½ O_2 \rightarrow H_2O$ (HC)

Figure 1. Scheme of the membrane reactor for the stepwise oxidative dehydrogenation of propane with a sequence of dehydrogenation (DH) and hydrogen combustion (HC).

Parallel, a direct oxy-dehydrogenation of the propane or of the abstracted hydrogen at the perovskite surface following a Mars and van Krevelen mechanism takes place. To be supportive of this sequence of reactions, the membrane is divided into passivated and non-passivated segments for oxygen permeation. This stepwise reaction can retain high selectivities and conversions beyond the thermodynamic equilibrium can be obtained. Furthermore, no regeneration of the reactor is required since no coke deposition could be observed.

In the following, different reactor set-ups with and without dehydrogenation catalyst and oxygen supply via the hollow fiber membrane at different reaction conditions will be compared.

Experimental

Preparation of the hollow fibers

The fabrication of the hollow fiber membrane of the composition $BaCo_xFe_yZr_zO_{3-\delta}$ (BCFZ, x+y+z=1, Figure 2) is described elsewhere.[14] The fibers with an outer diameter of ~1.1 mm and a wall thickness of ~0.14 mm were coated with gold paste (C 5754 B, Heraeus) and sintered at 950 °C for 5 hours to obtain 5 permeation zones (each 2 cm long) alternating with passivated areas (each 2 cm long, Figure 3). This procedure was repeated three times to ensure a leak-proof gold layer.

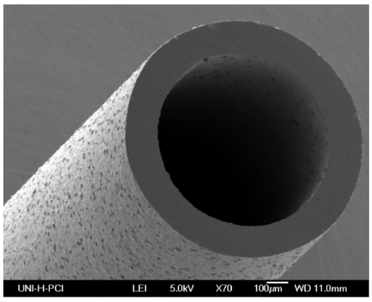
UNI-H-PCI
LEI
5.0kV
X70
100µm
WD 11.0mm

Figure 2. $BaCo_xFe_yZr_zO_{3-\delta}$ (BCFZ, x+y+z=1) hollow fiber membrane obtained by spinning at the Fraunhofer Institute for Interfacial and Biotechnology Stuttgart.[14]

Studies in the hollow fiber membrane reactor

For the ODP, propane (99.5%) diluted with steam and helium (99.996%) was fed to the shell side of the membrane, while synthetic (C_xH_y-free) air or oxygen (99.9996%) diluted with helium was fed to the core side. All gas flows were controlled by mass flow controllers (Bronkhorst Hi-Tech). The gases at the exit of the reactor were analyzed by a gas chromatograph (Agilent Technologies, HP 6890) equipped with a Carboxen 1000 column (Supelco). Concentrations of C_3H_8, C_3H_6, C_2H_6, C_2H_4, CH_4, CO, CO_2, H_2, N_2 and O_2 were determined by calibration against standard gases. The absolute flow of the effluents was determined by using neon (99.995%) as an internal standard. All data points collected in this work were taken at steady-state conditions which were obtained after 1-3 hours. For experiments using the dehydrogenation catalyst (PDH-964, BASF), the BCFZ hollow fiber was inserted into a porous alumina tube (outer diameter ~2.2 mm, wall thickness of ~0.4 mm) to avoid direct contact with the catalyst. The latter was milled in a mortar; a sieve fraction between 10 and 500 µm was sieved out and a portion of 0.25 g was dispersed between the inner porous alumina tube and the outer dense alumina tube (Figure 3).

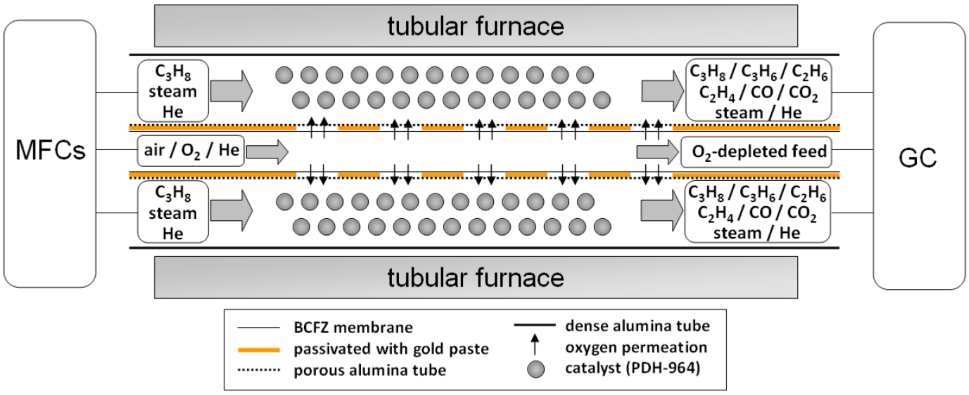

Figure 3. Schematic drawing of the reactor set-up and an incorporated multi-step BCFZ hollow fiber with five active zones for ODP. At both ends 6 cm of the 30 cm long fiber were coated with gold. The inner 18 cm of the fiber were alternately passivated over 2 cm with and without gold thus forming five active zones for oxygen permeation, each 2 cm long. The active surface area for the multi-step oxygen permeating BCFZ hollow fiber is 2.2 cm² with a total oxygen permeable length of 10 cm. The dehydrogenation catalyst was dipersed between the outer dense alumina tube and the fiber, which was inserted into a porous alumina tube.

Results and discussion

Conventional thermal dehydrogenation without and with oxygen supply via BCFZ hollow fiber membrane

Figure 4 shows as a reference case the propane conversion, product selectivities as well as propene yields in our reactor without oxygen supply and without any catalyst as a function of the temperature. A higher temperature leads to an increase in propane conversion, but also to a drop in propene selectivity due to augmented cracking of hydrocarbons to ethene and methane. Since the increase in propane conversion at the same time is higher than the decrease in propene selectivity, the propene yield rises with higher temperature.

According to a homogeneous gas phase reaction or wall reactions, the propene yield at 625 °C is around 0.3%, whereas at 725 °C already a 10% yield is obtained. The overall olefin selectivity ranges from ca. 50% to 80%.

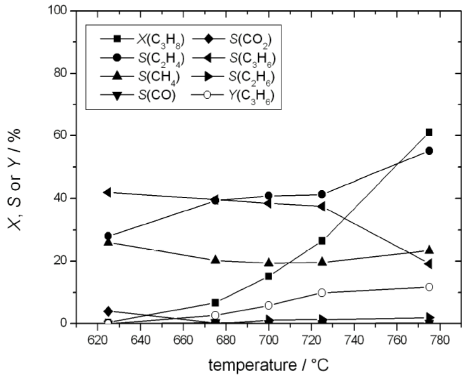

Figure 4. Reactor performance for the conventional thermal propane dehydrogenation (without oxygen addition and no catalyst). Propane conversion and product selectivities as a function of the temperature (5 mL_N min^{-1} propane, 10 mL_N min^{-1} steam, 35 mL_N min^{-1} helium).

By supplying oxygen separated from air via the BCFZ hollow fiber membrane into the reactor using no dehydrogenation catalyst, the propane conversion and propene yield could be enhanced significantly over the entire observed temperature range at a slightly lowered propene selectivity (Figure 5) compared to the pure thermal dehydrogenation in the empty reactor (Figure 4). For example, at 675 °C using the membrane reactor the obtained propene yield is almost four times higher than without oxygen supply. The higher the oven temperature, the higher the oxygen flux through the membrane according to the Wagner equation. Accordingly, more hydrogen can be burnt off, shifting the equilibrium towards the desired product.

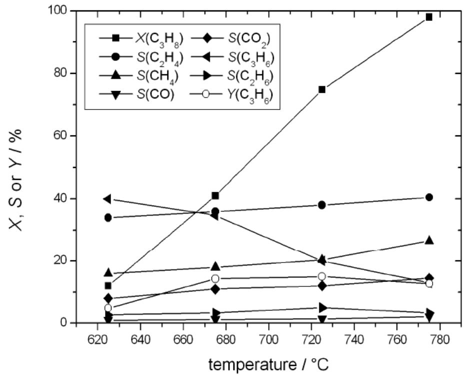

Figure 5. Temperature dependency of propane conversion, product selectivities and propene yield of the membrane reactor with oxygen supply through the BCFZ hollow fiber and no dehydrogenation catalyst (*shell*: 5 mL_N min^{-1} propane, 10 mL_N min^{-1} steam, 35 mL_N min^{-1} helium; *core*: 50 mL_N min^{-1} air; 5 x 0.44 cm^2 effective membrane surface).

For achieving good selectivities in our reactor, the kinetic compatibility between the reaction rates of the hydrogen forming dehydrogenation step and the amount of permeated oxygen is essential.

The latter can be influenced by either (i) the ratio of active membrane surface to passivated membrane surface, by (ii) varying the temperature or (iii) the oxygen partial pressure on the core side of the membrane. As we can see in Figure 6, by decreasing the oxygen concentration on the core side of the membrane - and therefore lowering the propane conversion - the propene selectivity could be increased, especially in the range of oxygen concentrations below 20%.

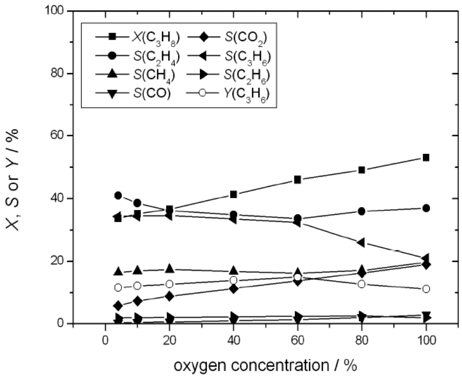

Figure 6. Effect of the oxygen partial pressure on the core side of the BCFZ hollow fiber membrane. Propane conversion, product selectivities and propene yield as a function of the oxygen concentration at a total pressure of 1 bar at *T* = 675 °C (*shell*: 5 mL$_N$ min^{-1} propane, 10 mL$_N$ min^{-1} steam, 35 mL$_N$ min^{-1} helium; *core*: F_{total} = 50 mL$_N$ min^{-1} oxygen diluted with helium; 5 x 0.44 cm² effective membrane surface).

For an industrial application of our membrane reactor, higher concentrations of propane/steam in the feed are more economic and desirable than those presented in the experiments so far. At a total propane and steam concentration of 10% in the feed, a propane conversion of approximately 60% at 21% propene selectivity is observed (Figure 7). By increasing the hydrocarbon/steam concentration, the propane conversion decreases continuously down to 10% for an undiluted feed. Above a total propane and steam concentration of 50% in the feed, the propene selectivity remains constant at 30% which seems to be the intrinsic selectivity of the reactor at these specific reaction conditions.

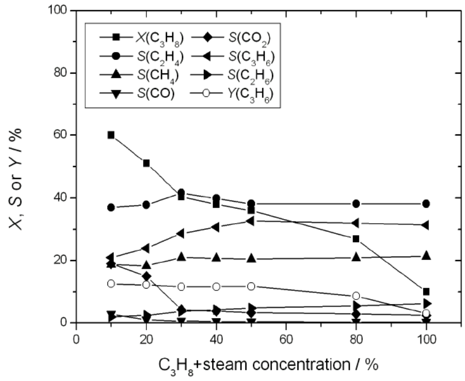

Figure 7. Effect of propane/steam concentration on propane conversion and product selectivities and propene yield in the BCFZ hollow fiber membrane reactor (*shell*: F_{total} = 50 mL_N min^{-1}, steam to carbon = 2:3 diluted with helium; *core*: 50 mL_N min^{-1} air; 5 x 0.44 cm^2 effective membrane surface; *T* = 675 °C).

Conventional catalytic dehydrogenation without and with oxygen supply via BCFZ hollow fiber membrane

Using a dehydrogenation catalyst in a fixed bed without oxygen supply through a BCFZ hollow fiber membrane, the propane conversion is enhanced over the total temperature range (Figure 8) compared to the blank reactor (Figure 4). Except the highest investigated temperature of 775 °C, also the propene selectivity is higher than without using the catalyst.

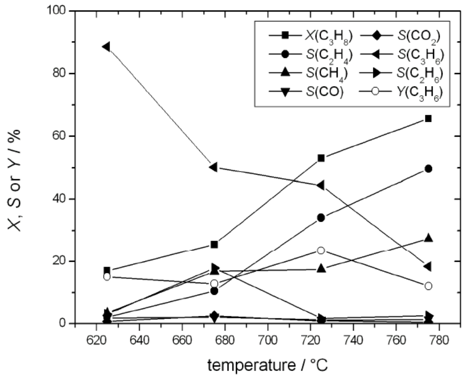

Figure 8. Reactor performance for the conventional catalytic propane dehydrogenation (without oxygen addition). Propane conversion, product selectivities and propene yield as a function of temperature (5 mL_N min^{-1} propane, 10 mL_N min^{-1} steam, 35 mL_N min^{-1} helium; 0.25 g of catalyst PDH-964; *WHSV* = 2.4 h^{-1}).

By feeding oxygen via the hollow fiber membrane into the catalytic reactor, the propane conversion could be increased in the whole observed temperature range between 625 °C and 775 °C (Figure 9). For the membrane reactor an improved propene yield with a maximum at 725 °C is found which equals an increase of around 50% in propene yield of the catalytic dehydrogenation without oxygen supply (Figure 8).

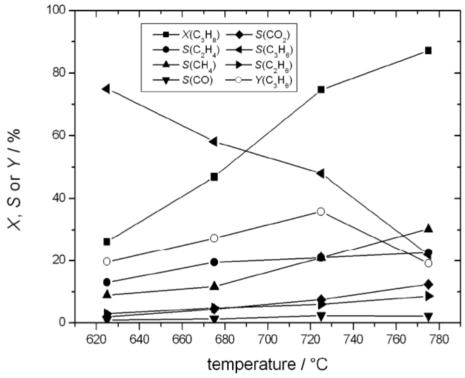

Figure 9. Impact of oxygen supply via a BCFZ hollow fiber membrane on the catalytic propane dehydrogenation. Propane conversion, product selectivities and propene yield as a function of temperature (*shell:* 5 mL$_N$ min^{-1} propane, 10 mL$_N$ min^{-1} steam, 35 mL$_N$ min^{-1} helium; *core:* 50 mL$_N$ min^{-1} air; 5 x 0.44 cm² effective membrane surface; 0.25 g of catalyst PDH-964; *WHSV* = 2.4 h^{-1}).

As shown for the reactor containing only the hollow fiber membrane (Figure 6), the amount of permeated oxygen can be influenced by varying the oxygen partial pressure on the feed side of the membrane (Figure 10). For example, when increasing the oxygen feed concentration from 10% to 20% while leaving the conditions on the permeate side untouched, the propane conversion can be increased from 51% to 75% while lowering the propene selectivity only from 52% to 46%.

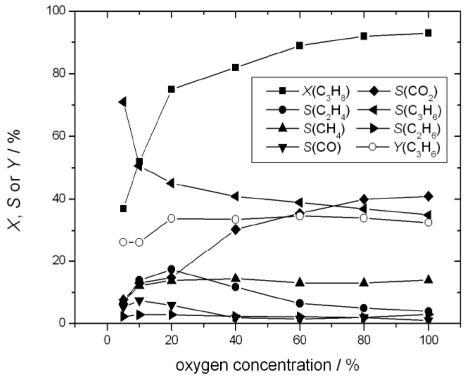

Figure 10. Interplay of oxygen partial pressure on the core side on propane conversion, product selectivities and propene yield (*shell:* 5 mL$_N$ min^{-1} propane, 10 mL$_N$ min^{-1} steam, 35 mL$_N$ min^{-1} helium; *core:* F_{total} = 50 mL$_N$ min^{-1} oxygen diluted with helium; 5 x 0.44 cm² effective membrane surface; 0.25 g of catalyst PDH-964; *WHSV* = 2.4 h^{-1}; *T* = 675 ℃).

Figure 11 shows the propane conversion and product selectivities as a function of the percentage of (propane + steam) in helium as feed on the shell side of the hollow fiber membrane. By decreasing this concentration to 10%, the propane conversion increases above 80% while the propene selectivity - as expected - drops to 28%. Most notably, if we feed only a mixture of propane and steam (no helium as a dilutant), the reactor gives rise to a propane conversion of 40% at 45% propene selectivity.

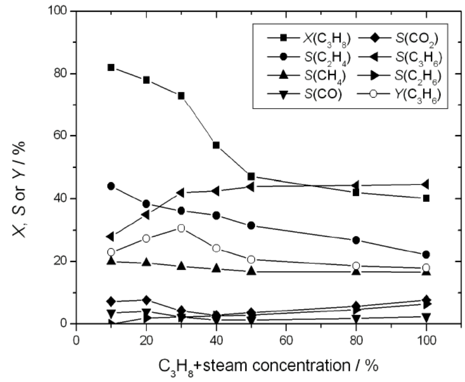

Figure 11. Effect of (propane + steam) concentration in helium on propane conversion and product selectivities in the membrane reactor with oxygen supply via the BCFZ hollow fiber and dehydrogenation catalyst (*shell*: F_{total} = 50 mL$_N$ min^{-1}, steam to carbon = 2:3 diluted with helium; *core*: 50 mL$_N$ min^{-1} air; 5 x 0.44 cm² effective membrane surface; 0.25 g of catalyst PDH-964; *WHSV* = 2.4 h^{-1}; *T* = 675 °C).

Table 1 gives an overview about the effects of the dehydrogenation catalyst and the oxygen permeating BCFZ hollow fiber membrane on the propane conversion as well as propene selectivity and yield. The pure thermal dehydrogenation in an empty reactor without catalyst and hollow fiber gives only 2% propene yield (Figure 4) at 675 °C. By supplying oxygen via the hollow fiber membrane at the same temperature the propane conversion is enhanced significantly from 6% to 41% whilst the selectivity towards propene only drops from 40% down to 35% (Figure 5).

The use of only the dehydrogenation catalyst leads to a comparable propene yield of 13% (at a lower propane conversion and higher propene selectivity). Combining the catalyst with the BCFZ hollow fiber membrane gives rise to an increase of around 2.5 times the propene yield versus only the catalyst or only the fiber inside the reactor (Table 1).

ID	cat	fiber	$X(C_3H_8)$ / %	$S(C_3H_6)$ / %	$Y(C_3H_6)$ / %	Fig.
1	-	-	6	40	2	4
2	-	x	41	35	14	5
3	x	-	26	50	13	8
4	x	x	74	45	34	10

Table 1: Propane conversion, propene selectivity and propene yield using 20% oxygen concentration in the gas feed on the core side of the membrane (ID 2 and 4) and a Pt/Sn/K dehydrogenation catalyst (ID 3 and 4) compared to the blank reactor with no oxygen supply and no dehydrogenation catalyst (ID 1) (*shell*: 5 mL$_N$ min^{-1} propane, 10 mL$_N$ min^{-1} steam, 35 mL$_N$ min^{-1} helium; *core*: F_{total} = 50 mL$_N$ min^{-1}, 20% oxygen; 0.25 g of catalyst PDH-964; *WHSV* = 2.4 h^{-1}; *T* = 675 °C).

Combining the catalyst with our hollow fiber, at a conversion of 93% at 675 °C a propene selectivity of 35% is obtained (39% total olefin selectivity; Figure 10). The highest propene selectivity of 75% is observed at a propane conversion of 26% and 625 °C (88% total olefin selectivity; Figure 9) whereas the best propene yield of 36% is achieved at 725 °C (69% total olefin selectivity; Figure 9).

The oxygen permeable membrane supplies oxygen in successive stages into the reactor (i) burning off selectively the hydrogen from thermal dehydrogenation and (ii) parallel the direct oxidation of propane/hydrogen by lattice oxygen of the perovskite takes place. Ongoing TAP-experiments will provide a deeper insight into the molecular mechanisms. The membrane not only separates the hydrocarbon feed from oxygen but also avoids the need of an oxygen separation plant.

Our membrane reactor using a dehydrogenation catalyst can compete with the best catalysts used in the co-feed mode of the ODP (Figure 12).

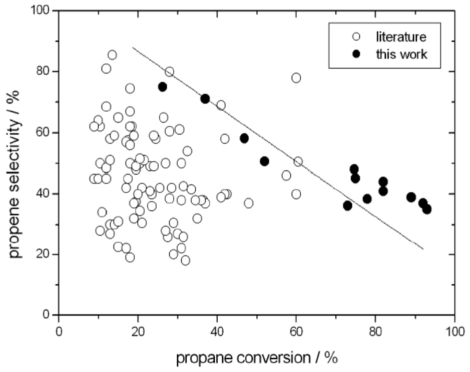

Figure 12. Propene selectivity as a function of propane conversion. The data for various catalytic systems reported in the literature between 2000 and 2006 and giving alkane conversion higher than 10% were taken from [5].

Conclusions

A membrane reactor for the oxidative dehydrogenation of short chain hydrocarbons combining the conventional catalytic dehydrogenation with the selective combustion of the abstracted hydrogen is presented.

To attain kinetic compatibility between the rates of dehydrogenation and oxygen supply via the $BaCo_xFe_yZr_zO_{3-\delta}$ perovskite hollow fiber membrane, certain parts of the hollow fiber have been passivated for oxygen transport by a gold coating.

Under our experimental conditions, the propene yield in the catalytic membrane reactor was twice the yield in the catalytic dehydrogenation without oxygen supply.

The propene yield shows a maximum at 725 °C and amount 36% (for 75% propane conversion and 48% propene selectivity). The total olefin yield (C_2 + C_3) amounts 69%.

Acknowledgements

The authors acknowledge the financial support of the project SynMem by the German Federal Ministry of Education and Research as well as BASF SE for providing the catalyst. Dr. Steffen Schirrmeister (Uhde GmbH) is thanked for the permit of publication.

Literature Cited

1. Eisele P, Killpack R. Propene. In: Ullmann's Encyclopedia of Industrial Chemistry, 7 th Edition. New York:John Wiley & Sons, Inc., 2001.
2. Caspary KJ, Gehrke H, Heinritz-Adrian M, Schwefer M. Dehydrogenation of Alkanes. In: Ertl G, Knözinger H, Schüth F, Weitkamp J. Handbook of Heterogeneous Catalysis. Weinheim: Wiley-VCH, 2008.
3. The Uhde STAR process, oxydehydrogenation of light paraffins to olefins, Uhde GmbH, 2009.
4. Imai T, Jan D-Y. European Patent 0 323 115, assigned to UOP, 1988.
5. Cavani F, Ballarini N, Cericola A. Oxidative dehydrogenation of ethane and propane: How far from commercial implementation?. Catal. Today 2007; 127:113-131.
6. Grasselli RK, Stern DL, Tsikoyiannis JG. Catalytic dehydrogenation (DH) of light paraffins combined with selective hydrogen combustion (SHC): I. DH → SHC → DH catalysts in series (co-fed process mode). Appl. Catal. A 1999; 189:1-8.
7. Wang H, Cong Y, Zhu X, Yang W. Oxidative dehydrogenation of propane in a dense tubular membrane reactor. React. Kinet. Catal. Lett. 2003; 79:351-356.
8. Wu Z, Hatim IMD, Kingsbury BFK, Gbenedio E, Li K. A Novel Inorganic Hollow Fiber Membrane Reactor for Catalytic Dehydrogenation of Propane. AIChe J. 2003; 49:3007-3017.
9. Jiang H, Wang H, Liang F, Werth S, Schiestel T, Caro J. Direct Decomposition of Nitrous Oxide to Nitrogen by In Situ Oxygen Removal with a Perovskite Membrane. Angew. Chem. Int. Ed. 2009; 48:2983-2986.
10. Jiang H, Wang H, Werth S, Schiestel T, Caro J. Simultaneous Production of Hydrogen and Synthesis Gas by Combining Water Splitting with Partial Oxidation of Methane in a Hollow-Fiber Membrane Reactor. Angew. Chem. Int. Ed. 2008; 47:9341-9344.
11. Czuprat O, Werth S, Schirrmeister S, Schiestel T, Caro J. Oxidative Dehydrierung niederer Alkane in einem selektiven Membranreaktor mit gestufter Sauerstoffzugabe und In-situ-Wasserstoffoxidation. Chem. Ing. Tech. 2009; 81:1591-1597.
12. Czuprat O, Werth S, Schirrmeister S, Schiestel T, Caro J. Olefin Production by a Multistep Oxidative Dehydrogenation in a Perovskite Hollow-Fiber Membrane Reactor. ChemCatChem 2009; 1:401-405.
13. Wang H, Tablet C, Caro J. Oxygen production at low temperature using dense perovskite hollow fiber membranes. J. Membr. Sci. 2008; 322:214-217.
14. Schiestel T, Kilgus M, Peter S, Caspary KJ, Wang H, Caro J. Hollow fibre perovskite membranes for oxygen separation. J. Membr. Sci. 2005; 258:1-4.

2.4 Dehydrogenation of Propane with Selective Hydrogen Combustion: A Mechanistic Study by Transient Analysis of Products

OLIVER CZUPRAT, JÜRGEN CARO, VITA A. KONDRATENKO, EVGENII V. KONDRATENKO

Catalysis Communications **2010**, *11*, 1211–1214.

Reprinted from Catalysis Communications, Vol. 11, OLIVER CZUPRAT, JÜRGEN CARO, VITA A. KONDRATENKO, EVGENII V. KONDRATENKO, Dehydrogenation of Propane with Selective Hydrogen Combustion: A Mechanistic Study by Transient Analysis of Products, 1211-1214, 2010, with permission from Elsevier.

Catalysis Communications 11 (2010) 1211–1214

Contents lists available at ScienceDirect

Catalysis Communications

journal homepage: www.elsevier.com/locate/catcom

Dehydrogenation of propane with selective hydrogen combustion: A mechanistic study by transient analysis of products

Oliver Czuprat [a], Jürgen Caro [a], Vita A. Kondratenko [b], Evgenii V. Kondratenko [b,]*

[a] *Institute of Physical Chemistry and Electrochemistry, Leibniz Universität Hannover, Callinstr. 3A, D-30167 Hannover, Germany*
[b] *Leibniz Institute for Catalysis at the University of Rostock, Albert-Einstein-Str. 29a, D-18059 Rostock, Germany*

ARTICLE INFO

Article history:
Received 31 May 2010
Received in revised form 9 July 2010
Accepted 13 July 2010
Available online 17 July 2010

Keywords:
TAP reactor
Pt catalyst
Mechanism
Membrane reactor
Oxidative dehydrogenation
Propane dehydrogenation
Oxygen transporting membrane
Perovskites

ABSTRACT

The role of lattice and adsorbed oxygen species in propane dehydrogenation in a perovskite hollow fiber membrane reactor containing a Pt–Sn dehydrogenation catalyst was elucidated by transient analysis of products with a sub-millisecond time resolution. Propane is mainly dehydrogenated non-oxidatively to propene and hydrogen over the catalyst, while lattice oxygen of the perovskite oxidizes preferentially hydrogen to water. For achieving high propene selectivity at high propane conversions, the formation of gas phase O_2 on the shell side of the membrane reactor should be avoided. Otherwise, oxygen species adsorbed over the Pt–Sn catalyst participate in non-selective C_3H_8/C_3H_6 transformations to C_2H_4 and CO_x.

© 2010 Elsevier B.V. All rights reserved.

1. Introduction

Oxidative dehydrogenation of light alkanes to olefins is a promising alternative to the industrially applied catalytic non-oxidative dehydrogenation due to no equilibrium constraint. However, the oxidative dehydrogenation with co-feeding of oxygen and alkane suffers from poor olefin selectivity at high alkane conversions. Grasselli et al. [1,2] suggested a concept for propane conversion to propene by combining the non-oxidative propane dehydrogenation over a Pt–Sn-containing catalyst with catalytic selective hydrogen combustion (SHC) over Sb_2O_4, In_2O_3, WO_3 and Bi_2O_3 supported on SiO_2. These both reactions can be performed in separated reactors or in one reactor with a mixture of these catalysts. However, this concept suffers from (i) separation of O_2 and N_2 or C_3H_6/C_3H_8 from N_2, if pure oxygen or air is used for the SHC, respectively or/and (ii) periodical catalyst regeneration in the one-reactor process scheme. Both drawbacks can be avoided by applying dense perovskite ceramic membranes exhibiting high oxygen ionic and electronic conductivity [3,4]. Such membranes of the composition of $BaCo_xFe_yZr_zO_{3-\delta}$ (BCFZ, $x+y+z=1$) are produced by the Fraunhofer Institute for Interfacial Engineering and Biotechnology (IGB) in Stuttgart in a hollow-fiber geometry [5]. The group at the Leibniz Universität Hannover has intensively applied BCFZ membranes for various reactions, e.g. direct decomposition of nitric oxide to nitrogen and oxygen in combination with syngas production from methane [6], oxidative coupling of methane [7] and the multi-step oxidative dehydrogenation of ethane [4] and propane [3].

Despite potential applications of such membrane reactors, mechanistic studies of the ongoing catalytic reactions are rare. Recently, we demonstrated that the temporal analysis of products (TAP) reactor provided useful mechanistic insights for optimizing ethane dehydrogenation to ethylene and methane oxidation to syngas in a BCFZ membrane reactor [8]. In the present study, we analyzed mechanistic aspects of previously investigated propane dehydrogenation with SHC in the membrane reactor containing a commercial Pt–Sn dehydrogenation catalyst [3]. The aim was to identify reaction pathways for the dehydrogenation and combustion. To this end, we investigated interactions of H_2 and C_3H_8 with the membrane and the catalyst in absence and presence of gas-phase ($^{18}O_2$ as isotopic tracer) oxygen.

2. Experimental

2.1. Membrane reactor for the multi-step dehydrogenation with SHC

Fig. 1 shows a scheme of the BCFZ membrane reactor for propane dehydrogenation with simultaneous hydrogen combustion [3]. The fibers were coated with gold paste to obtain five permeation zones (each 2-cm long) alternating with passivated areas (each 2-cm long) yielding a total effective surface area for oxygen permeation of 2.2 cm^2.

---

* Corresponding author. Tel.: +49 381 1281290; fax: +49 381 128151290.
E-mail address: evgenii.kondratenko@catalysis.de (E.V. Kondratenko).

1566-7367/$ – see front matter © 2010 Elsevier B.V. All rights reserved.
doi:10.1016/j.catcom.2010.07.009

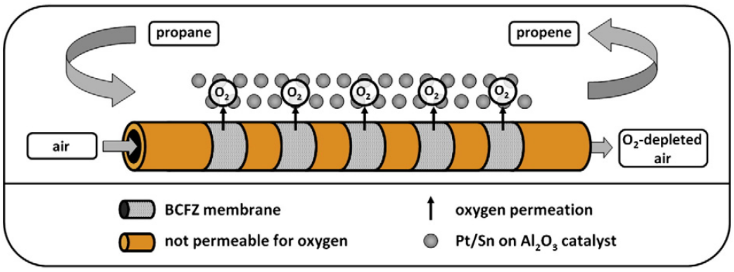

Fig. 1. Scheme of the hollow fiber membrane reactor for the multi-step catalytic dehydrogenation of propane with SHC.

The manufacturing of the membranes is described elsewhere [5]. The catalytic tests were performed at 1 bar and 948 K using 0.25 g Pt–Sn catalyst on the shell side of the membrane. Propane (5 $mL_N\ min^{-1}$, $WHSV = 2.4\ h^{-1}$), steam (10 $mL_N\ min^{-1}$) and helium (35 $mL_N\ min^{-1}$) were fed on the shell side, while synthetic air (50 $mL_N\ min^{-1}$) was supplied on the core side.

2.2. Transient experiments

Transient experiments were performed in the TAP-2 reactor at LIKAT, a transient pulse technique operating in vacuum with a sub-millisecond time resolution [9,10]. The crushed BCFZ membrane (70 mg, sieve fraction of 200–500 μm) or the Pt–Sn dehydrogenation catalyst (40 mg, sieve fraction of 200–500 μm) was packed within the isothermal zone of the quartz micro-reactor (40 mm length and 6 mm i. d.) between two layers of quartz particles of the same sieve fraction. The perovskite was pre-treated at ambient pressure in an O_2 flow (20 mL min^{-1}) at 948 K for 30 min followed by exposure to vacuum (10^{-5} Pa). A strong loss of oxygen observed upon the evacuation was recovered by $^{16}O_2$ pulsing. Pulse experiments over the Pt–Sn catalyst were performed without any pre-treatment.

In order to prove if lattice oxygen of the perovskite or adsorbed oxygen species participate in H_2 and C_3H_8 oxidation, single $H_2/Xe = 1/1$ or $C_3H_8/Xe = 1/1$ as well as simultaneous $^{18}O_2/Ar = 1/1$ and $H_2/Xe = 1/1$ ($C_3H_8/Xe = 1/1$) pulse experiments were performed. The ability of the Pt–Sn catalyst to react with H_2 and C_3H_8 was probed by single $H_2/Xe = 1/1$ or $C_3H_8/Xe = 1/1$ and simultaneous $^{18}O_2/Ar = 1/1$ and $H_2/Xe = 1/1$ ($C_3H_8/Xe = 1/1$) pulse experiments. In addition, H_2 multi-pulse experiments were carried out, in which an $H_2/Xe = 1/1$ mixture was repeatedly pulsed (in total ca. 200 pulses) over the perovskite and the catalyst. All experiments were performed at 948 K.

$^{18}O_2$ (95–98%, ISOCOM GmbH), $^{16}O_2$ (5.0), H_2 (5.0), C_3H_8 (3.5), Ar (5.0) and Xe (4.0) were used without further purification. Transient responses were recorded at the reactor outlet using a quadrupole mass spectrometer (HAL RD 301 Hiden Analytical) at the following atomic mass units (AMUs): 36 ($^{18}O_2$), 34 ($^{18}O^{16}O$), 32 ($^{16}O_2$), 20 (Ar, $H_2^{18}O$), 19 ($H_2^{18}O$), 18 ($^{18}O_2$, $H_2^{16}O$), 17 ($H_2^{16}O$), 2 (H_2), 40 (Ar), and 132 (Xe). The pulses were repeated 10 times for each AMU and averaged to improve the signal to noise ratio. In the H_2 multi-pulse experiments, the responses were treated without averaging. The concentration of feed components and reaction products was determined from the respective AMUs using standard fragmentation patterns and sensitivity factors.

3. Results and discussion

3.1. Steady-state catalytic results in the catalytic membrane reactor

The catalytic performance of the BCFZ hollow fiber membrane reactor for propane dehydrogenation in the presence and absence of oxygen flow through the membrane and with and without a Pt–Sn dehydrogenation catalyst has been previously reported [3]. The most meaningful results are summarized in Table 1. The perovskite alone showed low propene yield in the absence of oxygen (ID 1 in Table 1). The yield was increased by a factor of 7, when oxygen was supplied through the membrane (ID 2 in Table 1) due to a growth in the propane conversion indicating the importance of oxygen for the propane dehydrogenation. An increased propene yield was also achieved in the presence of the Pt–Sn catalyst but in the absence of oxygen (ID 3 in Table 1). The reactor performance was further improved in the presence of the Pt–Sn catalyst and oxygen supplied through the membrane (ID 4 in Table 1). The propene selectivity was very close to that in ID 3 but the propane conversion was approximately 3 times higher. This synergetic effect of the catalyst and oxygen was suggested to be due to SHC favouring the non-oxidative propane dehydrogenation [3]. In order to understand mechanistic origins governing activity and selectivity, we investigated C_3H_8 and H_2 interactions with the perovskite and the Pt–Sn catalyst by transient analysis of products.

3.2. Active oxygen species for propane dehydrogenation and hydrogen activation

Fig. 2 compares typical transient responses of carbon-containing products and unreacted propane after C_3H_8 ($C_3H_8/Xe = 1/1$) pulsing at 948 K. Clearly, the perovskite and the Pt–Sn catalyst differ in the reaction products formed. The shapes of the product transients are also dissimilar indicating that the mechanism and the kinetics of propane activation are different. C_3H_6 and CO_2 were formed over the perovskite (Fig. 2a). Since gas-phase O_2 was not present in the C_3H_8 pulse, lattice oxygen of the perovskite participated in the CO_2 formation. This is in agreement with our previous study [8]. No CO_2 but H_2 in addition to C_3H_6 was formed over the Pt–Sn catalyst (Fig. 2b) via non-oxidative propane

Table 1
Propane conversion, propene selectivity and yield in membrane reactor experiments [3]. ID1: blank reactor without BCFZ fixed bed/fiber and Pt-Sn catalyst, ID2: BCFZ hollow fiber membrane reactor without Pt-Sn catalyst, ID3: fixed bed of Pt–Sn catalyst, ID4: BCFZ hollow fiber membrane reactor with fixed bed of Pt–Sn catalyst. Experimental conditions: *shell side*: 5 $mL_N\ min^{-1}$ propane, 10 $mL_N\ min^{-1}$ steam, 35 $mL_N\ min^{-1}$ helium; *core side (only ID2 and ID3)*: $F_{total} = 50\ mL_N\ min^{-1}$, 20% oxygen; 0.25 g of Pt–Sn catalyst; $WHSV = 2.4\ h^{-1}$; $T = 948$ K.

ID	Pt-Sn Catalyst	Fiber	$X(C_3H_8)$/%	$S(C_3H_6)$/%	$Y(C_3H_6)$/%
1	–	–	6	40	2
2	–	+	41	35	14
3	+	–	26	50	13
4	+	+	74	45	34

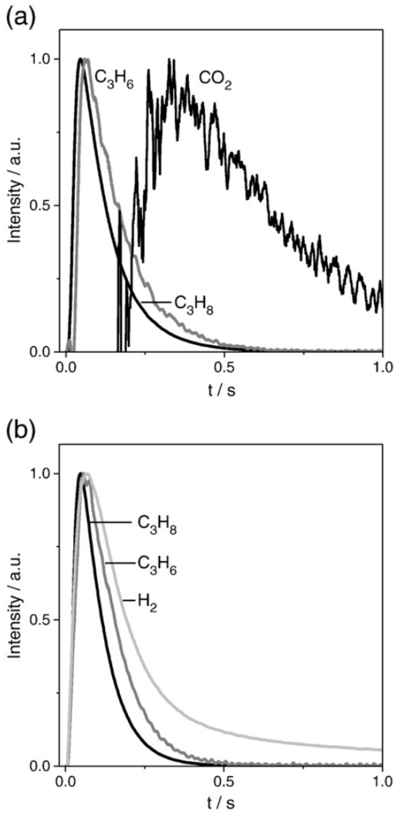

Fig. 2. Transient responses recorded after C_3H_8 (C_3H_8/Xe = 1/1) pulsing over (a) oxidized BCFZ perovskite and (b) Pt–Sn catalyst at 948 K.

dehydrogenation. Moreover, the propane conversion was higher than that over the perovskite. The difference in the activity of these two materials agrees well with the results of steady-state experiments (ID 1 vs. 3 in Table 1).

CO_x containing ^{18}O was not observed when $^{18}O_2$ ($^{18}O_2$/Ar = 1/1) and C_3H_8 (C_3H_8/Xe = 1/1) were simultaneously pulsed over the oxidized perovskite containing ^{16}O lattice oxygen. Therefore, only lattice oxygen of the perovskite oxidizes C_3H_8/C_3H_6. When $^{18}O_2$ and C_3H_8 were pulsed over the Pt–Sn catalyst, $C^{18}O$ was observed (Fig. 3), i.e. adsorbed oxygen species oxidize C_3H_8/C_3H_6 to $C^{18}O$. In addition, they participate in cracking propane to ethylene (Fig. 3). These both non-selective reactions are responsible for slightly lower propene selectivity in the membrane reactor in the presence of the Pt–Sn catalyst and oxygen flow through the membrane (ID 4 in Table 1) compared to the performance in the absence of the oxygen flow (ID 3 in Table 1); gas-phase O_2 is provided by the recombinative desorption of oxygen species diffused through the perovskite membrane.

To prove whether the perovskite and the Pt–Sn catalyst oxidize H_2 in the absence and presence of gas-phase O_2, single H_2 (H_2/Xe = 1/1) as well as simultaneous $^{18}O_2$ ($^{18}O_2$/Ar = 1/1) and H_2 (H_2/Xe = 1/1) pulse experiments were performed. The oxidized perovskite showed high activity towards H_2 oxidation in the absence of gas-phase O_2, i.e. lattice oxygen participated in this reaction. Taking also the results from Fig. 2 into account it is concluded that C_3H_8 and H_2 compete for the same lattice oxygen species. As for the C_3H_8 conversion, adsorbed oxygen does not participate in H_2 oxidation (results are not shown for brevity). However, the perovskite showed different activity for the oxidation of C_3H_8 and H_2. Typical H_2 transients are presented in Fig. 4. The outlet concentration of H_2 increases with increasing number of H_2 pulses. Correspondently, H_2 conversion decreases. This can be explained by continuous consumption of lattice oxygen of the perovskite for H_2 oxidation. The more H_2 is pulsed, the more lattice oxygen is removed resulting in a decrease in H_2 combustion and an increase of intensity of the H_2 transient. Such behaviour was not observed for C_3H_8 oxidation. Moreover, the H_2 conversion was higher than that of C_3H_8.

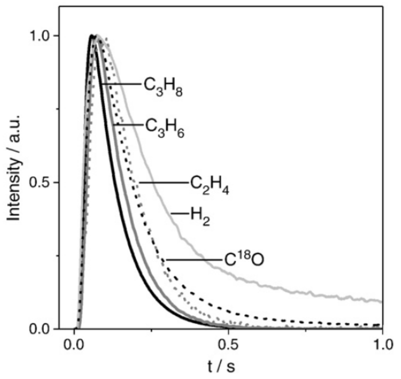

Fig. 3. Transient responses recorded after simultaneous pulsing of C_3H_8 (C_3H_8/Xe = 1/1) and $^{18}O_2$ ($^{18}O_2$/Ar = 1/1) over Pt–Sn catalyst at 948 K.

Furthermore, we analyzed the interaction of H_2 with the Pt–Sn catalyst in the absence and presence of gas-phase O_2. Fig. 5 compares H_2 transients obtained upon H_2 pulsing over the Pt–Sn catalyst and the perovskite. The very narrow shape of the H_2 transient over the perovskite is due to H_2 consumption. Contrarily, H_2 interacts reversibly and probably dissociatively with the catalyst as concluded from the broad shape of the H_2 response in Fig. 5. Moreover, since the shapes of the H_2 transients obtained in single H_2 and simultaneous $^{18}O_2$–H_2 pulse experiments are very similar, the presence of gas-phase O_2 does not significantly influence the interaction of H_2 with the catalyst. Only tiny amounts of $H_2^{18}O$ were detected in the latter experiments, i.e. the Pt–Sn catalyst is not active for H_2 oxidation even in the presence of gas-phase O_2.

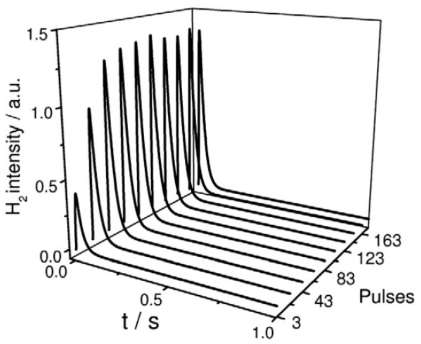

Fig. 4. Individual H_2 transient responses recorded after H_2 (H_2/Xe = 1/1) multi-pulsing over oxidized BCFZ perovskite at 948 K.

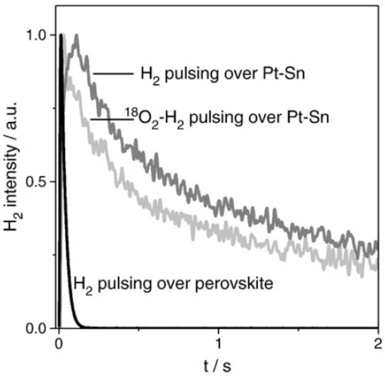

Fig. 5. Averaged H_2 transient responses recorded after H_2 (H_2/Xe = 1/1) pulsing and simultaneous pulsing of H_2 (H_2/Xe = 1/1) and $^{18}O_2$ ($^{18}O_2$/Ar = 1/1) over oxidized BCFZ perovskite and Pt–Sn catalyst at 948 K.

4. Summary and conclusions

The results of present transient and previous steady-state studies enabled us to develop the following mechanistic concept of propane dehydrogenation with SHC in the BCFZ perovskite membrane reactor containing a commercial Pt–Sn catalyst. Both solids catalyze propane dehydrogenation. In contrast to the perovskite, the Pt–Sn catalyst dehydrogenates propane non-oxidatively with a high activity. The low activity of the perovskite is due to the fact that its lattice oxygen is not active for breaking the C–H bond in propane at 948 K. However, these oxygen species oxidize hydrogen. The H_2 oxidation fulfills a double role: i) increasing non-oxidative propane conversion to propene and ii) increasing the reduction degree of the BCFZ perovskite.

If the rates of H_2 and C_3H_8/C_3H_6 oxidation over the perovskite are slower than the diffusion rate of oxygen ions through the BCFZ membrane, gas-phase O_2 can be formed on the shell side of the membrane. Our transient analysis demonstrated that the Pt–Sn catalyst converts C_3H_8 to C_2H_4 and CO in the presence of gas-phase O_2. For selective converting of C_3H_8 to C_3H_6 in the membrane reactor, the kinetic compatibility between the reaction rates of hydrogen production and its combustion over the perovskite is essential. The amount of oxygen permeated through the membrane can be tuned by varying oxygen partial pressure on the feed side of the membrane.

Acknowledgements

OC and JC acknowledge the financial support of the projects SynMem and NASA-OTM by the German BMBF and the European Union, respectively. BASF SE is thanked for providing the catalyst.

References

[1] R.K. Grasselli, D.L. Stern, J.G. Tsikoyiannis, Appl. Catal. A-Gen. 189 (1999) 1–8.
[2] R.K. Grasselli, D.L. Stern, J.G. Tsikoyiannis, Appl. Catal. A-Gen. 189 (1999) 9–14.
[3] O. Czuprat, S. Werth, T. Schiestel, AIChE J 56 (2010) 2390–2396.
[4] O. Czuprat, S. Werth, S. Schirrmeister, T. Schiestel, J. Caro, ChemCatChem 1 (2009) 401–405.
[5] T. Schiestel, M. Kilgus, S. Peter, K.J. Caspary, H. Wang, J. Caro, J. Membr. Sci. 258 (2005) 1–4.
[6] H. Jiang, L. Xing, O. Czuprat, H. Wang, S. Schirrmeister, T. Schiestel, J. Caro, Chem. Commun. 44 (2009) 6738–6740.
[7] O. Czuprat, T. Schiestel, H. Voss, J. Caro, Ind. Eng. Chem. Res. in press, doi: 10.1021/ie100282g.
[8] E.V. Kondratenko, H. Wang, V. Kondratenko, J. Caro, J. Mol. Catal. A-Chem. 297 (2009) 142–149.
[9] J.T. Gleaves, G.S. Yablonskii, P. Phanawadee, Y. Schuurman, Appl. Catal. A-Gen. 160 (1997) 55–88.
[10] J. Pérez-Ramírez, E.V. Kondratenko, Catal. Today 121 (2007) 160–169.

3 Oxidative Coupling of Methane

3.1 Summary

Due to the strong economic interest in developing processes transforming methane to higher-valued products, the oxidative coupling of methane (OCM) to C_2 products was evaluated in this paper, since it benefits from avoidance of sequential steps as required in synthesis routes based on reforming and FISCHER-TROPSCH.

A hollow fiber membrane reactor in combination with an established silica supported 2 wt% Mn/5 wt% Na_2WO_4 catalyst as a packed bed around the fiber was used for the OCM. The use of the membrane reduces the risks of explosive mixtures, redundantizes an oxygen plant and allows a precise control of the oxygen insertion to the hydrocarbon feed, which is necessary to initiate the thermodynamically feasible reaction pathway. Various reaction conditions like the effect of the oxygen partial pressure on the feed side of the membrane as well as the impact of the total methane flow rate and partial pressure on the sweep side were investigated.

Under optimum conditions, oxygen separation from air and C_2 formation could be established at 800 °C with a maximum in C_2 selectivity of 75% at a methane conversion of 6%. It could be demonstrated that the catalyst also promotes the oxidative dehydrogenation of ethane to ethene since the ethene to ethane ratio increases with a higher methane conversion due to a higher amount of oxygen supplied across the membrane. It was also figured out that using steam instead of helium as a diluent in order to increase the methane conversion can suppress CO_2 formation and maintain high olefin selectivities.

The aggregation of the catalyst particles as well as a loss of manganese on its surface after 100 hours on stream was confirmed by X-ray diffraction (XRD) analysis as well as scanning electron microscopy (SEM) in combination with energy-dispersive X-ray spectroscopy (EDXS). The aggregation of the particles and the related decrease of the specific catalyst surface were further proven by nitrogen adsorption measurement.

3.2 Oxidative Coupling of Methane in a BCFZ Perovskite Hollow Fiber Membrane Reactor

OLIVER CZUPRAT, THOMAS SCHIESTEL, HARTWIG VOSS, JÜRGEN CARO

Industrial & Engineering Chemistry Research **2010**, *49*, 10230–10236.

This is the pre-peer reviewed version of the published article.

Oxidative coupling of methane in a BCFZ perovskite hollow fiber membrane reactor

Oliver Czuprat,[*,†] *Thomas Schiestel,*[‡] *Hartwig Voss,*[§] *Jürgen Caro*[†]

Institute for Physical Chemistry and Electrochemistry (PCI), Leibniz Universität Hannover, Callinstr. 3,
30167 Hannover, Germany

Fraunhofer Institute for Interfacial Engineering and Biotechnology (IGB), 70569 Stuttgart, Germany

BASF SE, 67056 Ludwigshafen, Germany

oliver.czuprat@pci.uni-hannover.de

RECEIVED DATE (to be automatically inserted after your manuscript is accepted if required according to the journal that you are submitting your paper to)

---

[*] To whom correspondence should be addressed. E-mail: oliver.czuprat@pci.uni-hannover.de.

[†] PCI, Leibniz Universität Hannover.

[‡] IGB, Stuttgart.

[§] BASF SE, Ludwigshafen.

A membrane reactor incorporating a hollow fiber in combination with an established catalyst was used for the oxidative coupling of methane (OCM). The perovskite membrane of the composition $BaCo_xFe_yZr_zO_{3-\delta}$ (BCFZ, $x+y+z = 1$) allows a controlled oxygen feeding into the reactor over its axial length. By using this novel hollow fiber membrane reactor with a 2 wt% Mn/5 wt% Na_2WO_4 on SiO_2 catalyst as a packed bed around the fiber, oxygen separation from air and C_2 formation could be established at 800 °C with long-term stability. The highest C_2 selectivity of approximately 75% was observed at methane conversion of 6% with a C_2H_4 to C_2H_6 ratio of 2:1. The highest C_2H_4 to C_2H_6 ratio of 4:1 and maximum C_2 yield of 17% was obtained at 50% C_2 selectivity. It is known from literature that such results can be obtained without catalyst in a similar membrane reactor only at 150 °C higher temperature.

1. Introduction

Since methane is the main constituent of natural gas which will exceed the reserves of crude oil in the future, a strong economic interest exists in developing processes that transform methane to higher valued products. At present, methane is converted industrially to syngas via steam reforming[1] and to hydrocyanic acid by the Andrussow reaction.[2] The oxidative coupling of methane (OCM) to ethane and ethene is an attractive alternative for the existing processes based on crude oil and benefits from avoidance of sequential steps required to indirect routes involving CH_4 reforming and Fischer-Tropsch synthesis.[3] Most of the research on the highly exothermic catalytic OCM reaction started in the early 1980s with the pioneering works of Keller and Bhasin.[4]

The mayor difficulty to be overcome in CH_4 conversion is the scission of the first C-H bond (ca. 435 kJ mol^{-1}). For this reason, the direct pyrolitic route to H_2 and C_2H_4 will be disfavoured thermodynamically and requires high temperatures, consequently resulting in poor selectivity.

The OCM reaction usually occurs via a heterogeneous-homogeneous mechanism, i.e. the reaction involves the catalytic formation of methyl groups, which desorb as free radicals ($CH_3\cdot$)[5] that ultimately react via predominantly homogeneous pathways.[6] It is generally agreed that dissociated oxygen as lattice oxygen O_S^{2-} is supposed to be the active oxygen species, which presumably activates methane to generate $CH_3\cdot$ radicals. But there still exists noticeable disagreement or controversy concerning the active components or sites of the Na_2WO_4-Mn/SiO_2 catalyst. Li and coworkers related the excellent performance to WO_4 tetrahedral structures containing W=O and W-O-Si bonds[7,8]. This model was further developed with the emphasis on the combination of tetrahedral WO_4 and octahedral MnO_6 sites, respectively, responsible for the activation of methane and the oxygen lattice transport.[9] In contrast, Lunsford et al. proposed that Na-O-Mn species attributed to the activation of methane and tungsten ions apparently improved the catalyst stability.[10] Recently, it was claimed that both Na-O-Mn and Na-O-W species act as active sites for the OCM reaction.[11]

The ethane formed undergoes further transformations to ethene and carbon oxides. Both hydrocarbons can be consecutively oxidized to CO_x. Combustion of C_2 hydrocarbons becomes the main route to CO_x with increasing methane conversion, since ethane and ethene have a higher reactivity compared to methane. Therefore, the contribution of direct methane oxidation to CO_x decreases. All these pathways account for the inherently limited yield of OCM process of 28 % on a basis of fundamental kinetics.[12]

Palermo et al.[13] pointed out that Na plays a dual role: (i) crystallization of amorphous silica to the crystalline form and (ii) stabilization and dispersion of surface WO_x species with WO_4 as a possible candidate.[14]

According to DFT calculations by Chen et al.[15], the tetrahedral [WO_4] site with a single bridge oxygen is the most probable active center responsible for methane activation.

The surface methyl radical generation reaction is temperature-dependent and dramatically slower than the temperature-independent radical coupling reaction in the gas phase.[16] Based on these observations it can be inferred that, in the absence of combustion, the C_2 production rate is limited by the generation rate of free methyl radicals and can be increased by increasing the temperature, since at low temperatures, active sites are less active. At low temperatures, most of the oxygen ions do not generate methyl radicals but recombine to gaseous oxygen and cause combustion, resulting in low selectivities. C_2 products are favored by high $CH_3\cdot$ radical concentrations because their recombination is a bimolecular event.

On the other hand, high concentrations of oxygen are disadvantageous to high C_2 selectivities. Low oxygen concentrations are, however, unfavourable for high degrees of methane conversion and high C_2 yields. An alternative to staged oxygen delivery is the use of membrane reactors. Dosing the oxygen through a perovskite membrane shows several advantages: (i) due to the distributed feeding of oxygen over the whole reactor (or at least over the length of the oxygen permeable zone of the membrane) the oxygen partial pressure is low and homogeneous which thereby supports the partial oxidation and not the total oxidation, thus increasing the selectivity, (ii) in the sense of process intensification, two operation units become combined: the oxygen separator and the chemical reactor for the OCM reaction thus increasing the space-time-yield by 50%. It is estimated that about 30% of the costs in the C_2 synthesis stem from cryogenic air distillation according to Linde. Air separation using oxygen transport membranes operating at process temperature of the chemical reaction makes the use of methane as feedstock economically and ecologically attractive by energy saving resulting in reduction of CO_2 emission.

This method of contacting the reactants can also increase selectivity and yield to the desired products in reacting systems where several reactions take place since the kinetic order of oxygen for the desired reactions is lower than for the other reactions (usually deep oxidation reactions).

All models and experimental results of the OCM reaction have in common incomplete conversion of methane due to a high stoichiometric excess of methane with respect to oxygen; thereby the formation of side products, CO and CO_2, is partly suppressed.

Non-porous oxygen-ion-conducting perovskite oxides have potential as OCM catalytic membrane reactors using air as an economical oxygen source.[17] At the membrane surface of the reactive side of the membrane reactor, oxygen ions (O_S^{2-}) are competitively consumed by two reactions – methane activation

$$2\ CH_4 + O_S^{2-} \rightarrow 2\ CH_3\cdot + H_2O \qquad \text{(I)}$$

and recombination of oxygen ions according to

$$2\ O_S^{2-} \rightarrow O_2 + 4e^-. \qquad \text{(II)}$$[18]

Kao et al. showed that the use of a mixed-conducting ceramic membrane of the composition $La_{0.8}Sr_{0.2}Co_{0.6}Fe_{0.4}O_{3-\delta}$ for oxygen insertion to the reaction zone could increase the C_2 selectivity compared to the fixed bed reactor (FBR).[19] Wang et al. packed an active OCM catalyst in a $Ba_{0.5}Sr_{0.5}Co_{0.8}Fe_{0.2}O_{3-\delta}$ membrane tube and obtained a C_2 yield which is similar to that in a FBR, though a higher ratio of C_2H_4/C_2H_6 was observed in the membrane tube reactor.[20] The selectivities in these materials appear to be limited by high oxygen ion recombination rates that compete for oxygen with the desired coupling reaction.

Systems using dense perovskite hollow fiber membranes have been presented by our group, e.g. for the direct decomposition of nitrous oxide to nitrogen by in situ oxygen removal,[21] the simultaneous production of hydrogen and synthesis gas by combining water splitting with partial oxidation of methane[22] and recently the multi-step oxidative dehydrogenation of ethane (ODE)[23] and propane (ODP).[24]

In this publication we present the use of a dense mixed oxygen ion and electron conducting (MIEC) perovskite hollow fiber membrane of the composition $BaCo_xFe_yZr_zO_{3-\delta}$ (BCFZ, $x+y+z = 1$) for the oxidative coupling of methane employing 2 wt% Mn/5wt% Na_2WO_4 on SiO_2 as an OCM catalyst. To the best of our knowledge, it is the first time that a perovskite hollow fiber membrane reactor of the composition above is used for the oxidative coupling of methane.

2. Experimental Section

2.1. Preparation of the hollow fibers

The hollow fiber membranes of the composition $BaCo_xFe_yZr_zO_{3-\delta}$ (BCFZ, $x+y+z=1$, Figure 1) were manufactured by phase inversion spinning followed by sintering as described elsewhere.[25] In order to obtain the isothermal condition, two ends of the fibers with an outer diameter of ~1.1 mm and a wall thickness of ~0.14 mm were coated with gold paste (C 5754 B, Heraeus) and sintered at 950 °C for 5 hours to obtain a 3 cm long permeation zone in the middle of the furnace. This procedure was repeated three times to ensure a leak-proof gold layer not permeable to oxygen.

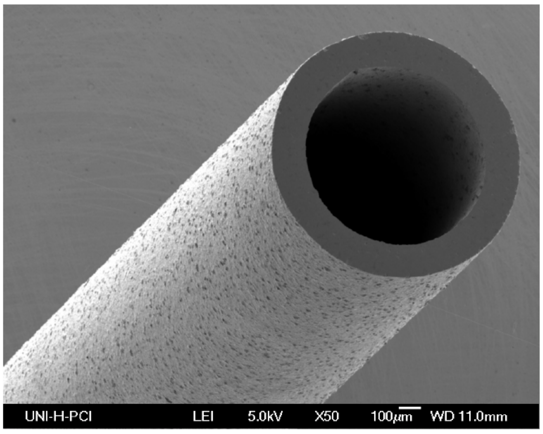

Figure 1: $BaCo_xFe_yZr_zO_{3-\delta}$ (BCFZ, $x+y+z = 1$) hollow fiber membrane obtained by spinning at the Fraunhofer Institute for Interfacial Engineering and Biotechnology.

2.2. Preparation of the catalyst

Appropiate amounts of $Mn(NO_3)_2 \cdot 4\ H_2O$ (Sigma-Aldrich) and $Na_2WO_4 \cdot 2\ H_2O$ (Sigma Aldrich) were dissolved in deionized water and contacted with SiO_2 (Davisil, Grade 636, Sigma-Aldrich) under stirring at 130 °C for 5 h. Finally, the impregnated silica gel was treated for 8 h at 800 °C. In order to characterize the obtained catalyst before and after reaction, XRD were conducted with monochromated Cu $K_{\alpha 1}$ radiation in the range of 10-70° 2θ at room temperature (Philips X'Pert-PW1710). Figure 2 shows the XRD patterns for the 2 wt% Mn/5 wt% Na_2WO_4 on SiO_2 catalyst. The fresh as well as the spent catalyst (on stream for 100 h) possess the reflections for the three SiO_2 modifications quartz, cristobalite and tridymite, whereas the first appears to increase during reaction. The amount of active Na_2WO_4 decreases slightly while being on stream under reaction conditions as can be inferred from the characteristic peaks at $2\theta = 17.1$ and 32.5°.

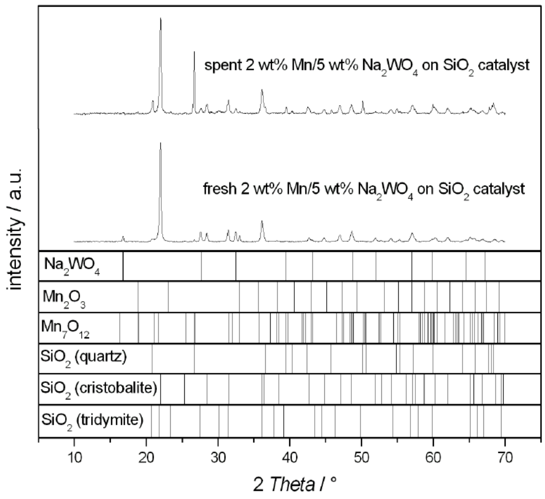

Figure 2. Powder XRD pattern of fresh and spent (on stream for 100 h) 2 wt% Mn/5 wt% Na_2WO_4 on SiO_2 catalyst.

SEM was carried out on a JEOL JSM-6700F field-emission instrument using a secondary electron detector (SE) at an accelerating voltage of 2 kV. EDX spectra were obtained at an accelerating voltage of 15 kV using a light-element detector (INCA 300, Oxford Instruments).

The elemental distribution by EDXS shown in Figure 3 qualitatively confirms also the loss of manganese species on the catalyst's surface after being on stream for 100 h as well as an agglomeration of the catalyst particles.

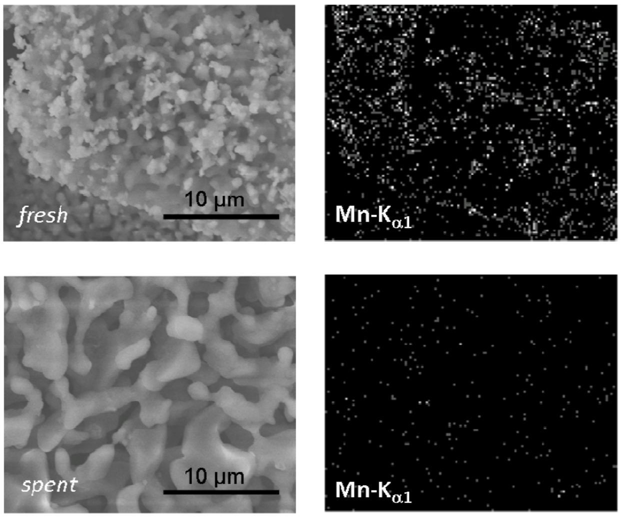

Figure 3. SEM micrographs and corresponding elemental distribution for manganese by EDXS of the fresh and spent catalyst (on stream for 100 h), respectively.

2.3. Studies in the hollow fiber membrane reactor

For the OCM, pure methane (99.5%) - or diluted with steam and helium (99.996%) where specified - was fed to the shell side of the membrane, while synthetic (C_xH_y-free) air was fed to the core side. All gas flows were controlled by mass flow controllers (Bronkhorst High-Tech). The gases at the exit of the reactor were analyzed by a gas chromatograph (Agilent Technologies, HP6890N) equipped with a Carboxen 1000 column (Supelco). Concentrations of C_2H_6, C_2H_4, CH_4, CO, CO_2, H_2, N_2 and O_2 were determined by calibration against standard gases. The absolute flow of the effluents was determined by using neon (99.995%) as an internal standard. All data points collected in this work were taken at steady-state conditions which were obtained after 1-3 hours. For experiments using the OCM catalyst (2 wt% Mn/5 wt% Na_2WO_4 on SiO_2), the BCFZ hollow fiber was inserted into a porous alumina tube (outer diameter ~2.2 mm, wall thickness of ~0.4 mm) to avoid direct contact with the catalyst. The catalyst was milled in a mortar; a sieve fraction between 10 and 500 µm was sieved out and a portion of 0.25 g was dispersed between the inner porous alumina tube and the outer dense alumina tube (Figure 4).

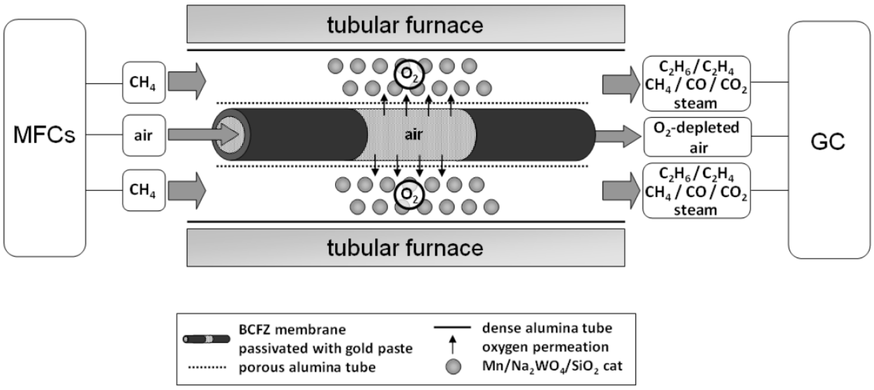
tubular furnace
MFCs
CH_4
air
CH_4
O_2
air
O_2
C_2H_6/C_2H_4 CH_4 / CO / CO_2 steam
O_2-depleted air
C_2H_6/C_2H_4 CH_4 / CO / CO_2 steam
GC
tubular furnace
BCFZ membrane passivated with gold paste
porous alumina tube
dense alumina tube
oxygen permeation
$Mn/Na_2WO_4/SiO_2$ cat

Figure 4. Schematic drawing of the reactor set-up and an incorporated BCFZ hollow fiber for OCM. At both ends the 30 long fiber was coated with gold to obtain a 3 cm long isothermal oxygen permeation zone. The active surface area for the oxygen permeating BCFZ hollow fiber is 0.78 cm². The OCM catalyst was dispersed between the outer dense alumina tube and the fiber, which was inserted into a porous alumina tube.

3. Results and discussion

3.1. Intrinsic catalytic activity of the BCFZ perovskite for the OCM as packed bed

First, we studied the OCM in a packed bed reactor. Figure 5 shows methane conversion as well as product selectivities as a function of the co-fed oxygen flow rate for constant methane feed rate evaluating the intrinsic catalytic activity of BCFZ powder for the OCM. A higher flow rate of co-fed oxygen increases methane conversion and the CO_2 to CO ratio. The C_2 selectivity decreases with increasing oxygen content in the co-feed and shows a maximum at a methane to oxygen ratio of 25:1. This finding is in complete accordance with previous TAP (temporal analysis of products) studies on the same BCFZ material, showing that the selectivity ratio $S(C_2):S(CO_2)$ increases with increasing amounts of lattice oxygen removed from the perovskite, i.e. OCM is favoured for an increased reduction degree of the perovskite which is obtained at low oxygen concentrations in the co-feed.[26] However, the low methane conversion and the poor C_2 selectivities indicate that no substantial catalytic performance towards the OCM can be assigned to the pure BCFZ perovskite. We decided therefore to apply Mn-Na_2WO_4/SiO_2 as a well-established catalyst in the following membrane reactor experiments. This is in agreement with the literature, where in similar membrane reactors studies with perovskite hollow fiber membranes at 800 °C only 1% C_2 yield was obtained when working without catalyst.[27]

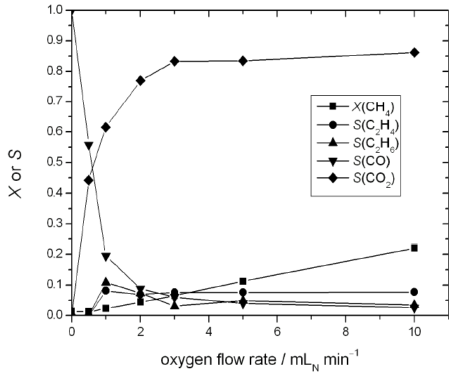

Figure 5. Evaluation of the intrinsic catalytic activity of BCFZ powder in a fixed bed reactor showing methane conversion and product selectivities as a function of the co-fed oxygen flow rate (25 mL$_N$ min^{-1} methane, 0-10 mL$_N$ min^{-1} oxygen) at 800 °C.

3.2. Effect of air dilution on core side of the hollow fiber membrane reactor

Since it is known that the oxygen partial pressure controls methane conversion and C_2 selectivity, the oxygen transport through the BCFZ hollow fiber membrane was varied by diluting the air with helium. Diluted air shows a lower oxygen partial pressure and, consequently, the reduced driving force causes a reduced oxygen transport into the reactor.

Introducing the BCFZ hollow fiber membrane and the 2 wt% Mn/5 wt% Na_2WO_4 on SiO_2 catalyst as a fixed packed bed around the fiber as shown in Figure 4, the methane conversion as well as C_2 selectivities are increased dramatically (see Figure 6). Lowering the oxygen concentration on the core side increases the C_2 selectivity, where ethane selectivity increases more compared to the ethene selectivity. A higher oxygen concentration on the core side of the membrane leading to a higher oxygen transport through the membrane favors hydrocarbon oxidation. The ethene to ethane ratio varies between 2.3 and 3.5. At a higher concentration of oxygen it is more likely that the ethane formed during the OCM reaction undergoes further transformations, e.g. oxidative dehydrogenation.

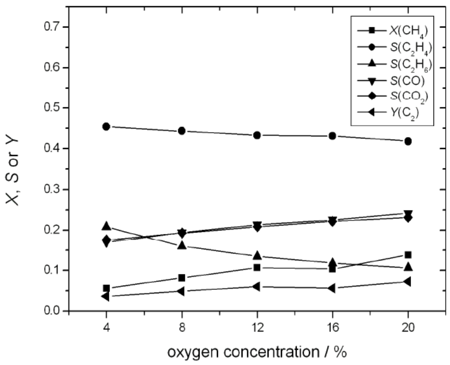

Figure 6. Effect of the oxygen concentration obtained by air dilution on the core side while feeding pure methane at 25 $\mathrm{mL_N\,min^{-1}}$ on the shell side of the membrane. Methane conversion, product selectivities and C_2 yield as a function of the oxygen concentration on the core side of the membrane at 1 bar and $T = 800$ °C (*shell*: 25 $\mathrm{mL_N\,min^{-1}}$ methane; *core*: $F_{\mathrm{total}} = 50$ $\mathrm{mL_N\,min^{-1}}$ air diluted with helium; 0.78 $\mathrm{cm^2}$ effective membrane surface; 0.25 g of catalyst; $WHSV = 4.32\ \mathrm{h^{-1}}$).

3.3. Effect of total methane flow rate

Parallel to the variation of the oxygen supply to the reaction through the membrane by diluting air, the oxygen to methane ratio was controlled by varying the methane flux rate. By applying lower total flow rates of methane on the shell side than shown in Figure 6, its conversion can be increased (see Figure 7) due to a longer residence time of methane inside the reactor. A longer residence time, on the other hand, leads to an increased hydrocarbon oxidation and therefore to a drop in C_2 selectivity. Especially, ethene and ethane are the precursers for CO_x due to their higher reactivity compared to methane.

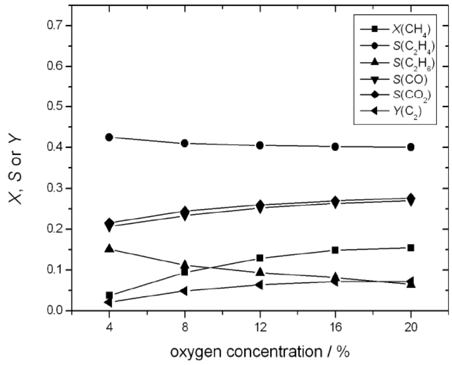

Figure 7. Higher C_2 selectivity due to air dilution on the core side of the membrane while feeding methane at 15 mL$_N$ min^{-1} on shell side. Methane conversion, product selectivities and C_2 yield as a function of the oxygen concentration on the core side of the membrane at 1 bar and T = 800 °C (*shell*: 15 mL$_N$ min^{-1} methane; *core*: F_{total} = 50 mL$_N$ min^{-1} air diluted with helium; 0.78 cm² effective membrane surface; 0.25 g of catalyst; $WHSV$ = 2.59 h^{-1}).

It can be seen from the results shown in Figures 6 and 7 that a shorter contact time is helpful for the increase of the C_2 selectivity by preventing hydrocarbon deep oxidation. On the other hand, a shorter contact time decreases the rate of reaction probability on the catalyst surface. Additionally, the gas can not get the optimum temperature for a high conversion due to the short residence time inside the heated reactor.

3.4. Dilution of methane

A dilutant is often used to control the excess heat of the reaction of OCM. In our experiments, helium and steam were selected as diluents. Diluting methane with an inert gas, e.g. helium, increases the methane conversion at a constant residence time inside the reactor (Figure 8) as expected, since the ratio of oxygen to methane is increased. A higher amount of oxygen can lead to an increased transformation of methane, but also to a higher degree of oxidation to CO_x since the rate constant for CO_x formation from C_2H_4 oxidation is up to six times greater than that from the direct oxidation of CH_4.[28] The ethene selectivity at 100% methane concentration drops to approximately 35% when feeding 20% methane in helium.

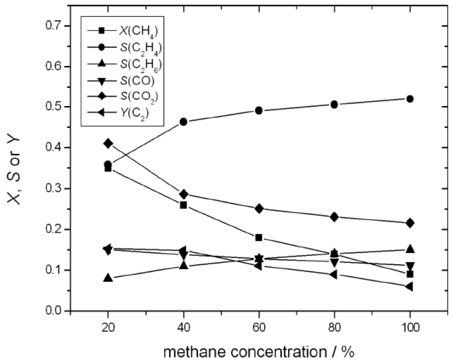

Figure 8. Dilution of methane leading to its higher conversion at a constant total flow rate of 25 $mL_N\,min^{-1}$ on the shell side of the membrane while feeding pure air on the core side. Methane conversion, product selectivities and C_2 yield as a function of the oxygen concentration on the core side at 1 bar and $T = 800$ °C (*shell*: $F_{total} = 25$ $mL_N\,min^{-1}$ methane diluted with helium; *core*: 50 $mL_N\,min^{-1}$ air; 0.78 cm^2 effective membrane surface; 0.25 g of catalyst; $WHSV = 0.86\text{-}4.32\ h^{-1}$).

At a total flow rate of 50 $mL_N\,min^{-1}$ on the shell side, the ethene selectivity can be maintained at a constant level above 50% even at low methane concentrations in the feed (results not shown). The shorter rentention time within the reactor suppresses the hydrocarbon oxidation up to a certain extent. Summarizing, the methane concentration of the feed should be as high as possible for a high C_2 selectivity.

Using steam instead of helium as a dilutant can suppress CO_2 formation and maintain high ethene selectivities especially at low methane concentrations (see Figure 9) in comparison to results shown in Figure 8. The results indicate that steam not only has a dilution effect, but also suppresses the deep oxidation. Most importantly, the steam can distribute the temperature more evenly along the catalyst bed during the reaction. Consequently, the gas-phase reaction is suppressed and more C_2 product is preserved in the outlet.

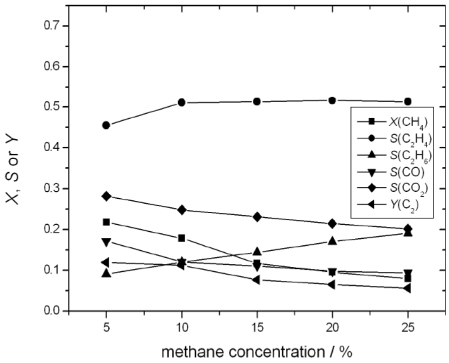

Figure 9. Steam as dilutant for methane allowing high ethene selectivities at higher degrees of dilution at a constant total flow rate of 25 mL$_N$ min^{-1} on the shell side of the membrane while feeding pure air on core side. Methane conversion, product selectivities and C_2 yield as a function of the oxygen concentration on the core side of the membrane at 1 bar and T = 800 °C (*shell*: F_{total} = 50 mL$_N$ min^{-1} methane diluted with steam; *core*: 50 mL$_N$ min^{-1} air; 0.78 cm^2 effective membrane surface; 0.25 g of catalyst; *WHSV* = 0.86-4.32 h^{-1}).

Takanabe and Iglesia reported that the utilization of steam as dilutant introduces OH· radicals that result in improved C_2 selectivities and yields. One of the reasons discussed is that the presence of OH· radicals avoids strong adsorption of C_2H_4 on surfaces that favour its oxidation.[29]

3.5. Effect of diluting air at lowered methane concentration

Figures 10 and 11 illustrate the effect of diluting the air on core side of the hollow fiber membrane while feeding diluted methane at two different flow rates. This set-up could realize the kinetic compatibility of oxygen supply for the methyl radical formation and gave rise to the maximum C_2 yield of 17% and C_2 selectivity of 74% observed in this work at 800 °C. It should be noted that similar yields and selectivities have been obtained for the OCM in a $La_{0.6}Sr_{0.4}Co_{0.2}Fe_{0.8}O_{3-\delta}$ (LSCF) hollow fiber membrane reactor.[27] However, when not using a catalyst like in our experiments, a temperature of 950 °C instead of 800 °C was necessary.

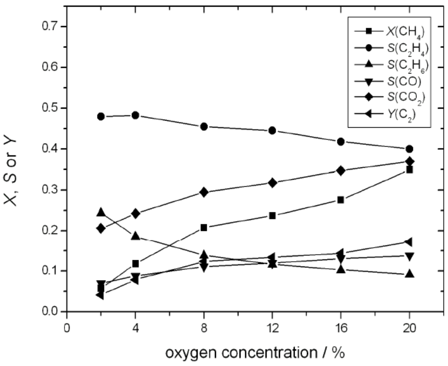

Figure 10. Improved C_2 selectivities and C_2 yields by feeding diluted oxygen on core side while feeding 10% methane on shell side of the hollow fiber membrane at a total flow rate of 25 $mL_N\ min^{-1}$. Methane conversion, product selectivities and C_2 yield as a function of the oxygen concentration on the core side of the membrane at 1 bar and $T = 800$ °C (*shell*: 5 $mL_N\ min^{-1}$ methane, 20 $mL_N\ min^{-1}$ helium; *core*: $F_{total} = 50\ mL_N\ min^{-1}$ air diluted with helium; 0.78 cm² effective membrane surface; 0.25 g of catalyst; $WHSV = 0.86\ h^{-1}$).

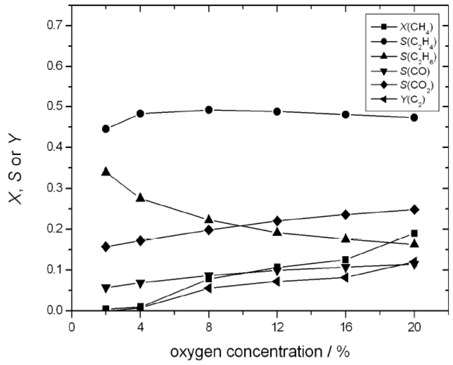

Figure 11. Effect of reducing the oxygen partial pressure by air dilution with helium on core side while feeding 10 % methane at a total flow rate of 50 $\mathrm{mL_N\ min^{-1}}$ on shell side of the hollow fiber membrane. Methane conversion, product selectivities and C_2 yield as a function of the oxygen concentration on the core side of the membrane at 1 bar and T = 800 °C (*shell*: 10 $\mathrm{mL_N\ min^{-1}}$ methane, 40 $\mathrm{mL_N\ min^{-1}}$ helium; *core*: F_{total} = 50 $\mathrm{mL_N\ min^{-1}}$ air diluted with helium; 0.78 cm² effective membrane surface; 0.25 g of catalyst; *WHSV* = 1.72 $\mathrm{h^{-1}}$).

Generally speaking, a higher methane conversion due to a higher amount of oxygen supplied across the membrane to the hydrocarbon side, increases the ethylene to ethane ratio. This can be explained by the fact that catalysts used for the OCM reaction are – for a certain extent - also good for the oxidative dehydrogenation of ethane to ethylene.[30] At a higher concentration of oxygen it is more likely that the ethane formed undergoes further transformations, e.g. oxidative dehydrogenation on the catalyst's surface.

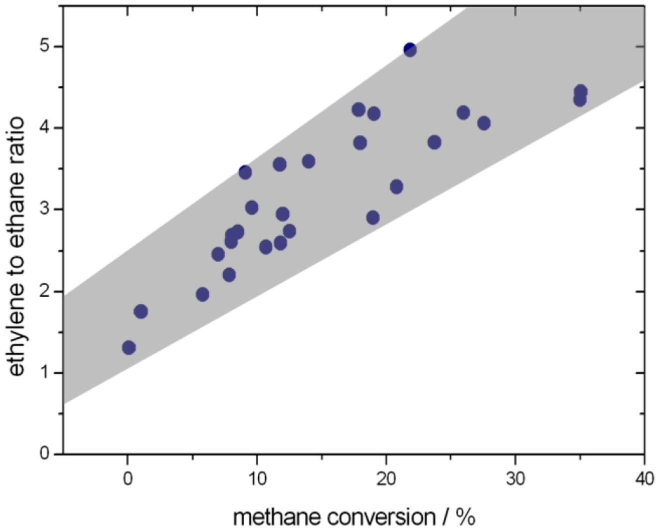

Figure 12. Controlling the ethylene to ethane ratio by the degree of methane conversion.

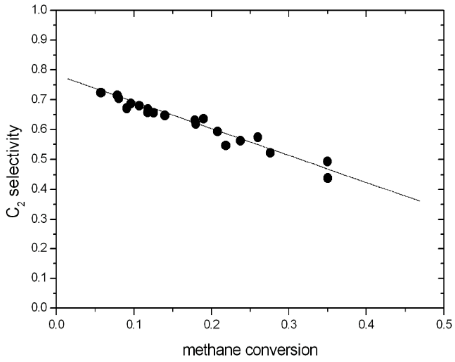

Figure 13. Performance of the hollow fiber membrane reactor for the OCM using a 2 wt% Mn/5 wt% Na_2WO_4 on SiO_2 catalyst. C_2 selectivity as a function of methane conversion (> 5%).

All processes for the oxidative coupling of methane suffer from the high costs for low-temperature separations of C_2 products from the reactor effluent containing a high concentration of unconverted methane besides the various side products. A process concept for converting natural gas into ethene and hydrogen or hydrocarbon liquids has been described recently by Hall[31], being licensed by SynFuels International. This technology, which has been explored in an industrial pilot plant, is claimed to be economically viable depending on the methane price entering the overall cost scheme; thus, it can be considered attractive for remote gas or in situations where the gas is just flared off. For a 1.4 MSCMD (million standard cubic meters per day) plant US$25 per barrel of liquid product has been estimated assuming remote gas at US$0.018 m^{-3}, 10-year straight line amortization, 25% fixed costs and US$1-3 per barrel operating costs. As claimed in a patent[32], the economy of methane-to-ethene processing can be improved when both the catalytic OCM reaction and the separation of ethene from the reactor-effluent components (methane, ethane, carbon oxides) are performed at elevated pressure. Elevated pressures reduce not only the size of the various process units due to an increase of the reaction rates but they improve also the efficiency of the separation process. For separating the ethene an aqueous silver-nitrate solution was used as a complexing absorbent.

When arranged in bundles, with hollow fibre geometry a high membrane area per reactor/permeator volume can be achieved. Economic goals, e.g. membrane area per m^3 permeator of the order of 5000 m^2 at a price of well below 1000 €/m^2 can be met by the perovskite hollow fibres. Furthermore, thin walled hollow fibres show a better mechanical stability than disk-shaped membranes of the same wall thickness. The successful development of perovskite hollow fibre is considered a remarkable step towards their industrial application, e.g. for the oxidative coupling of methane.

Based on our results, the oxygen necessary for a methanol-plant with a capacity of 2000 tons/day based on partial oxidation of methane could be delivered by 4600 km fibres. Such fibres would need a relatively small volume of 3–4 m^3 depending on the packing density. When comparing this volume to a classical air separation unit, the enhancement in space–time–yield (in terms of oxygen per plant size) is obvious.

4. Conclusions

A membrane reactor with oxygen supply via a $BaCo_xFe_yZr_zO_{3-\delta}$(BCFZ, x+y+z = 1) perovskite hollow fiber for the oxidative coupling of methane is presented. Having a dense membrane that separates hydrocarbon and oxygen feed, reduces the risks of explosive mixtures as well as saves costs since no oxygen plant for the separation of oxygen from air is required. Furthermore, it allows a precise control of the oxygen insertion thus increasing C_2 selectivity. Using a 2 wt% Mn/5 wt% Na_2WO_4 on SiO_2 catalyst, C_2 formation could be studies at 800 °C with long-term stability and a maximum ethene to ethane ratio of 4:1. The highest C_2 selectivity of approximately 75% was observed at a methane conversion of 6%, whereas the highest C_2H_4 to C_2H_6 ratio of 4:1 and maximum C_2 yield of 17% was obtained at 50% C_2 selectivity (see Figure 10). It is known from literature that 950 °C are necessary to get the same results for the OCM in a hollow fiber membrane reactor when working without catalyst. For industrial implementation of such a system, one could use a multitude of hollow fiber bundles in a catalytic fixed bed. Furthermore, it can be inferred from the presented results that the gaseous oxygen produced accelerates the non-catalytic gas phase methane combustion leading to a decrease of the C_2 selectivity. The C_2 selectivity and yield might be improved by packing an active OCM catalyst on the membrane surface.

According to the present results, also more steam should be added to the reactants in further experiments to prevent hydrocarbon from deep oxidation in the gas-phase due to the better removal of excess heat from the catalyst bed.

Acknowledgment

The authors acknowledge the financial support of the project NASA-OTM by the European Union as well as BASF SE for the permit of publication.

Literature Cited

(1) van den Oosterkamp, P.F. *Encyclopedia of Catalysis*; Wiley-VCH: Weinheim, 2003.

(2) Gail, E.; Gos, S.; Kulzer, R.; Lorösch, J.; Rubo, A.; Sauer, M. *Ullmann's Encyclopedia of Industrial Chemistry, Vol. 10, Cyano Compounds, Inorganic*; Wiley-VCH: Weinheim, 2003.

(3) Lercher, J.A.; Bitter, J.H.; Steghuis, A.G.; van Ommen, J.G.; Seshan, K. *Environmental Catalysis*; Imperial College Press: London, 1999.

(4) Keller, G.F.; Bhasin, M.M. Synthesis of ethylene via oxidative coupling of methane: I. Determination of active catalysts *J. Catal.* **1982**, *73*, 9.

(5) Ito, T.; Wang, J.X.; Lin, C.H.; Lunsford, J.H. Oxidative dimerization of methane over a lithium-promoted magnesium oxide catalyst *J. Am. Chem. Soc.* **1985**, *107*, 5062.

(6) Takanabe, K.; Iglesia, E. Mechanistic Aspects and Reaction Pathways for Oxidative Coupling of Methane on Mn/Na_2WO_4/SiO_2 Catalysts *J. Phys. Chem. C* **2009**, *113*, 10131.

(7) Jiang, Z.; Yu, C.; Fang, X.; Li, S.; Wang, H. Oxide support Interaction and Surface Reconstruction in the Na_2WO_4/SiO_2 System *J. Phys. Chem.* **1993**, *97*, 12870.

(8) Wu, J.; Li, S. The role of Distorted WO_4 in the Oxidative Coupling of Methane on Tungsten Oxide supported Catalysts *J. Phys. Chem.* **1995**, *99*, 4566.

(9) Kou, Y.; Zhang, B.; Niu, J.; Li, S.; Wang, H.; Tanaka, T.; Yoshida, S. Amorphous features of Working Catalysts: XAFS and XPS Characterization of Mn/Na_2WO_4/SiO_2 as Used for the Oxidative Coupling of Methane, *J. Catal.* **1998**, *173*, 399.

(10) Wang, D.; Rosynek, M.P.; Lunsford, J.H. Oxidative Coupling of Methane over Oxide-Supported Sodium-Manganese catalysts *J. Catal.* **1995**, *155*, 390.

(11) Ji, S.; Xiao, T.; Li, S.; Xu, C.; Hou, R.; Coleman, K.S.; Green, M.L.H. The relationship between the Structure and the Performance of Na-W-Mn/SiO_2 Catalysts for the Oxidative Coupling of Methane *Appl. Catal. A* **2002**, *225*, 271.

(12) Su, Y.S.; Ying, J.Y.; Green, W.H. Upper bound on the yield for oxidative coupling of methane *J. Catal.* **2003**, *218*, 321.

(13) Palermo, A; Vazquez, J.P.H.; Lee, A.F.; Tikhov, M.S.; Lambert, R.M. Critical influence of the amorphous silica-to-cristobalite phase transition on the performance of Mn/Na_2WO_4/SiO_2 catalysts for the oxidative coupling of methane *J. Catal.* **1998**, *177*, 259.

(14) Kondratenko, E.V.; Baerns, M. *Handbook of Heterogeneous Catalysis*; Wiley-VCH : Weinheim, 2008.

(15) Chen, H.S.; Niu, J.Z.; Zhang, B.; Li, S.B. DFT Study on the Active Sites in Mn-Na_2WO_4/SiO_2 Catalyst *Acta. Phys. Chim. Sin.* **2001**, *17*, 111.

(16) Machin, I.; Pereira, P.; de Gouveia, V.; Rosa, F. *ACS Preprints-Symposia* **1992**, *37*, 173.

(17) Xu, S.J.; Thomson, W.J. Perovskite-type oxide membranes for the oxidative coupling of methane *AIChE J.* **1997**, *43*, 2731.

(18) Bouwmeester, H.J.M.; Kruidhof, H.; Burggraaf, A.J. Importance of the surface exchange kinetics as rate limiting step in oxygen permeation through mixed-conducting oxides *Solid State Ionics* **1994**; *72*; 185.

(19) Zeng, Y.; Lin, Y.S. Oxygen Permeation and Oxidative Coupling of Methane in Yttria Doped Bismuth Oxide Membrane Reactor *J. Catal.* **2000**, *193*, 58.

(20) Wang, H.; Cong, Y.; Yang, W. *Catal. Today* **2005**, *104*, 160.

(21) Jiang, H.; Wang, H.; Liang, F.; Werth, S.; Schiestel, T.; Caro, J. Direct Decomposition of Nitrous Oxide to Nitrogen by In Situ Oxygen Removal with a Perovskite *Membrane. Angew. Chem. Int. Ed.* **2009**, *48*, 2983.

(22) Jiang, H.; Wang, H.; Werth, S.; Schiestel, T.; Caro, J. Simultaneous Production of Hydrogen and Synthesis Gas by Combining Water Splitting with Partial Oxidation of Methane in a Hollow-Fiber Membrane Reactor. *Angew. Chem. Int. Ed.* **2008**, *47*, 9341.

(23) Czuprat, O.; Werth, S.; Schirrmeister, S.; Schiestel, T.; Caro, J. Olefin Production by a Multistep Oxidative Dehydrogenation in a Perovskite Hollow-Fiber Membrane Reactor. *ChemCatChem* **2009**, *1*, 401.

(24) Czuprat, O.; Werth, S.; Caro, J.; Schiestel, T. Oxidative dehydrogenation of propane in a perovskite membrane reactor with multi-step oxygen insertion *AIChE J.*, DOI: 10.1002/aic.12158.

(25) Schiestel, T.; Kilgus, M.; Peter, S.; Caspary, K.J.; Wang, H.; Caro, J. Hollow fibre perovskite membranes for oxygen separation. *J. Membr. Sci.* **2005**, *258*, 1.

(26) Kondratenko, E.V.; Wang, H.; Kondratenko, V.; Caro, J. Selective oxidation of CH_4 and C_2H_6 over a mixed ion and electron conducting perovskite – A TAP and membrane reactor study. *J. Mol. Catal. A-Chem.* **2009**, *297*, 142.

(27) Tan, X.; Li, K. Oxidative Coupling Of Methane in a Perovskite Hollow-Fiber Membrane Reactor. *Ind. Eng. Chem. Res.* **2006**, *45*, 142.

(28) Pak, S.; Qiu, P.; Lunsford, J.H. Elementary Reactions in the Oxidative Coupling of Methane over $Mn/Na_2WO_4/SiO_2$ and $Mn/Na_2WO_4/MgO$ Catalysts. *J. Catal.* **1998**, *179*, 222.

(29) Takanabe, K.; Iglesia, E. Mechanistic Aspects and Reaction Pathways for Oxidative Coupling of Methane on $Mn/Na_2WO_4/SiO_2$ Catalysts. *J. Phys. Chem. C* **2009**, *113*, 10131.

(30) Banares, M.A. Supported metal oxide and other catalysts for ethane conversion: a review. *Catal. Today* **1999**, *51*, 319.

(31) Hall, K.R. A new gas to liquids (GTL) or gas to ethylene (GTE) technology. *Catal. Today* **2005**, *106*, 243.

(32) Culp, G.L.; Stricker, V.J.; Nelson, R.; Bhasin, M.M.; Nielsen, K.A., US Patent 6 518 476 B1, assigned to Union Carbide Chemicals & Plastics Technology Corporation, 2003.

4 Effect of Carbon Dioxide on the BCFZ Perovskite

4.1 Summary

In all hydrocarbon activation reactions involving oxygen species, CO_2 is an occuring by-product. This chapter presents investigations on the poisoning effect of CO_2 on BCFZ perovskite-type hollow fiber membranes under different experimental conditions. The influence of the CO_2 partial pressure, temperature and time on stream were evaluated.

Application of CO_2 containing sweep gases have yielded a gradual stop of the oxygen permeation as demonstrated by quantitative on-line gas chromatography. Subsequent sweeping with helium recovered the oxygen permeation as well as microstructure of the membrane proven by XRD measurements. The higher the CO_2 partial pressure and lower the temperature, the faster the decrease in oxygen permeation flux. Moreover, it was shown by SEM and EDXS that under exposure of 50% CO_2 in He for 5 hours at 800 °C, the perovskite structure is impaired up to a depth of ca. 15 µm and approximately 30 µm after 10 hours, respectively.

Thermodynamic calculations were carried out to plot an ELLINGHAM diagram of the carbonates with the cations of BCFZ. It revealed that barium carbonate is the most stable among all possible carbonates and is most likely to be formed. Investigations on the microstructure by SEM and EDXS as well as XRD proved that treatment with CO_2 results in the formation of barium carbonate. The dense carbonate layer functions as a protective layer for further carbonate formation, because the reaction rate is limited by transport phenomena through the product layer. Barium migrates through the carbonate layer to the surface of the membrane in order to form new carbonate.

Time-dependent experiments show that the decrease as well as the regeneration of the oxygen flux take place in a time-span of about 15 min, which can be related to the diffusion-controlled decomposition and regeneration of perovskite structure.

In-situ XRD analysis further demonstrated formation of high temperature rhombohedral $BaCO_3$ polymorph after exposure to CO_2 at 900 °C. This structure is not quenchable and stable at temperatures between 800 °C and 960 °C. The reversible phase transition of $BaCO_3$ from orthorhombic at temperatures below 800 °C to rhombohedral to cubic at 1000 °C was also demonstrated. Additionally, formation of CoO as well as traces of tetragonal disordered Fe-enriched perovskite phase could be assigned as by-products of BCFZ decomposition.

4.2 Influence of CO_2 on the Oxygen Permeation Performance of Perovskite-type $BaCo_xFe_yZr_zO_{3-\delta}$ Hollow Fiber Membranes

OLIVER CZUPRAT, MIRKO ARNOLD, STEFFEN SCHIRRMEISTER, THOMAS SCHIESTEL, JÜRGEN CARO

Journal of Membrane Science **2010**, *364*, 132-137.

This is the pre-peer reviewed version of the published article.

Influence of CO_2 on the oxygen permeation performance of perovskite-type $BaCo_xFe_yZr_zO_{3-\delta}$ hollow fiber membranes

Oliver Czuprat[a,*], Mirko Arnold[b], Steffen Schirrmeister[c], Thomas Schiestel[d], Jürgen Caro[a]

[a] Institute of Physical Chemistry and Electrochemistry, Leibniz Universität Hannover,
Callinstr. 3A, D-30167 Hannover, Germany

[b] BASF Catalysts Germany GmbH, Große Drakenburger Str. 133, D-31582 Nienburg/Weser,
Germany

[c] Uhde GmbH, Friedrich-Uhde-Str. 15, D-44141 Dortmund, Germany

[d] Fraunhofer Institute for Interfacial Engineering and Biotechnology, Nobelstraße 12,
D-70569 Stuttgart, Germany

*corresponding author: oliver.czuprat@pci.uni-hannover.de

Keywords: perovskite membrane; BCFZ; CO2 stability; membrane reactor; oxygen conductor

Abstract

The influence of CO_2 on the oxygen permeation performance of perovskite-type $BaCo_xFe_yZr_zO_{3-\delta}$ (BCFZ, $x+y+z=1$) hollow fiber membrane under different experimental conditions is presented. Helium with various partial pressures of CO_2 was applied as sweep gas at different temperatures on the shell side of the hollow fiber leading to a decrease and finally drop to zero of the oxygen permeation while feeding air on the core side due to carbonate formation. Repeated cycles of changing the sweep gas between the CO_2/He mixture and pure He were conducted in order to check the reversibility of the carbonate formation. The analysis of the micro structure after permeation experiments was carried out by X-ray diffraction (XRD) as well as by scanning electron microscope (SEM). It was found that both micro structure as well as oxygen permeation are recovered in a CO_2-free atmosphere like pure He on the shell side while feeding air on the core side. Under exposure of 50% CO_2 in He for 5 hours, the perovskite structure is impaired up to a depth of ca. 15 μm and approximately 30 μm after 10 hours, respectively.

1. Introduction

Intensive research in the past years has been focused on solid oxide membranes regarding their ability to separate oxygen from air at infinite selectivity. Specifically, mixed ionic-electronic conductors (MIECs) with perovskite structure have potential for many industrial processes in which a constant supply or removal of oxygen is required [1]. Various straightforward applications of MIECs as cathode material in solid oxide fuel cells (SOFCs) as well as in the conversion of hydrocarbons have been reported [2].

For prospective industrial applications not only high oxygen permeability but also sufficient stability especially in reducing gas atmospheres or atmospheres containing CO_2 is essential. The poisoning effect of CO_2 is due to the fact that earth alkali metal cations of the perovskite tend to form carbonates. Wang et al. observed a good phase stability of a perovskite of the composition $(Ba_xSr_{1-x})(Co_{0.8}Fe_{0.2})O_{3-\delta}$ (BSCF) down to an oxygen partial pressure of $2 \cdot 10^{-5}$ bar [3]. Yan and co-workers investigated the effect of CO_2 between 450 and 750 °C on the cell performance of solid oxide fuel cells made of the same material [4]. They found a negative but reversible effect on the cell performance even at relatively low CO_2 partial pressures.

Summarizing, the impact of CO_2 on the membrane performance plays an important role and thus needs to be examined since CO_2 is a constituent in natural air as well as a by-product in various oxidative hydrocarbon activation reactions. Eminently, in zero emission plants in which oxygen permeable membranes are flushed with CO_2-containing exhaust gases, the demand for CO_2 stable membranes becomes crucial [6].

As early as in 1995 Pei et al. observed the chemical decomposition of $Sr(Co_{1-x}Fe_x)O_{3-\delta}$ (SCF) hollow fiber membranes after partial oxidation of methane to synthesis gas. They found Sr carbonate as well as a mixture of Fe and Co oxides on the reaction side of the membrane leading to membrane failures [7]. High-temperature in situ neutron powder diffraction on SCF ceramics in CO/CO_2 atmospheres were carried out while diffraction pattern of whole membrane profiles show no or even low contents of earth alkali carbonates but the formation of various oxides [8,9].

Depending on the potential application of membranes with perovskite-type structure either the feed side or the permeate side needs to be investigated regarding its CO_2 stability as presented in publications in recent years [7-9]. Recently, Arnold et al. reported that the impact of CO_2 on the oxygen permeation of BSCF membranes in the sweep gas is superior to that on the feed gas [10], but the cessation of oxygen permeation was reversible.

Dense perovskite type membranes of the composition $BaCo_xFe_yZr_zO_{3-\delta}$ (BCFZ, $x+y+z = 1$) have been produced by the Fraunhofer Institute for Interfacial Engineering and Biotechnology (IGB) in Stuttgart in hollow fiber geometry [11] and have been used in our group in membrane reactors for example for direct decomposition of N_2O [12] and NO [13] or the production of hydrogen by thermal water splitting [14,15]. Furthermore, we presented the concept for a membrane reactor performing a repeated catalytic dehydrogenation of ethane and propane with selective hydrogen combustion [16,17]. Recently, we applied our membrane reactor for the oxidative coupling of methane [18].

Figure 1 shows the Ellingham diagram for possible carbonate formations from the BCFZ perovskite. The three parallel lines with a positive slope in the diagram represent the chemical potential of the corresponding carbonates which have been taken into account. Among those, Barium carbonate is the most stable. The dotted lines correspond to the chemical potential of CO_2 at different partial pressures. The rectangle equals the regime of the reaction parameters applied in this work (T = 800-900 °C, $p(CO_2)$ = 0-1 bar). As long as the potential of Barium carbonate is higher than that of CO_2 at a certain partial pressure and temperature, the first is not stable. Consequently, high temperatures and low CO_2 partial pressure suppress carbonate formation.

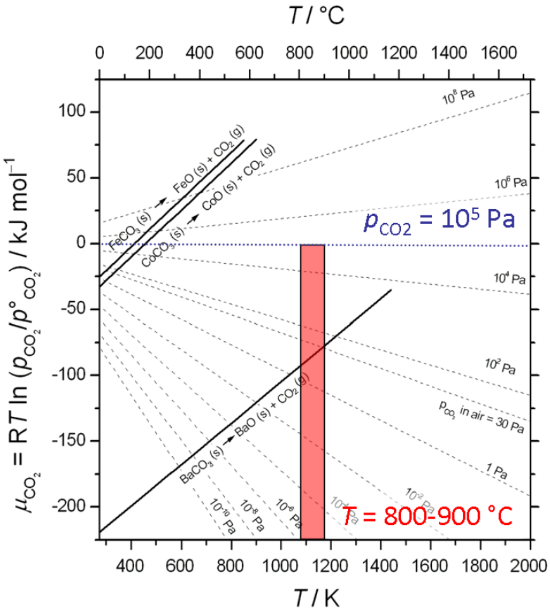

Figure 1: Ellingham diagram for the stability of carbonates under different CO_2 partial pressures. Chemical potentials of Ba, Co and Fe carbonates have been calculated with thermodynamic data [5] and are shown as continuous lines. The dotted lines represent the chemical potential of CO_2. The box indicates the range of reaction parameters. If the chemical potential of the carbonate is higher than that of CO_2, the carbonate decomposes.

To the best of our knowledge, it is the first time that the impact of CO_2 in the sweep gas on a BCFZ perovskite and its oxygen permeability is investigated. Energy dispersive x-ray spectroscopy (EDXS) as well as scanning electron microscopy (SEM) and x-ray diffraction (XRD) experiments were applied for analytical purposes.

2. Experimental

The above mentioned hollow fiber membranes of the composition $BaCo_xFe_yZr_zO_{3-\delta}$ (BCFZ, $x+y+z = 1$, Figure 2) were manufactured by phase inversion spinning followed by sintering as described elsewhere. [11]

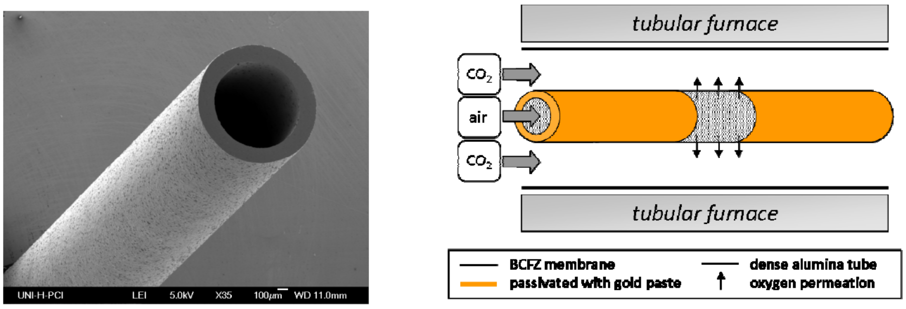
UNI-H-PCI LEI 5.0kV X35 100μm WD 11.0mm
tubular furnace
CO_2
air
CO_2
tubular furnace
BCFZ membrane
passivated with gold paste
dense alumina tube
oxygen permeation

Figure 2: $BaCo_xFe_yZr_zO_{3-\delta}$ (BCFZ, $x+y+z = 1$) hollow fiber membrane obtained by phase inverse spinning at the Fraunhofer Institute for Interfacial Engineering and Biotechnology (IGB, left). Schematic drawing of the reactor set-up and an incorporated BCFZ hollow fiber (right). At both ends the 30 long fiber was coated with gold to obtain a 3 cm long isothermal oxygen permeation zone. The active surface area for the oxygen permeating BCFZ hollow fiber is 0.78 cm².

.

In order to study the effect of CO_2 on the O_2 permeation of the BCFZ hollow fiber membrane, several permeation experiments were carried out on a high-temperature permeation reactor which is described in detail elsewhere. [11] To ensure isothermal conditions, two ends of the fibers with an outer diameter of 1.1 mm and a wall thickness of 0.14 mm were coated with gold paste (C 5754 B, Heraeus) and sintered at 950 °C for 5 hours to obtain a 3 cm long permeation zone in the middle of the furnace. This procedure was repeated three times to ensure a leak-proof gold layer not permeable to oxygen. The effective permeation area of the membrane was 0.78 cm².

All gases were supplied into the reactor by mass flow controllers (Bronkhorst Hi-Tech) and the outlets were continuously analyzed by an on-line gas chromatograph (Agilent Technologies, HP6890N, equipped with a carboxen 1000 column). The sweep side of the membrane was flushed either with pure He (99.996%) or selected concentrations of CO_2 in helium. On the feed side synthetic air was applied. The total flow rate on the feed side was set to be 150 mL_N min^{-1}, the total flow rate on the shell side to 50 mL_N min^{-1}, respectively. The absolute flow of the effluents was determined by using Ne as an internal standardization. After permeation experiments, the membranes were quenched to room temperature under indicated atmospheres.

SEM combined with EDXS as well as XRD were conducted on fraction surfaces. SEM studies were carried out on a JEOL JSM-6700F field-emission instrument using a lower secondary electron detector (LEI) at an accelerating voltage of 2 kV. EDX spectra were obtained at an accelerating voltage of 15 kV using a light-element detector (INCA 300, Oxford Instruments). To determine the crystal structure of membrane surfaces, XRD were conducted with monochromated Cu $K_{\alpha1}$ radiation in the range of 20°-80° 2θ at room temperature (Bruker D8 Advance).

3. Results and discussion

Figure 3 shows the O_2 permeation fluxes of a BCFZ hollow fiber membrane as a function of the CO_2 concentration in the sweep gas (left) at three different temperatures (T = 800, 850, 900 °C). The data points were collected after a constant O_2 permeation flux could be detected (after approximately 60 min). Subsequently, the sweep gas was changed to pure He and the recovering of the O_2 permeation flux in the CO_2 free atmosphere was measured as a function of time (Figure 3, right). At each temperature, this cycle has been repeated for additional four times to ensure reproducibility. A new cycle at a certain temperature was started after the O_2 flux regained its former value (before the exposition to CO_2) while sweeping with pure He.

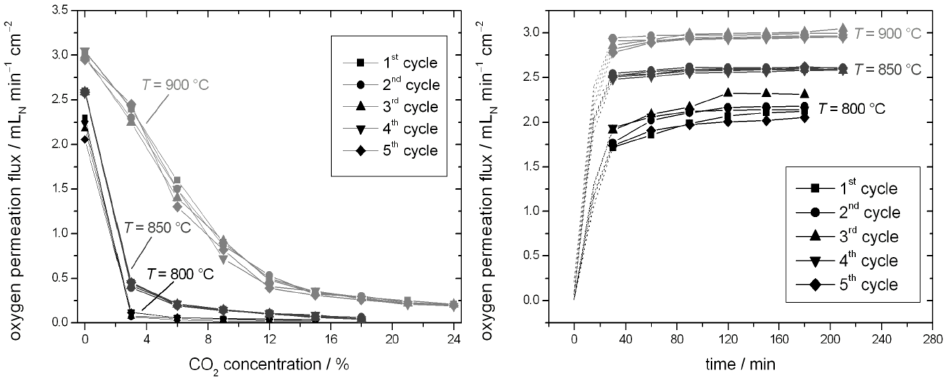

Figure 3: O_2 permeation flux while increasing the CO_2 concentration in the sweep gas He (left, equilibrium time between data points 60 min) and during recovering of the O_2 permeation flux while sweeping with pure He (right) at different temperatures. (*core*: 150 mL$_N$ min^{-1} air; *shell*: F_{total} = 50 mL$_N$ min^{-1}). Number of cycles indicates how many times carbonate formation and recovery have been repeated at each temperature.

As expected, the O_2 permeation flux across the membrane decreases with an increasing CO_2 concentration in the sweep gas due to a higher rate of carbonate formation on the permeate side of the membrane. The higher the temperature, the less distinctive is the decrease of the O_2 permeation, because of the exothermic carbonate formation (see Figure 1).

The recovering of the O_2 permeation flux while sweeping with pure He can be seen in Figure 3 (right). Most of the recovering from the decreased flux due to carbonate formation takes place in the first 40 min. Reducing the CO_2 content in the sweep gas to zero, favors the carbonate decomposition and therefore increasing the O_2 permeation. Notably, the original O_2 flux can be restored during the recovering, i.e. the micro structure of the perovskite is re-established ensuring a migration of the oxygen ions which is apparently not affected by the former phase change.

Taking a closer look on the kinetics of the carbonate formation and its decomposition, further experiments were carried out investigating the O_2 permeation flux as a function of time. Figure 4 illustrates the O_2 permeation while sweeping with 3% CO_2 in He and feeding air on the core side of the membrane at 800 and 850 °C.

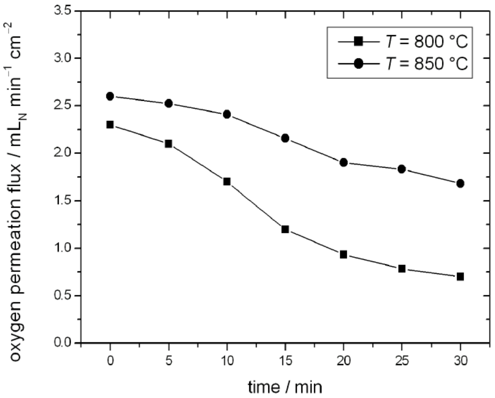

Figure 4: Impact of time and temperature on the O_2 permeation flux while sweeping with 3% CO_2 in He (*core*: 150 mL_N min^{-1} air at 1 bar; *shell*: F_{total} = 50 mL_N min^{-1} 3% CO_2 in He at 1 bar).

Within 30 min the O_2 permeation flux at 800 °C decreases from ca. 2.3 to 0.7 $mL_N\,min^{-1}$ cm^{-2} while feeding air on the core side of the membrane and sweeping with 3% CO_2 in He. At a higher temperature (T = 850 °C) the decrease is less significant, i.e. from 2.6 down to ca. 1.7 $mL_N\,min^{-1}$ cm^{-2} in the same time span, which can be related to the lower stability of carbonates at higher temperatures. Applying even higher CO_2 concentrations leads to an even more significant loss of O_2 permeability (see Figure 5).

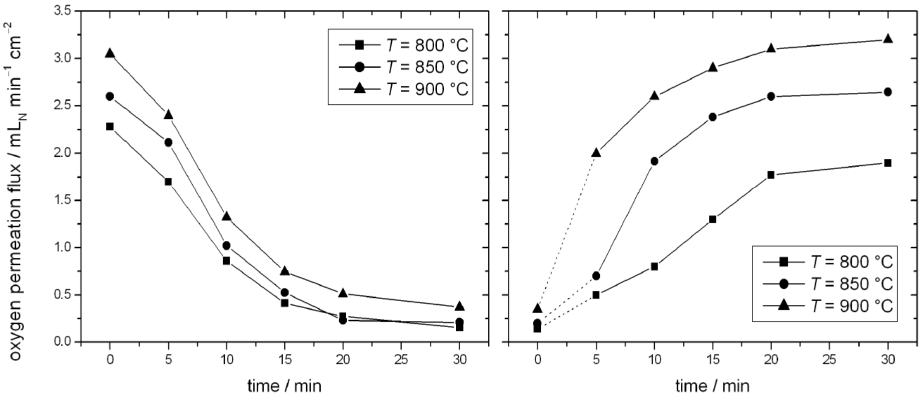

Figure 5: Decrease of O_2 permeation under CO_2 exposure on the sweep side (left, *core*: 150 mL$_N$ min^{-1} air at 1 bar; *shell*: F_{total} = 50 mL$_N$ min^{-1} 10% CO_2 in He at 1 bar) and recovery as a function of time while sweeping with pure He (right, *core*: 150 mL$_N$ min^{-1} air at 1 bar; *shell*: 50 mL$_N$ min^{-1} He at 1 bar).

Applying 10% CO_2 in He on the sweep side while feeding air on the core side of the membrane yields to almost a total decrease in O_2 permeation for all three investigated temperatures within 30 min. In contrast, the recovering of the O_2 flux across the membrane due to carbonate decomposition seems more temperature dependent. At 900 °C the original O_2 flux of 3.1 mL$_N$ min^{-1} cm^{-2} is nearly regained after 20 min of sweeping pure He on the shell side, whereas at 800 °C only 1.8 mL$_N$ min^{-1} cm^{-2} are obtained (original flux approximately 2.3 mL$_N$ min^{-1} cm^{-2}).

Figure 6 shows cross section of a fresh membrane (left), after exposure to a 1:1 mixture of CO_2 and He after five hours at 800 °C (middle), and after regeneration with He (right).

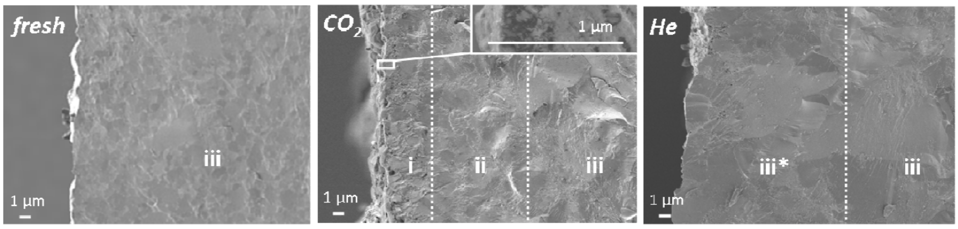

Figure 6: SEM micrographs showing the cross section at the shell side of the BCFZ hollow fiber membrane as freshly calcined in air at 1320 °C (left), after 5 hours in a 1:1 mixture of CO_2 and He (middle, *shell:* F_{total} = 50 mL$_N$ min^{-1} He:CO_2 = 1:1 at 1 bar for 5 hours; *core:* 150 mL$_N$ min^{-1} air at 1 bar) and after recovering the total O_2 flux through the membrane by sweeping with pure He (right, *shell:* 50 mL$_N$ min^{-1} He at 1 bar; *core:* 150 mL$_N$ min^{-1} air at 1 bar). The different areas are indicated as: (i) $BaCO_3$-enriched top layer, (ii) Ba-depleted layer, (iii) untouched original perovskite composition, and (iii*) with He as CO_2-free sweep gas regenerated perovskite phase, respectively.

As shown in Figure 6 (left), the fresh fiber exhibits a homogeneous micro structure over the entire cross section. After CO_2 treatment (Figure 6, middle), three zones can be distinguished in the cross section as indicated by the morphology as well as by EDXS. The decomposed region after CO_2 exposure consists of two zones: zone (i) with a thickness of approximately 5 µm followed by an additional 5-10 µm thick layer (ii). Region (iii) has been not affected by CO_2 exposure. Replacing CO_2 with He as sweep gas (right) leads to a regeneration of zones i and ii (labelled as iii*) yielding a homogeneous micro structure again.

The elemental distribution at the permeate side of the membrane by EDXS is visualized in Figure 7, revealing that layer (i) is Ba-enriched. Regions (iii) and (iii*) represent the untouched and restored BCFZ perovskite structures, respectively.

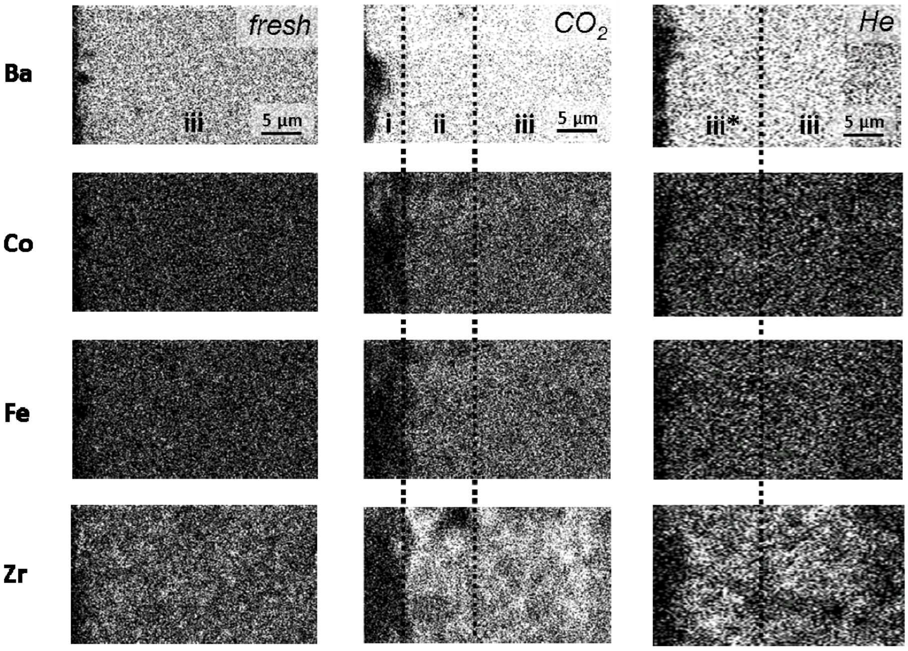

Figure 7: Elemental distribution by EDXS at the sweep side of a fresh fiber (left column), after 5 hours permeation of a 1:1 CO_2:He mixture (middle column, *shell:* F_{total} = 50 mL_N min^{-1} He:CO_2 = 1:1 at 1 bar for 5 hours; *core:* 150 mL_N min^{-1} air at 1 bar) and after recovering the total O_2 flux through the membrane by sweeping with pure He (right column, *shell:* 50 mL_N min^{-1} He at 1 bar; *core:* 150 mL_N min^{-1} air at 1 bar).

In order to confirm the formation of a carbonate top layer as well as the total reversibility of both the structural changes as well as of the O_2 permeation flux, in situ XRD measurements of BCFZ hollow fiber membrane were conducted at 800 °C before and after exposure of the BCFZ hollow fiber membrane to a 50% CO_2 in N_2 atmosphere for 5 hours and after regeneration by sweeping with pure He on shell side for 60 min. The resulting XRD pattern indicates the formation of $BaCO_3$ with an additional reflex at approximately 27° 2θ (see Figure 8).

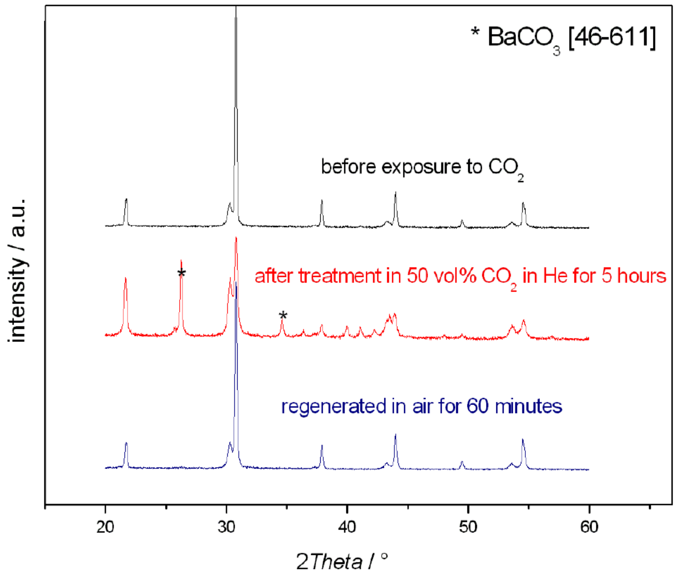

Figure 8: Powder XRD pattern of BCFZ before exposure to CO_2, after treatment in 50% CO_2 in He for 5 hours and after regeneration in He for 60 min at 800 °C.

While treating BCFZ with a gas mixture of 50% CO_2 in He at 800 °C, barium carbonate is formed (middle pattern). The subsequent sweeping with He on the shell side for 60 min leads to a full regeneration (lower pattern). It is rational to infer from this observation that the perovskite structure is reconstructed which is in full accordance to the oberserved regenerated O_2 flux through the membrane as described earlier.

Table 1 shows the elemental distribution of the different layers of the perovskite membrane. It is obvious that layer (i) is Ba-enriched and consequently layer (ii) is Ba-depleted.

Table 1: Summary of the elemental distribution of Ba, Co, Fe, Zr obtained by EDXS at different regions of the cross section of the BCFZ hollow fiber membranes before (zone iii), after treatment for 5 hours in a 1:1 CO_2:He mixture (layers i and ii), and after recovering of the total O_2 flux through the membrane by sweeping with pure He (iii*).

	elemental distribution / at%			
	iii	i	ii	iii*
Ba	52.58	71.82	49.90	50.79
Co	17.67	8.05	19.11	19.50
Fe	18.73	7.41	18.02	18.99
Zr	11.03	12.72	12.97	10.73

The standard deviation for quantification data of Ba, Co, Fe, Zr is assumed to be ±12%, according to [19].

Since the thickness of the carbonate layer is only approximately 5 μm after treatment with CO_2 for 5 hours, it can be concluded that this layer (i) is dense and can be regarded as a protective layer for further carbonate formation. Obviously CO_2 does not diffuse into the perovskite structure to form internal clusters of barium carbonate. In contrast, Ba^{2+} migrates through the carbonate layer to the surface of the membrane in order to form new carbonate. If the reaction product forms a compact, non-porous layer, the reaction rate is limited by transport phenomena through the product layer as described by Gomes and Dekeyser [20] and carbonate formation rate is decreased. Consequently, layer (ii) is Ba-depleted as already shown above.

After doubling the time of treatment with a 1:1 mixture of CO_2 and He, thicker layers (i) and (ii) have been formed. The Ba-enriched layer (i) has gained a thickness of approximately

10 µm, whereas die following Ba-depleted layer (ii) has increased up to ca. 20 µm (see Figure 9). Zone (iii) represents the untouched original perovskite structure.

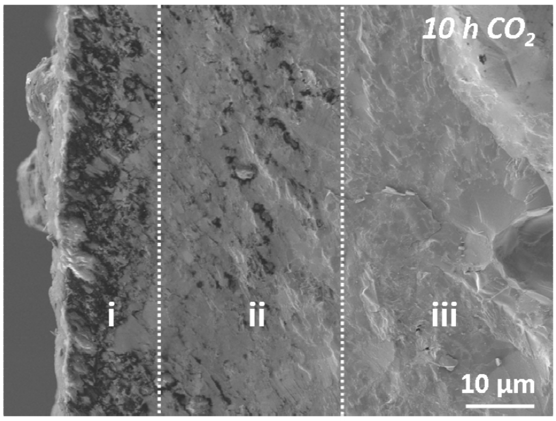

Figure 9: SEM micrograph of the cross section of the shell side of a BCFZ hollow fiber membrane after exposition to 50% CO_2 in He as sweep gas on the shell side for 10 hours while feeding air on the core side at 800 °C: (i) Ba-enriched top-layer, followed by a Ba-depleted layer (ii), and the untouched original perovskite structure (iii).

The elemental quantification of Ba, Co, Fe, Zr as well as the relative C content resulting from EDXS mapping analysis of the cross section of the membrane as a function of the distance to the surface on the shell side is shown in Figure 10 (5 hours 50% CO_2, left side, 10 hours 50% CO_2, right side). It can be seen clearly that a prolonged exposition to CO_2 in the sweep gas gives rise to a growth of the Ba-enriched layer (i) as well as an increase of the relative C content of the latter. The Ba-enriched layer is followed by a Ba-depleted zone (ii) and the untouched perovskite structure (iii).

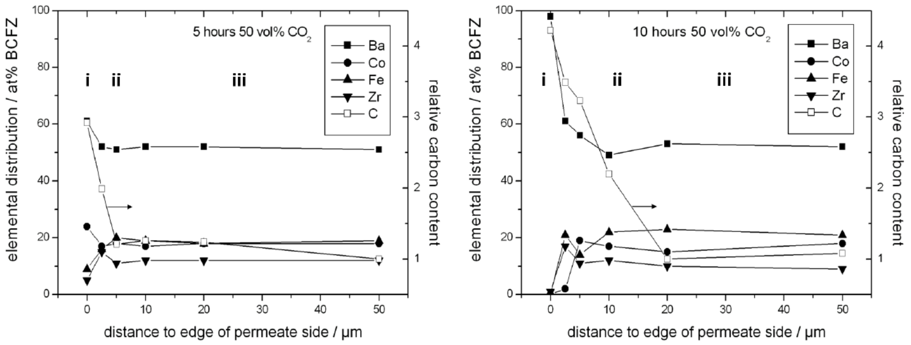

Figure 10: Elemental distribution of Ba, Co, Fe and Zr as well as the relative C content as a function of the distance to shell side surface exposure to 50% CO_2 in He for 5 hours (left) and 10 hours (right) at 800 °C.

4. Conclusion

The poisoning effect of CO_2 on the oxygen permeation flux as well as the changes in the micro structure of BCFZ hollow fiber under CO_2 exposure have been investigated as a function of CO_2 concentration, temperature and time. Using CO_2-containing sweep gases decrease and finally stop the O_2 permeation flux but this effect can be easily recovered by sweeping with pure He. This process is fully reversible. Time-dependent experiments show that the decrease as well as the regeneration of the oxygen flux take place in a time-span of about 15 min, which can be related to the diffusion-controlled decomposition of the perovskite to form barium carbonate and the regeneration of the homogenous stoichiometric Barium distribution in the perovskite structure.

The decomposition of the original perovskite structure takes place up to a depth of approximately 10 µm when exposed to a 50% CO_2 in He stream for 5 hours and ca. 25 µm after 10 hours, respectively. The outer zone of 5 (10) µm is $BaCO_3$-enriched followed by an approximately 5-10 (15) µm thick Ba-depleted zone as indicated by SEM, EDXS and XRD observations after treatment with 50% CO_2 in He for 5 (10) hours.

Acknowledgments

The authors gratefully acknowledge the financial support by Uhde GmbH and their permit for publication.

References

[1] H.J.M. Bouwmeester, A.J. Burggraaf, Dense ceramic membranes for oxygen separation, in: A.J. Burggraaf, L. Cot (Eds.), Fundamentals of Inorganic Membrane Science and Technology, Elsevier, Amsterdam, 1996, p. 435.

[2] R. Dittmeyer, J. Caro, Catalytic Membrane Reactor, in: G. Ertl, H. Knözinger, F. Schüth, J. Weitkamp (Eds.), Handbook of Heterogeneous Catalysis, Vol. 4, Wiley-VCH, Weinheim, 2008, p. 2198.

[3] H. Wang, S. Werth, T. Schiestel, J. Caro, Perovskite hollow-fiber membranes for the production of oxygen-enriched air, Angew. Chem. Int. Ed. 44 (2005) 6906-6909.

[4] A. Yan, M. Cheng, Y. Dong, W. Yang, V. Maragou, S. Song, P. Tsiakaras, Investigation of $Ba_{0.5}Sr_{0.5}Co_{0.8}Fe_{0.2}O_{3-\delta}$ based on cathode IT-SOFC. Part I. The effect of CO_2 on the cell performance, Appl. Catal. B 66 (2006) 64-71.

[5] I. Barin, F. Sauert, G. Patzki, Thermochemical Data of Pure Substances, 3rd edition, Vols. I and II. VCH, Weinheim, 1995.

[6] J.H. Horlock, Advanced Gas Turbine Cycles, Pergamon, Oxford, 2003.

[7] S. Pei, M.S. Kleefisch, T.P. Kobylinski, J. Faber, C.A. Udovich, V. Zhang-McCoy, B. Dabrowski, U. Balachandran, R.L. Mieville, R.B. Peoppel, Failure mechanism of ceramic membrane reactors in partial oxidation of methane to synthesis gas, Catal. Lett. 30 (1995) 201-212.

[8] B.J. Mitchell, R.C. Rogan, J.W. Richardson Jr., B. Ma, U. Balachandran, Stability of the cubic perovskite $SrFe_{0.8}Co_{0.5}O_{3-\delta}$, Solid State Ionics 146 (2002) 313-321.

[9] Y. Li, E.R. Maxey, J.W. Richardson Jr., Structural behaviour of oxygen permeable $SrFe_{0.2}Co_{0.8}O_x$ ceramic membranes with and without pO_2 gradients, J. Am. Ceram. Soc. 88 (2005) 1244-1252.

[10] M. Arnold, H. Wang, A. Feldhoff, Influence of CO_2 on the oxygen permeation performance and the micro structure of perovskite-type $(Ba_{0.5}Sr_{0.5})(Co_{0.8}Fe_{0.2})O_{3-\delta}$ membranes, J. Membr. Sci. 293 (2007) 44-52.

[11] T. Schiestel, M. Kilgus, S. Peter, K.J. Caspary, H. Wang, J. Caro, Hollow fibre perovskite membranes for oxygen separation, J. Membr. Sci. 258 (2005) 1-4.

[12] H. Jiang, H. Wang, F. Liang, S. Werth, T. Schiestel, J. Caro, Direct Decomposition of Nitrous Oxide to Nitrogen by In Situ Oxygen Removal with a Perovskite Membrane, Angew. Chem. Int. Ed. 48 (2009) 2983-2986.

[13] H. Jiang, L. Xing, O. Czuprat, H. Wang, S. Schirrmeister, T. Schiestel, J. Caro, Highly effective NO decomposition by in situ removal of inhibitor oxygen using an oxygen transporting membrane, Chem. Commun. 44 (2009) 6738-6740.

[14] H. Jiang, H. Wang, S. Werth, T. Schiestel, J. Caro, Simultaneous Production of Hydrogen and Synthesis Gas by Combining Water Splitting with Partial Oxidation of Methane in a Hollow-Fiber Membrane Reactor, Angew. Chem. Int. Ed. 47 (2008) 9341-9344.

[15] H. Jiang, Z. Cao, S. Schirrmeister, T. Schiestel, J. Caro, A Coupling Strategy to Produce Hydrogen and Ethylene in a Membrane Reactor, Angew. Chem. Int. Ed., DOI: 10.1002/anie.201000664.

[16] O. Czuprat, S. Werth, S. Schirrmeister, T. Schiestel, J. Caro, Olefin Production by a Multistep Oxidative Dehydrogenation in a Perovskite Hollow-Fiber Membrane Reactor, ChemCatChem 1 (2009) 401-405.

[17] O. Czuprat, S. Werth, J. Caro, T. Schiestel, Oxidative dehydrogenation of propane in a perovskite membrane reactor with multi-step oxygen insertion, AIChE J., DOI: 10.1002/aic.12158.

[18] O. Czuprat, T. Schiestel, H. Voss, J. Caro, Oxidative Coupling of Methane in a BCFZ Perovskite Hollow Fiber Membrane Reactor, Ind. Eng. Chem. Res. 2010, **DOI:** 10.1021/ie100282g.

[19] P.J. Statham, Limitations to accuracy in extracting characteristic line intensities from X-Ray spectra. J. Res. Natl. Inst. Stand. Technol. 107 (2002) 531-546.

[20] W.P. Gomes, W. Dekeyser, Factors influencing the reactivity of solids, in: N.B. Hannay (Ed,), Treatise on Solid State Chemistry, vol. 4, Plenum Press, New York, 1976, p. 61.

4.3 *In-situ* X-ray Diffraction Study on Carbonate Formation in Perovskite-Type $BaCo_xFe_yZr_zO_{3-\delta}$

KONSTANTIN EFIMOV, OLIVER CZUPRAT, ARMIN FELDHOFF

Journal of Solid State Chemistry **2010**, *submitted for publication*.

This is the pre-peer reviewed version of the published article.

In-situ X-ray diffraction study of carbonate formation and decomposition in perovskite-type $BaCo_xFe_yZr_zO_{3-\delta}$

Konstantin Efimov, Oliver Czuprat, Armin Feldhoff*

Institute of Physical Chemistry and Electrochemistry
Leibniz Universität Hannover
Callinstr. 3A, D-30167 Hannover, Germany

*corresponding author: Konstantin.Efimov@pci.uni-hannover.de

Abstract

The effect of CO_2 on the perovskite-type structure of $BaCo_xFe_yZr_zO_{3-\delta}$ (BCFZ, x+y+z = 1) is investigated by in-situ X-ray diffraction (XRD) as well as transmission electron microscopy (TEM). Partial decomposition of the BCFZ into high-temperature rhombohedral $BaCO_3$ polymorph was observed during annealing in an atmosphere, which contained 50 vol% CO_2 / 50 vol% N_2 at 900 °C. This carbonate structure is not quenchable and cannot be detected by ex-situ methods. Additionally, the reversible phase transition of $BaCO_3$ from orthorhombic to rhombohedral to cubic at different temperatures accompanied by formation of CoO was shown by in-situ XRD and TEM. Furthermore, complete regeneration of perovskite phase was obtained after high-temperature treatment under CO_2-free conditions.

1. Introduction

Doped perovskites (ABO_3) with multivalent cations as mixed ionic and electronic conductors are a hot topic in materials science today, e.g. as membrane materials for the separation of oxygen from oxygen containing gases like air with unrivalled selectivities [1] or as cathode material in solid-oxide fuel cells [2]. In the last decade, these membranes have attracted great academic and industrial interest, since they have also large potential applications in chemical processes in which a constant supply or removal of oxygen is required [3]. For prospective industrial applications as membrane reactors for oxidative activation reactions of light hydrocarbons [4] or as oxygen separators in zero emission plants in which oxygen permeable membranes are flushed with CO_2-containing exhaust gases [5], a sufficient stability especially in reducing gas atmospheres or atmospheres containing CO_2 is essential. The poisoning effect of CO_2 arises from alkaline earth metal cations in the perovskite structure, which tend to form carbonates. CAROLAN *et al.* reported that the oxygen permeation flux of $La_{0.8}Ba_{0.2}Co_{0.8}Fe_{0.2}O_{3-\delta}$ decreased significantly when 430 ppm CO_2 was introduced into the operation gas [6]. It was further discovered that $BaCe_{0.9}Y_{0.1}O_{3-\delta}$ is converted to the carbonate at 850-1000 °C under pure CO_2 atmosphere and the perovskite structure is disrupted [7].

ARNOLD *et al.* investigated the influence of CO_2 on the oxygen permeation performance and the microstructure of perovskite-type $Ba_{0.5}Sr_{0.5}Co_{0.8}Fe_{0.2}O_{3-\delta}$ membranes [8]. It was found that when having air on the feed side, using pure CO_2 as sweep gas at 875 °C caused an immediate stop of the oxygen permeation flux, which could be recovered by sweeping with pure helium. A detailed surface analysis of a BSCF cathode after operation in 1% CO_2/O_2 at 450 °C for 24 h revealed that its surface was destroyed and mixed barium-strontium carbonate was formed as a top layer [9].

Systems using dense perovskite hollow fiber membranes of the composition $BaCo_xFe_yZr_zO_{3-\delta}$ (BCFZ, $x+y+z$ = 1), which is a novel oxygen permeable membrane material with high O_2 permeation fluxes and excellent thermal and mechanical stability [10], have been presented by our group, e.g. for the direct decomposition of nitrous oxide to nitrogen by in-situ oxygen removal [11], the simultaneous production of hydrogen and synthesis gas by combining water splitting with partial oxidation of methane [12] as well as the multi-step oxidative dehydrogenation of ethane [4] and propane (ODP) [13]. Furthermore, the oxidative coupling of methane to C_2 products could be successfully demonstrated in a BCFZ hollow fiber membrane reactor [14]. Summarizing, the effect of CO_2 on the membrane permeation performance plays an important role and thus was examined recently [15]. Under exposure of 50% CO_2 in He, the perovskite structure is impaired up to a depth of ca. 15 µm after 5 hours and approximately 30 µm after 10 hours, respectively. Furthermore, it was found that both micro structure as well as oxygen permeation are recovered in a CO_2-free atmosphere.

In order to get a deeper understanding of the processes occurring during application in CO_2 containing atmospheres, we carried out an *in-situ* X-ray diffraction (XRD) as well as transmission electron microscopy (TEM) study on the BCFZ powder.

2. Experimental

The BCFZ powder was obtained from the Fraunhofer-Institute for Ceramic Technologies and Systems (IKTS, Hermsdorf). Hollow fiber membranes were manufactured by phase inversion spinning followed by sintering as described elsewhere [1]. The O_2 permeation experiments of the BCFZ hollow fiber membrane, were carried out in a high-temperature permeation reactor which is described in detail elsewhere [1]. *In-situ* powder XRD was conducted on the Bruker D8 Advance diffractometer in Bragg-Brentano geometry using Cu-K_α radiation. The diffractometer was equipped with an Anton Paar 1200 N high-temperature chamber and superfast 1D Lynxeye detector. XRD data were analyzed using TOPAS 4.0 software (Bruker AXS). Structural data for the known phases were taken from ICSD database (FIZ Karlsruhe) with file numbers: $BaCoO_{2.23}$ [28865], $BaZrO_3$ [27048], $BaCO_3$ (orthorhombic) [15196], $BaCO_3$ (rhombohedral) [158389], $BaCO_3$ (cubic) [27449], CoO [28505], FeO [24635]. Scanning TEM (STEM) was conducted at 200 kV on a JEOL JEM-2100F-UHR field-emission instrument. A light element EDX spectrometer, Oxford Instruments INCA-200 TEM, was used for elemental analysis. In order to obtain a TEM sample, the powder was glued between two alumina bodies, polished, and finally Ar^+ sputtered to electron transparency.

3. Results and discussion

The effect of CO_2 on the oxygen permeation performance of the BCFZ hollow fiber at 900 °C is shown in Figure 1. Insertion of 10% CO_2 on the sweep side of a membrane leads to the diminution of oxygen permeation flux already after a few minutes. Then, the oxygen flux through perovskite hollow fiber is almost stopped after dwell time of 30 minutes. However, the fast recovery of the oxygen permeation can be observed, if the sweep gas is changed to pure He. The value of oxygen flux reaches two-thirds of the initial performance after 5 minutes. The complete regeneration occurs after testing for 30 minutes.

According to CZUPRAT *et al.*, the decline of oxygen permeation flux in presence of CO_2 is due to formation of barium carbonate, which was observed by XRD and SEM on the surface of quenched BCFZ perovskite hollow fiber [15]. The full recovery of the flux points out to the regeneration of the perovskite structure. The high-temperature *in-situ* XRD affords to prove these statements.

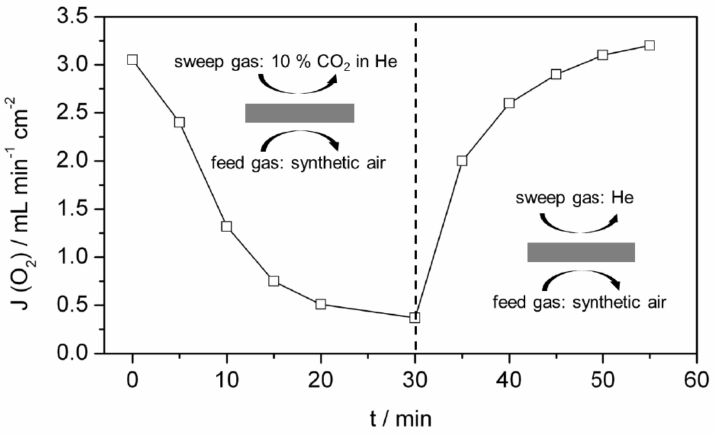

Figure 1: Decline of O_2 permeation through a BCFZ hollow fiber membrane with effective thickness of 140 µm under CO_2 exposure on the sweep side (sweep side: F_{total} = 50 mL min^{-1} 10% CO_2 in He; feed side: 150 mL min^{-1} synthetic air) and recovery as a function of time while sweeping with pure He at 900 °C (sweep side: 50 mL min^{-1} He; feed side: 150 mL min^{-1} synthetic air).

Figure 2 shows *in-situ* XRD patterns of BCFZ collected at (a) room temperature, (b) at 900 °C in flowing synthetic air, (c) and at 900 °C in an atmosphere containing 50% CO_2 and 50% N_2. As can be seen in the room temperature XRD (Figure 2a), the origin BCFZ powder consists of two perovskite systems as reported by Caro et al. previously [16]. The main compound is a $BaCo_xFe_yZr_{1-x-y}O_{3-\delta}$ with cubic structure (space group Pm-3m, *a* = 4.072 Å). Furthermore, the powder contains a low amount of cubic $BaZrO_3$ perovskite (space group Pm-3m, *a* = 4.18 Å). Note, the co-existence of two cubic perovskite phases after doping of more than 10% Zr was also reported for similar perovskite systems like $Ba_{0.5}Sr_{0.5}Co_{0.8}Fe_{0.2-x}Zr_xO_{3-\delta}$ and $SrCo_{0.4}Fe_{0.6-x}Zr_xO_{3-\delta}$ [17,18]. The high-temperature XRD pattern taken from the BCFZ powder annealed at 900 °C for 30 minutes in the flowing synthetic air evidences no structural changes. Only slightly shift of Bragg-reflection positions to smaller angles can be recognized here due to thermal lattice expansion. The annealing of the BCFZ powder at 900 °C for 90 minutes under 50 vol% CO_2 / 50 vol% N_2 leads to the partial decomposition of perovskite structure. $BaCO_3$ can be detected in the *in-situ* XRD pattern (Figure 2c) alongside of BCFZ. The pattern of $BaCO_3$ relates to the high-temperature rhombohedral polymorph (space group R3m), which is stable in the temperature range from approximately 800 °C to 960 °C as reported by Antao et al [19]. The structure of this phase is not quenchable and cannot be detected by ex-situ methods. Quantitative Rietveld analysis was applied to determine the $BaCO_3$ content in the sample to be 29%. Additionally, the presence of a third phase is obvious by weak intensities at 36.3° and 42.1° 2Θ. This phase can be understood as Co^{2+} or Fe^{2+} oxide. A precise attribution of oxide composition by XRD is unfeasible as the Bragg-positions of the XRD patterns are arranged very closely to each other. Change-over of the gas ambience to the synthetic air or pure N_2 results in complete decomposition of $BaCO_3$ and regeneration of perovskite structure. In order to elucidate the kinetic of the carbonate formation and decomposition, series of *in-situ* XRD experiments accompanied by quantitative analysis were carried out determining the content of $BaCO_3$ in the BCFZ powder as function of time. Figure 3 summarizes the results of quantitative analysis of diffraction patterns collected at 900 °C in time intervals of 15 minutes at different gas atmospheres. In presence of 50 vol% CO_2 in N_2, the content of $BaCO_3$ amounts to 15% after the first 15 minutes. After half an hour, the content of $BaCO_3$ reaches 24%. Then, the amount of carbonate increases slowly and reaches the value of 29% during 90 minutes. The sluggish kinetic of carbonate formation after the dwell time of 30 minutes may be explained by the development of the dense carbonate layer on the surface of perovskite particles, which can be considered as a protective layer regarding further carbonate formation. Moreover, thermodynamical considerations deliver further approach to

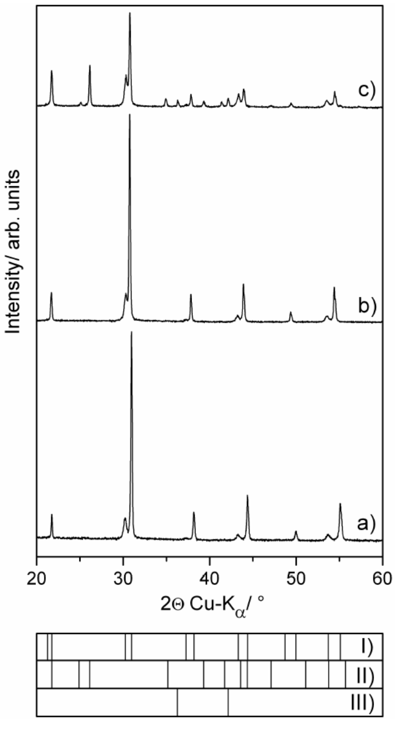

Figure 2. *In-situ* XRD-patterns of BCFZ powder collected a) at room temperature; b) at 900 °C in flowing synthetic air after 30 minutes; c) at 900 °C in an atmosphere containing 50% CO_2 / 50% N_2 after 90 minutes. I-III) Calculated Bragg-position of I) BCFZ (two phase system); II) $BaCO_3$ rhombohedral polymorph; III) Co^{2+}/Fe^{2+} oxide.

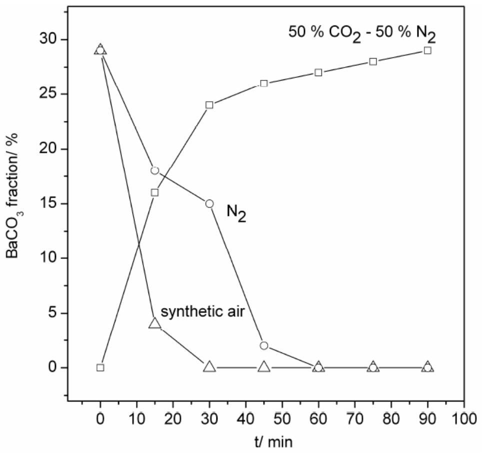

Figure 3. Amount of $BaCO_3$ in the BCFZ sample as function of time at different atmospheres as observed by *in-situ* XRD.

understand partial BCFZ decomposition. According to the Ellingham diagram presented by Feldhoff *et al*. $BaCO_3$ is stable at $5 \cdot 10^4$ Pa CO_2 up to 1330 °C [20]. However, Kumar *et al*. reported that the reaction of $BaCO_3$ with transition metal oxide like TiO_2 leading to the formation of perovskite is thermodynamically possibly above 376 °C in 10^5 Pa CO_2 [21]. Thus, we assume that the reaction of the carbonate with transition metal oxide counteracts the formation of the carbonate at 900 °C in $5 \cdot 10^4$ Pa CO_2 and the both processes are in equilibrium state. The composition of remaining BCFZ perovskite, which consists of the two above mentioned perovskite phases was also changed during the annealing in CO_2. We found that the ratio of $BaCo_x$FeyZr$_{1-x-y}O_{3-\delta}$ component was significantly decreased in contrast to the ratio of $BaZrO_3$ phase, which remained almost constant. It seems that carbonate formation occurs at the costs of Co- and Fe- containing perovskite phase. These phenomena points out to the higher stability of Zr-based perovskite as postulated by Yokokawa *et al*. [22]. Figure 3 shows also the kinetics of the BCFZ regeneration, if the CO_2 atmosphere was changed over to synthetic air or pure N_2. In air, the carbonate was decomposed very rapidly. After 15 minutes, only 4% carbonate can be detected in the sample. After 30 minutes, the carbonate was removed completely. Carbonate decomposition proceeds in the N_2 ambience a little slower. The perovskite structure was fully recovered after testing for 60 minutes. The decomposition of $BaCO_3$ in CO_2-free atmospheres corresponds to thermodynamical calculations, which indicate that carbonate becomes unstable at 900 °C if CO_2 partial pressure is lower than 30 Pa [20]. Then, solid state reaction between carbonate and transition metal oxides can be considered as thermodynamically favored.

Effect of temperature on the carbonate formation in the atmosphere containing 50 vol% CO_2 in N_2 was also studied by *in-situ* XRD during heating and cooling in the range of 30-1000 °C with steps of 100 °C. Before each data acquisition, an equilibrium time of 30 minutes was set. Figure 4a,b displays selected XRD data. An appreciable amount of $BaCO_3$ was detected not until 600 °C by heating of the sample (Figure 4a).

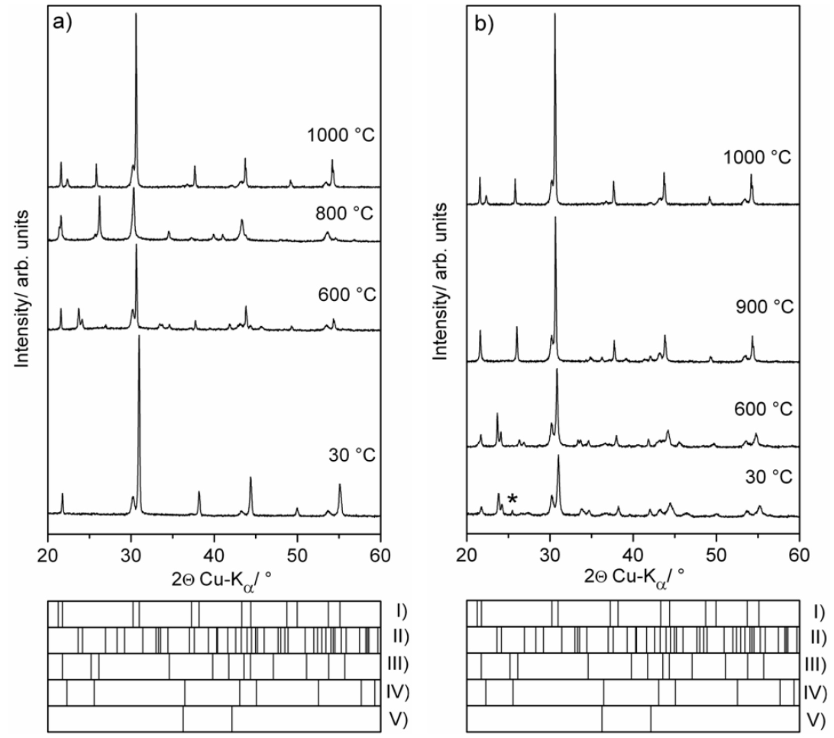

Figure 4. *In-situ* XRD of BCFZ powder in the atmosphere containing 50 vol% CO_2 and 50 vol% N_2 a) during heating; b) during cooling. Before each data acquisition an equilibrium time of 30 minutes was set. I-V) Calculated Bragg-positions for I) BCFZ; II) orthorhombic $BaCO_3$; III) rhombohedral $BaCO_3$; IV) cubic $BaCO_3$; V) Co^{2+} / Fe^{2+} oxide. Asterisk marks a reflection of tetragonal perovskite phase.

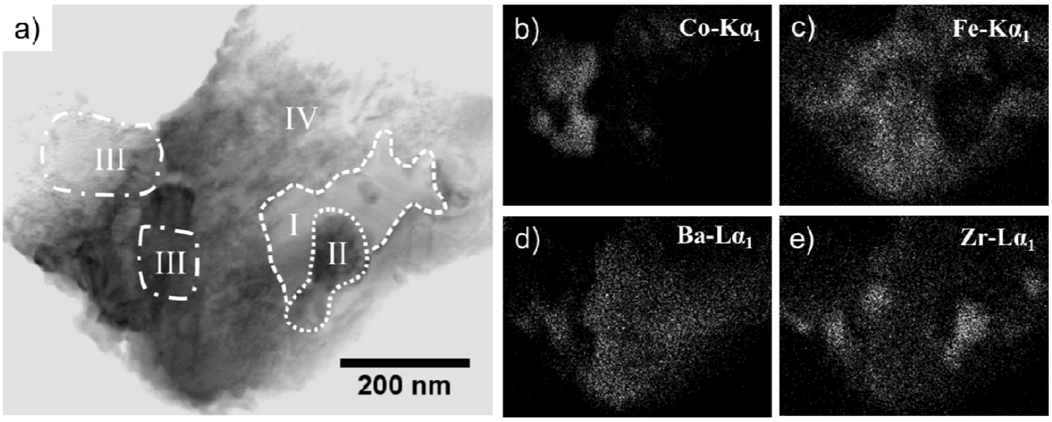

Figure 5. a) STEM bright field micrograph of BCFZ powder annealed and cooled in 50 vol% CO_2 and 50 vol% N_2. b-e) Elemental distributions by EDXS.

A low temperature orthorhombic polymorph (space group Pmcn) was formed under these conditions. Additionally, a low amount of Co/Fe oxide can be observed in the powder. The carbonate remains in orthorhombic symmetry up to 700 °C. Raising the temperature leads to the phase transition of the orthorhombic $BaCO_3$ to rhombohedral polymorph at 800 °C and to cubic carbonate phase at 1000 °C. The high-temperature cubic carbonate (space-group Fm-3m) exists only at temperatures above 960 °C as reported by STRØMME *et al.* [23]. Interestingly, the carbonate content in the sample was diminished from 40% at 800 °C to 10% at 1000 °C. This finding can be related to an increasing of the Gibbs free enthalpy of carbonate formation with rising temperature accompanied by decline of the Gibbs free enthalpy of the reaction between carbonate and oxides leading to shift of equilibrium of the processes [21]. During cooling, $BaCO_3$ structure changes to rhombohedral polymorph at 900 °C (Figure 4b) and the carbonate content reaches the value of 21 %. Further cooling to 600 °C leads to formation of orthorhombic carbonate phase and rising of their ratio to 27%. The composition of the sample was marginally changed after the complete cooling in CO_2. However, at room temperature we detected a new compound in XRD pattern, which cannot be attributed to the mentioned phases. The intensity of the phase at 25.4° 2Θ, which is marked by asterisk in Figure 4b, relates to a tetragonal perovskite structure as reported by MARTYNCZUK *et al.* [24].

In order to verify the results of *in-situ* XRD experiments, we investigated the sample, which was annealed and cooled down in CO_2 by TEM methods. STEM bright-field micrograph in Figure 5a shows a BCFZ powder particle, which is consist of several grains. EDXS elemental distribution (Figure 5b-e) clearly demonstrates that the grains exhibit a different chemical composition. The grain marked in Figure 5a with “I” contains no metal cations besides of Ba and can be indicated as $BaCO_3$. Obviously, the carbonate phase does not form a dense layer around the BCFZ powder particle in contrast to the hollow fiber ceramic membrane [15]. Instead, the carbonate is located inside of the particle. This kind of behavior was also observed by MARTYNCZUK *et al.*, who investigated the effect of CO_2 on the functional performance of related Zn-doped $(Ba,Sr)FeO_{3-\delta}$ perovskite [24]. The phase “II” consisting of Ba and Zr in the ratio 1:1 relates to $BaZrO_3$. Cliff-Lorimer quantification of EDXS data reveals a dramatical enrichment of Co in area “III” collateral to an almost entire absence of other cations. Thus, this phase can be considered as CoO. Finally, the main phase marked with “IV” can be described as a Co-depleted $Ba(Co,Fe,Zr)O_{3-\delta}$ perovskite.

Based on the *in-situ* XRD study as well as TEM investigations, we summarize the BCFZ decomposition process in presence of CO_2. Firstly, the CO_2 reacts with BCFZ under formation of $BaCO_3$. The carbonate can exhibit different polymorphs dependent on the temperature. The formation of carbonate does not lead to the complete destruction of perovskite. Based on TEM, partial BCFZ decomposition cannot be explained by slow kinetic of the reaction due to formation of protective layer on the surface of perovskite particle. The chemical equilibrium between formation of carbonate and reaction to the perovskite can be rather considered as an applicable approach. Second, we found that the carbonate formation occurs predominantly at the cost of Co/Fe containing component of BCFZ accompaned by development of CoO as by-product. Poor stability of Co-containing perovskite caused by flexible redox behavior of Co-cations was already discussed in some details in our previous reports [25-27]. The remaining perovskite phase was found to be Fe-enriched. According to the report of YÁNG *et al.*, structures of perovskites with Ba/Fe-rich composition exhibit several distorted variants [28]. One of them, the tetragonal distorted perovskite phase, we observed in the room temperature XRD pattern (Figure 4b).

4. Conclusions

Decomposition process of BCFZ powder in the CO_2 containing atmosphere was investigated by *in-situ* XRD as function of dwell time and temperature. Rapid formation of high-temperature rhombohedral $BaCO_3$ polymorph was observed after exposure of the CO_2 at 900 °C. This non-quenchable carbonate structure, which is stable at temperatures between 800 °C and 960 °C, can be declared as the phase terminating the oxygen permeation transport through BCFZ membrane materials. Time-dependent experiments at isothermal conditions deliver the partial decomposition of two phase BCFZ system at the costs of Co- and Fe- containing perovskite phase, which is in close agreement with thermodynamical considerations. Furthermore, the complete regeneration of BCFZ was proven after removing of CO_2 from the gas ambience.

The reversible phase transition of $BaCO_3$ from orthorhombic at temperatures below 800 °C to rhombohedral to cubic at 1000 °C was shown by *in-situ* XRD. Finally, formation of CoO as well as traces of tetragonal disordered Fe-enriched perovskite phase was observed as by-products of BCFZ decomposition by XRD and TEM methods.

Acknowledgments

K.E. and A.F. gratefully acknowledge financial support by the State of Lower Saxony (Germany, NTH bottom-up project, No. 21-71023-25-7/09). O.C. appreciates funding from the European Union's Seventh Framework Programme FP7/2007-2013 under grant agreement No. 228701. The authors gratefully acknowledge fruitful discussions with Prof. JÜRGEN CARO.

References

[1] T. SCHIESTEL, M. KILGUS, S. PETER, K.J. CASPARY, H. WANG, J. CARO, *J. Membr. Sci*. 258 (2005) 1.
[2] Z. Shao, S. HAILE, *Nature* 431 (2004) 170.
[3] H.J.M. BOUWMEESTER, A.J. BURGGRAAF, Dense ceramic membranes for oxygen separation, in: A.J. BURGGRAAF, L. COT (Eds.), Fundamentals of Inorganic Membrane Science and Technology, Elsevier, Amsterdam, 1996, p. 435.
[4] O. CZUPRAT, S. WERTH, S. SCHIRRMEISTER, T. SCHIESTEL, J. CARO, *Chem. Cat. Chem.* 1 (2009) 401.
[5] J.H. HORLOCK, Advanced Gas Turbine Cycles, Pergamon, Oxford, 2003.
[6] M.F. CAROLAN, P.N. DYER, J.M LABAR, R.M. THOROGOOD, US Patent 5240473 (1993).
[7] N. ZAKOWSKY, S. WILLIAMSON, J.T.S. IRVINE, *Solid State Ionics* 176 (2005) 3019.
[8] M. ARNOLD, H. WANG, A. FELDHOFF, *J. Membr. Sci*. 293 (2007) 44.
[9] A. YAN, V. MARAGOU, A. ARICO, M. CHENG, P. TSIAKARAS, *Appl. Catal. B* 76 (2007) 320.
[10] S.M. LIU, G.R. GAVALAS, *J. Membr. Sci.* 246 (2005) 103.
[11] H. JIANG, H. WANG, F. LIANG, S. WERTH, T. SCHIESTEL, J. CARO, *Angew. Chem. Int. Ed.* 48 (2009) 2983.
[12] H. JIANG, H. WANG, S. WERTH, T. SCHIESTEL, J. CARO, *Angew. Chem. Int. Ed.* 47 (2008) 9341.
[13] O. CZUPRAT, S. WERTH, J. CARO, T. SCHIESTEL, *AIChE J*. 56 (2010) 2390.
[14] O. CZUPRAT, T. SCHIESTEL, H. VOSS, J. CARO, *Ind. Eng. Chem. Res.* (2010) DOI:10.1021/ie100282g.
[15] O. CZUPRAT, M. ARNOLD, S. SCHIRRMEISTER, T. SCHIESTEL, J. CARO' *J. Membr. Sci*. (2010) DOI:10.1016/j.memsci.2010.08.019.
[16] J. CARO, H. WANG, C. TABLET, A. KLEINERT, A. FELDHOFF, T. SCHIESTEL, M. KILGUS, P. KÖLSCH, S. WERTH, *Catal. Today* 118 (2006) 128.
[17] S. YAKOVLEV, C.Y. YOO, S. FANG, H.J.M. BOUWMEESTER, *Appl. Phys. Lett.* 96 (2010) 254101.
[18] L. YANG, L. TAN, X. GU, W. JIN, L. ZHANG, N. XU, *Ind. Eng. Chem. Res*. 42 (2003) 2299.
[19] S.M. ANTAO, E.I. HASSAN, *Phys Chem Minerals* 34 (2007) 573.
[20] A. FELDHOFF, M. ARNOLD, J. MARTYNCZUK, Th.M. GESING, H. WANG, *Solid State Sciences,* 10 (2008) 689.
[21] S. KUMAR, G.L. MESSING, W.B. WHITE, *J. Amer. Cer. Soc.* 76 (1993) 617.
[22] H. YOKOKAWA, N. SAKAI, T. KAWADA, M. DOKIYA, *Solid State Ionics* 52 (1992) 43.

[23] K.O. STRØMME, *Acta Chem. Scand.* A 29 (1975) 105.
[24] J. MARTYNCZUK, K. EFIMOV, L. ROBBEN, A. FELDHOFF. *J. Membr. Sci.* 344 (2009) 62.
[25] K. EFIMOV, T. HALFER, A. KUHN, P. HEITJANS, J. CARO, A. FELDHOFF, *Chem. Mater.* 22 (2010) 1540.
[26] A. FELDHOFF, J. MARTYNCZUK, M. ARNOLD, M. MYNDYK, I. BERGMANN, V. ŠEPELÁK, W. GRUNER, U. VOGT, A. HÄHNEL, J. WOLTERSDORF, *J. Solid State Chem*. 182 (2009) 2961.
[27] K. EFIMOV, Q. XU, A. FELDHOFF, *Chem. Mater*. (2010) DOI:10.1021/cm101745v.
[28] Z. YÁNG, A.S. HARVEY, A. INFORTUNA, L. GAUCKLER, *J. Appl. Crystallogr*. 42 (2009) 153.

5 Conclusion and Perspectives

Oxygen is one of the top five chemical feedstocks in the world [1] and is currently produced by cryogenic distillation and pressure swing adsorption (PSA). Since these are very cost intensive technologies a novel way to obtain pure oxygen in a more economic process has been of outrageous interest.

Polymeric or perovskite-type membrane based approaches have been developed in the past decades, but have not led to a commercial breakthrough yet. Polymeric membranes have a sufficient selectivity to oxygen and high fluxes, but they generally have a low separation factor. The maximum oxygen concentration produced by such a single stage system is only up to 50%. In the case of oxygen separation from air using ceramic membranes, recent progress has been made leading to a demonstration unit using BSCF membranes developed by the Institute for Technical Ceramics of Hermsdorf (Germany) as part of the research consortium *mem-brain* [39] and to a pilot plant by the Chinese Weiton Group [40]. The German device is able to produce 150 L_N oxygen per hour.

However, there is still no industrial application of perovskite-type membranes on a large scale today - 20 years after the pioneering studies of TERAOKA *et al.* [41] on a $La_{1-x}A_xCo_{1-y}Fe_yO_{3-\delta}$ membrane. This lack of applications is mainly due to the long-term stability problems of perovskites, especially at low oxygen partial pressure at the usual operation temperature of approximately 850 °C. Either the stability or the oxygen flux is insufficient.

In this thesis, the perovskite composition BCFZ, which is a novel O_2-permeable membrane material with high O_2 permeation fluxes and excellent thermal and mechanical stability [42], was used for experiments. Earlier investigations confirmed that the thermal expansion coefficient of BCFZ is smaller than those of BSCF or SCF ($SrCoFeO_3$) leading to a higher operation stability [43], which makes BCFZ used throughout this work more practical under hard conditions on an industrial scale.

In order to develop the ceramic membrane system for industrial applications, it is essential to optimize the membrane configuration such as flat sheet, tubular or hollow fiber. Disk-shaped membranes implicate many problems such as the high temperature sealing, the connection and the pressure resistance. Tubular membranes were developed to solve the problems associated with the high temperature seal, but their small surface area to volume ratio and their relative thick wall leading to a low oxygen permeation flux make them unfavorable in practice.

In contrast, hollow fiber membranes as employed in the present work solve the problems mentioned above. Such hollow fiber membranes possess much larger membrane area per unit volume for oxygen permeation and a significantly thinner wall.

In this thesis, BCFZ hollow fiber membranes have been successfully applied for various oxidative activation reactions of light hydrocarbons combined with suitable catalysts in a packed-bed around the fiber. A novel concept for the production of light alkenes from their corresponding saturated analogues has been presented, based on a repeated sequence of thermal/catalytic dehydrogenation (DH) and selective hydrogen combustion (SHC) steps (c.f. chapter 2). It combines high selectivities obtained in a catalytic/thermal DH with the absence of thermodynamic limitations in terms of alkane conversion achievable in the conventional oxidative dehydrogenation. The SHC leads to a higher educt conversion since the latter is not limited anymore in terms of thermodynamics and the precise controlled oxygen insertion increases the olefin selectivity compared to the conventional co-feed mode of operation, besides a higher safety due to separation of hydrocarbon and air/oxygen. For both ethane and propane dehydrogenation, the kinetic compatibility of DH and SHC was established by varying the reaction parameters, e.g. temperature, flow rates of reactants etc. Summarizing, this novel and straightforward concept for the production of light alkenes using standard catalysts can compete with the best catalysts used in the conventional co-feed mode of operation. It was demonstrated that an ethene yield comparable to those in industrial steam crackers can be obtained at a temperature which is approximately 100 °C lower and the propene yield in the catalytic membrane reactor is twice the yield in the catalytic DH without oxygen supply.

Reaction pathways for propane dehydrogenation and the mechanism of hydrogen combustion were successfully elucidated by transient analysis of product experiments. Furthermore, the role of solid and gaseous oxygen species in the above described membrane reactors for propane dehydrogenation was studied in detail with isotopic labeled $^{18}O_2$. Altogether, these kinetic insights allow the user to control the selectivity reasonably and effectively.

Additionally, the supply of oxygen through a BCFZ hollow fiber membrane in a reactor in combination with a suitable catalyst was also effectually utilized for the catalytic oxidative coupling of methane to C_2 hydrocarbons (c.f. chapter 3).

In all oxidation reactions involving hydrocarbons, the formation of CO_2 has to be taken into account, since barium in the perovskite-type membrane tends to form the corresponding carbonate under exposure to CO_2. The resulting effect of decreasing the oxygen permeation flux was measured as well as its full reversibility of carbonate formation. Moreover, the impact on the microstructure of the membrane material was comprehensively investigated (c.f. chapter 4). With this knowledge in mind, the operating conditions for CO_2 involving processes can be optimized in order to maintain a constant and sufficient oxygen flux across the membrane.

Summarizing, the present work demonstrates not only several applications of an oxygen transporting perovskite-type hollow fiber membrane for oxidative activation reactions of light hydrocarbons which are already of large-scale industrial importance (ODH) or will arise growing interest in the near future (OCM). All reactor set-ups in this thesis have shown improved performance regarding long-term stability compared to those reported in the literature up to now, thus attracting industrial and economic attention. Also a mechanistic insight into the pathways of selectivity control for the dehydrogenation of propane with hydrogen combustion is presented as well as a comprehensive study on the effect of CO_2 on the membrane and its oxygen permeability. Taking these two investigations in account, the product selectivity in case of propane dehydrogenation as well as the overall performance of the catalytic membrane reactor can be controlled, optimized and taken to the next level.

Above all, since no separate and energy-consuming oxygen plant is required for producing pure oxygen for conversion of light hydrocarbons, the membrane reactor presented in this thesis contributes to process intensification due to a combination of an oxygen plant and reactor in a single device as well as an economic and ecologic overall process design.

Possible problems which need to be considered on the road to a large scale industrial application are, in particular, a trouble-free module concept of fiber bundles. The (hot) sealing between fibers and the outer module itself has to fulfill the requirements in terms of chemical inertness and thermal expansion coefficients. Such modules would take advantage of an extreme high surface to volume ratio of the membrane reactor as well as allow a user-friendly plant, where broken fibers can be exchanged rapidly just by replacing an easy-to-handle module. Furthermore, to lower the cost for the fibers and making the processes described in this thesis even more economically viable, the gold-sealing can be replaced by operating the fiber bundles in cross-flow mode.

6 Bibliography

[1] International Energy Agency, World Energy Outlook **2006**.

[2] I. CHORKENDORFF, J.W. NIEMANTSVERDRIET, *Concepts of Modern Catalysis and Kinetics*, Wiley-VCH, Weinheim, **2003**, pp. 452.

[3] National Research Council Panel on New Directions in Catalytic Sciences and Technology, *Catalysis Looks to the Future,* National Academic Press, Washington D.C., **1992**, pp. 1.

[4] W. VIELSTICH, A. LAMM, H. GASTEIGER, *Handbook of Fuel Cells: Fundamentals, Technology, Applications,* Wiley, Chichester, **2003**, pp. 2690.

[5] R.A. SHELDON, *Green Chem.* **2005**, *7*, 267.

[6] R. BORGNA, L. BALZANO, J.E. HERRERA, W.E. ALVAREZ, D.E. RESASCO, *J. Catal.* **2001**, *204*, 131.

[7] G.W. HUBER, J.N. CHHEDA, C.J. BARRETT, J.A. DUMESIC, *Science* **2005**, *308,* 1446.

[8] A.G. DIXON, *Int. J. Chem. Reactor Eng.* **2003**, *1*, 1.

[9] J. CARO, *Chem. Ing. Tech.* **2006**, *78*, 899.

[10] R. BAKER, *Membrane Technology in the Chemical Industry: Further Directions, 1st edition*, Wiley-VCH, Weinheim, **2001**.

[11] R.V. JASRA, N.V. CHOUDARY, S.G.T. BHAT, *Separation Science and Technology* **2001**, *26*, 885.

[12] H.J.M. BOUWMEESTER, A.J. BURGGRAAF in *Fundamentals of Inorganic Membrane Science and Technology, Membrane Science and Technology Series, Vol. 4* (Eds.: A.J. BURGGRAAF, L. COT), Elsevier, Amsterdam, **1996**.

[13] E.K. RIDEAL, H.S. TAYLOR, *Catalysis in Theory and Practice*, Macmillan, London, **1919**, Chapter 2.

[14] W. OSTWALD, *Nature* **1902**, *65*, 522.

[15] O. DEUTSCHMANN, H. KNÖZINGER, K. KOCHLOEFL, T. TUREK in *Ullmann's Encyclopedia of Industrial Chemistry, 7th edition*, Wiley-VCH, Weinheim, **2010**.

[16] P. SABATIER, J. B. SENDERENS, *C. R. Acad. Sci.* **1902**, *134*, 514.

[17] M. BOUDART in *Handbook of Heterogeneous Catalysis* (Eds.: G. ERTL, H. KNÖZINGER, J. WEITKAMP), Wiley-VCH, Weinheim, **1997**.

[18] G.A. SAMORJAI, *Introduction to Surface Chemistry and Catalysis*, John Wiley, New York, **1994**, pp. 667.

[19] G. EIGENBERGER in *Handbook of Heterogeneous Catalysis*, *Vol. 4* (Eds.: G. ERTL, H. KNÖZINGER, F. SCHÜTH, J. WEITKAMP), Wiley-VCH, Weinheim, **2008**, pp. 2076.

[20] K.R. WESTERTERP, *Chem. Eng. Sci.* **1992**, *47*, 2195.

[21] W.J. KOROS, Y.H. MA, T. SHIMIDZU, *Pure & Appl. Chem.* **1996**, *68*, 1479.

[22] R. DITTMEYER, J. CARO in *Handbook of Heterogeneous Catalysis, Vol. 4* (Eds.: G. ERTL, H. KNÖZINGER, F. SCHÜTH, J. WEITKAMP), Wiley-VCH, Weinheim, **2008**, pp. 2198.

[23] J. CARO in *Comprehensive Membrane Science and Engineering, Vol. 3* (Eds.: E. DRIOLI, L. GIORNO), Academic Press, Oxford, **2010**, pp. 1.

[24] J. CORONAS, J. SANTAMARIA, *Catal. Today* **1999**, *51*, 377.

[25] J. CARO, *Chem. Ing. Tech.* **2010**, *82*, 837.

[26] K. SUNDMACHER, L.K. RIHKO-STRUCKMANN, V. GALVITA, *Catal. Today* **2005**, *104*, 185.

[27] H.J.M. BOUWMEESTER, *Catal. Today* **2003**, *82*, 141.

[28] U. MÜLLER in *Anorganische Strukturchemie, 3rd edition* (Eds.: C. ELSCHENBROICH, F. HENSEL, H. HOPF), Teubner Studienbücher Chemie, Teubner, Stuttgart, **1996**.

[29] H. WANG, C. TABLET, W. YANG, J. CARO, *Mater. Lett.* **2005**, *59*, 3750.

[30] J.B. GOODENOUGH in *Localized to Itinerant Electronic Transition in Perovskite Oxides in Structure and Bonding, 1st edition* (Ed.: D.M.P. MINGOS) Springer, Berlin, **2000**.

[31] R. BREDESEN, K. JORDAL, O. BOLLAND, *Chem. Eng. Process.* **2004**, *43*, 1129.

[32] Y. TAKEDA, K. KANNO, T. TAKADA, O. YAMAMOTO, M. TAKANO, N. NAKAYAMA, Y. BANDO, *Solid State Sci.* **1986**, *63*, 237.

[33] S. MCINTOSH, J.F. VENTE, W.G. HAIJE, D.H.A. BLANK, H.J.M. BOUWMEESTER, *Chem. Mater.* **2006**, *18*, 2187.

[34] T. SCHIESTEL, M. KILGUS, S. PETER, K.J. CASPARY, H. WANG, J. CARO, *J. Membr. Sci.* **2005**, *258*, 1.

[35] J. CARO, H. WANG, C. TABLET, A. KLEINERT, A. FELDHOFF, T. SCHIESTEL, M. KILGUS, P. KÖLSCH, S. WERTH, *Catal. Today* **2006**, *118*, 128.

[36] S. BASU, A.L. KHAN, A. CANO-ODENA, C. LIU, I.F.J. VANKELECOM, *Chem. Soc. Rev.* **2010**, *39*, 750.

[37] C. WAGNER, *Prog. Solid State Chem.* **1975**, *10*, 3.

[38] J. MAIER, *Festkörper – Fehler und Funktion, Prinzipien der Physikalischen Festkörperchemie, 1st edition*, Teubner, Stuttgart-Leipzig, **2000**.

[39] www.mem-brain-allianz.de, accessed on 8th of July 2010.

[40] www.weiton.com, accessed on 8th July 2010.

[41] Y.Y. TERAOKA, T. NOBUNAGA, N. YAMAZOE, *Chem. Lett.* **1988**, *3*, 503.

[42] J.TONG, W. YANG, R. CAI, B. ZHU, L. LIN, *Catal. Lett.* **2002**, *78*, 129.

[43] H. WANG, C. TABLET, W. YANG, J. CARO, *Mater. Lett.* **2005**, *59*, 3750.

7 List of Figures

Figure 1.1: Energy diagram comparing a catalyzed and non-catalyzed reaction (E_A: activation energy). 13

Figure 1.2: Basic type of a catalytic fixed-bed reactor. 14

Figure 1.3: Simplified scheme for diffusion, sorption and reaction in heterogeneous catalysis. 15

Figure 1.4: Selective removal of products (a) and selective supply of reactants (b) via a permselective membrane. The reaction defines the reaction zone in a non-permselective membrane (c). 17

Figure 1.5: Packed-bed catalytic reactor incorporating an inert membrane (a) in comparison to catalytic membrane reactor (b) and a packed-bed catalytic membrane reactor (c). 19

Figure 1.6: Classification of ceramic membranes for oxygen transport. σ denotes the conductivity (ionic or electronic); μ is the chemical potential. 21

Figure 1.7: Oxygen concentration in axial direction in the catalyst bed. (a) Co-Feed reactor with strongly decreasing oxygen concentration. (b) Membrane as oxygen distributor with constant or even increasing oxygen concentration. 22

Figure 1.8: Layered AO_3 structure with hexagonal arrangement of the A site cations (blue). Oxygen ions are colored gray. 23

Figure 1.9: Structure of perovskite-type oxide. 24

Figure 1.10: Geometric construction of GOLDSCHMIDT's tolerance factor in the ideal cubic perovskite structure. 25

Figure 1.11: Overview of various ABO_3 perovskite-type structures. Displayed are the BO_6 and $A(B)O_6$ octahedra in the case of ilmenite, respectively. Differently distorted perovskite-type structures have been reported. 26

Figure 1.12: Photograph (left) and SEM micrograph (right) of sintered BCFZ hollow fiber membranes. 28

Figure 1.13: The principle of oxygen permeation through dense perovskite membranes resulting from the gradient $\nabla\mu_{O_2}$ between the oxygen chemical potentials of the feed side ($\mu_{O_2}^1$) and the permeate side ($\mu_{O_2}^2$). $\mu_{O_2}^0$ denotes the standard potential, p_1 the oxygen partial pressure on the feed side, p_2 the oxygen partial pressure on the permeate side, p_0 the standard pressure, $h^{\prime}$ the electron holes and $V_O^{\prime\prime}$ the oxygen ion vacancies 30

Figure 1.14: Oxygen diffusion along oxygen vacancies in the perovskite crystal lattice. 31

Appendix A

Oxygen Ion Migration in $Ba_{0.5}Sr_{0.5}Co_{0.8}Fe_{0.2}O_{3-\delta}$ Perovskite - a Molecular Mechanics Study

OLIVER CZUPRAT

unpublished results, 2010.

Computer modeling techniques have been used to examine the mechanistic features of oxygen ion transport in the $Ba_{0.5}Sr_{0.5}Co_{0.8}Fe_{0.2}O_{3-\delta}$ (BSCF) at the atomistic level. Defect simulations have evaluated the lowest energy interstitial site as well as oxygen migration pathway. Interstitial oxygen migration is predicted via a non-linear pathway. The model study proves the use of a simple molecular mechanics model to describe the oxygen migration accurately and confirms that the high ionic conductivity in perovskite type oxides is mediated by oxygen interstitial migration.

Keywords: perovskite, molecular mechanics, BSCF, Oxygen migration, GULP.

A.1. Introduction

Oxide materials that exhibit high ionic conductivity have attracted considerable attention for the last decades not only due to the wide range of straightforward applications, e.g. fuel cells, gas sensors, catalysts, membrane materials for oxygen separation or removal [1-3]. The investigation of diffusion mechanisms and defect phenomena supports the understanding of macroscopic transport behavior and the ability to predict transport parameters in solid materials. However, most of the experiments on diffusion or conductivity have difficulties to supply enough information to identify the atomistic mechanisms controlling ionic transport.

Computer modeling techniques are well established tools in the field of materials chemistry of solids at the atomic level [4]. The development of computational chemistry has also been assisted by the enormous growth in computer hardware power and by advances in theoretical methodologies.

One type of oxides that has attracted significant attention is based on the perovskite structure ABO_3 which exhibits a diversity of chemical compositions and properties. In the cubic type the BO_3 octahedra are corner-linked with the A cation in a 12-coordination site.

About 20 years ago, TERAOKA *et al.* first reported $SrCo_{0.8}Fe_{0.2}O_{3-\delta}$ (SCF) membranes with very high oxygen permeation flux, which is attributed to the high concentration of oxygen vacancy, caused by the substitution of A^{3+} metal ion by Sr^{2+} in the A-site of the perovskite [5]. Unfortunately, a perovskite brownmillerite transition could occur at lower oxygen partial pressure and at low temperatures, making the membrane fractured [6]. With the purpose of improving phase stability and keeping the high-performance, SHAO et al. developed $Ba_{0.5}Sr_{0.5}Co_{0.8}Fe_{0.2}O_{3-\delta}$ (BSCF) perovskite by a partly substitution of Sr^{2+} in SCF with Ba^{2+} [7].

The series of compounds based on cubic BSCF are some of the most fascinating members of the perovskite family, not only due to their applications in SOFCs, ceramic membranes and heterogeneous catalysis and is considered as one of the most promising materials [8,9]. Exceptionally high concentrations of mobile oxygen vacancies in combination with a distinctive phase stability are responsible for the high oxygen transport rates of BSCF.

Our group has thoroughly investigated the phase structure, sintering process and permeability of BSCF in membrane geometry [10], as well as an in situ high temperature X-ray diffraction studies [11] and evaluated the material for application in catalytic membrane reactors or oxygen separators [12].

Most of the attention has been focused on the modeling of simple ABO_3 types of perovskite by now. In the present study the energy profile for a migrating oxygen ion of the $Ba_{0.5}Sr_{0.5}Co_{0.8}Fe_{0.2}O_{3-\delta}$ perovskite regarding to its oxygen deficient character has been mapped out as well as a possible interstitial position for oxygen within its lattice as part of the migration process has been evaluated. To the best of our knowledge, it is the first time that this issue is presented in the literature.

A.2. Material and Methods

In the present study, atomistic (static lattice) modeling technologies which determine the lowest energy configuration of the crystal structure by employing efficient energy minimization procedures embodied in the GULP code [13] were used to model the perovskite material. These well-established techniques are comprehensively reviewed elsewhere [4].

The calculations are based upon the BORN model for polar solids which are commonly employed for ceramic oxides. Each ion is assigned a charge corresponding to its formal oxidation state, with the long-term COULOMBic as well as short-range repulsive and VAN DER WAALS interactions. These short-range interactions were modeled using the BUCKINGHAM potential:

$$V_{ij}(r_{ij}) = A \exp(-r_{ij}/\rho) - C/r_{ij}^6 \tag{A.1}$$

where r is the interatomic distance and A, ρ and C are empirically derived parameters specific to each species.

Since charged defects will polarize nearby ions in the lattice, accurate calculation of defect energies requires the consideration of ionic polarizibility, especially when “soft” ions like O^{2-} are present in the model. Therefore the shell model of DICK and OVERHAUSER [14] is incorporated as a simple but effective description of polarizibility by treating each ion as a massless shell and an ionic core connected via a harmonic spring. The potential of this interaction is calculated as

$$E_{\text{core–shell}}(r) = (1/2)\, k_2\, r^2 \tag{A.2}$$

Only the shells are allowed to interact via the short range potential.

The MOTT-LITTLETON approach [15] was used to model point defects. A defect is introduced to the energy-minimized lattice and the surrounding ions are classified into two regions. An inner sphere of ions surrounding the point defect (region 1) are relaxed explicitly whilst the crystal bulk (region 2), where the defect forces are relatively weak, is treated by computationally less expensive quasi-continuum methods. In this way local relaxation is effectively modeled and the crystal is not considered simply as a rigid lattice.

In the static lattice approach it is assumed that transport is effected by discrete jumps (or hops) of atoms by either vacancy or interstitial mechanisms (Figure A.1). Simulating the potential energy surface for the migrating ion allows identifying the most favored pathway.

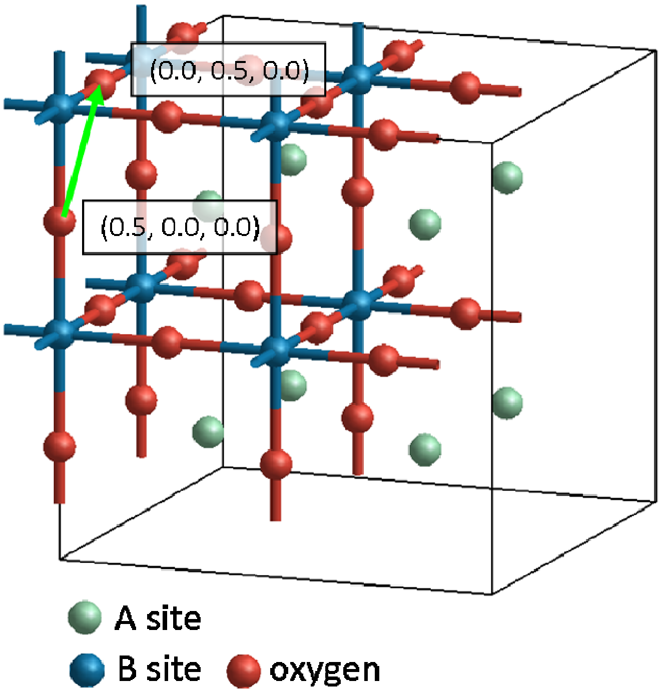

Figure A.1: Schematic illustration of a migrating oxygen ion in the lattice of the BSCF perovskite within the *z*-plane.

It has been commonly assumed that the migrating ion within the perovskite lattice takes a direct linear path into a neighboring vacancy. However, an important result of the search of the potential energy surface is that deviation from direct path for vacancy migration is revealed (Figure A.2).

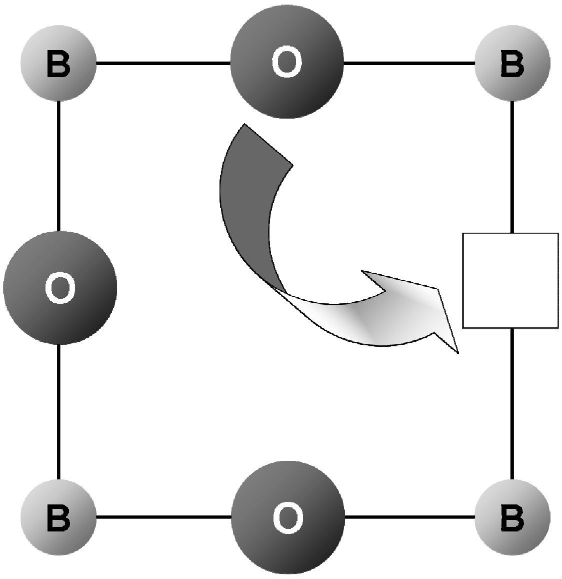

Figure A.2: Curved path for oxygen ion migration between adjacent vacancy sites in ABO_3.

A.3. Results and Discussion

A.3.1. Structural Modeling

The structure was described in terms of the *Pm3m* space group. Our approach to modeling the BSCF perovskite was to apply a selection of published potentials as presented in Table A.1 and details of our structural simulation are given in Table A.2. In general, there is good agreement between experimental and simulated structure, thus supporting the validity of the potentials used for the subsequent defect calculations. Notably, the ratio of Co^{2+} to Co^{3+} is chosen to be 1:2 giving rise to an average valence of the all B site cations of 2.2+ which is in accordance with earlier findings [16] and corresponds to a an statistic occupation of the oxygen positions in the perovskite lattice of approximately 78% and $\delta = 0.635$, respectively.

Table A.1: Interatomic potentials for $Ba_{0.5}Sr_{0.5}Co_{0.8}Fe_{0.2}O_{3-\delta}$.

(a) Short range (potential cut-off = 10 Å)

Interaction	A/eV	ρ/Å	C/eV Å^{-6}	Ref.
Ba^{2+} - O^{2-}	931.700	0.3949	0	[17]
Co^{2+} - O^{2-}	696.300	0.3362	0	[18]
Co^{3+} - O^{2-}	1329.820	0.3087	0	[18]
Fe^{3+} - O^{2-}	1156.360	0.3299	0	[19]
Sr^{2+} - O^{2-}	1956.702	0.3252	0	[18]
O^{2-} - O^{2-}	22764.000	0.1490	43	[19]

(b) Shell model

Ion	Y/e	k/eV Å^{-2}	Ref.
O^{2-}	-2.24	42.0	[19]

Table A.2: Calculated and experimental [20] structural parameters for $Ba_{0.5}Sr_{0.5}Co_{0.8}Fe_{0.2}O_{3-\delta}$ (Co^{2+}:Co^{3+} = 1:2).

.	Experimental a / Å	Calculated a / Å
$Ba_{0.5}Sr_{0.5}Co_{0.8}Fe_{0.2}O_{3-\delta}$	3.989	4.012

A.3.2. Oxygen Ion Migration

Although conductivitiy studies provide accurate activation energies, it is not always possible to associate the observed values with a particular diffusion mechanism. Atomistic calculations have been used to investigate these problems by an extensive search of the potential energy surface for oxygen migration. The energy profile for oxygen ion migration was mapped out by calculating the defect energy of the migrating ion within the z-plane and allowing relaxation of the lattice at each position in order to determine the diffusion path (Figure A.3).

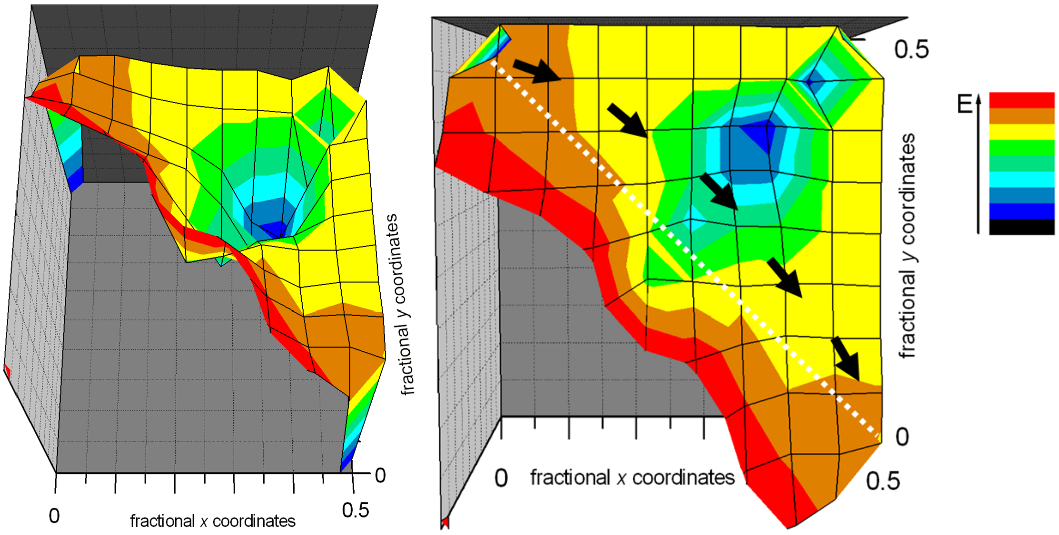

Figure A.3: Potential energy hypersurface for oxygen ion migration as a function of the fractional coordinates in the *z*-plane. Right: Black arrows illustrate the deviation of the oxygen migration pathway from a linear one.

It is obvious that the interstitial position of an oxygen ion at super-stoichiometric conditions is located at approximately $x = 0.4$, $y = 0.4$. The dotted line in Figure A.3 (right) equals a direct linear way between the two oxygen vancancies. Because of areas of lower potential energy above this line, the lowest energy migration path for interstitial O^{2-} is predicted to be a curved route which is in accordance with earlier findings in Molecular Dynamics simulations [21]. In the saddle-point configuration, the migrating ion must pass through the opening of a triangle defined by two A site (Ba,Sr) ions and one B site (Co,Fe) ion.

A.4. Conclusion

The present study demonstrates how computer modeling techniques can be used to examine oxygen transport properties in perovskite-type oxides that are relevant to their use in oxidation catalysis, fuel cells and separation membranes. Even simple simulation methods like a molecular mechanics approach which is less demanding for calculating capacity are capable to act as a powerful tool supporting experimental techniques.

Diffusion is mediated by hopping of oxygen ions along the anion octahedral edge, but not in a linear manner; rather migration takes place via a curved path, resulting in a significantly lower energy barrier.

Acknowledgments

The author gratefully acknowledges fruitful discussion with A.M. Schneider. Prof. J. Caro is thanked for general support.

[1] H.J.M. BOUWMEESTER, A.J. BURGRAFF in *Fundamentals of Inorganic Membrane Science and Technology,* (Eds.: A.J. BURGRAFF, L. COT), Elsevier, Amsterdam, **1996**.

[2] H.L. TULLER, M. BALKANSKI; *Science and Technology of fast-ion conductors*, Plenum Press, New York, **1987**.

[3] R. DITTMEYER, J. CARO in *Handbook of Heterogeneous Catalysis, Vol. 4* (Eds.: G. ERTL, H. KNÖZINGER, F. SCHÜTH, J. WEITKAMP), Wiley-VCH, Weinheim, **2008**, pp.2198.

[4] C.R.A. CATLOW, *Computer Modelling in Inorganic Crystallography*, Academic Press, San Diego, **1997**.

[5] Z.P. SHAO, S.M. HAILE, *Nature* **2004**, *431*, 170.

[6] S. PEI, M.S. KLEEFISCH, T.P. KOBYLINSKI, J. FABER, C.A. UDOVICH, V. ZHANG-MCCOY, *Catal. Lett.* **1995**, *30*, 201.

[7] Z. SHAO, G. XIONG, J. TONG, H. DONG, W. YANG *Sep. Purif. Technol.* **2001**, *25*, 419.

[8] Y. TERAOKA, H.M. ZHANG, S. FURUKAWA, N. YAMAZOE, *Chem. Lett.* **1985**, *11*, 1743.

[9] C.S. CHEN, S.J. FENG, S. RANM, D.C. ZHU, W. LIU, H.J.M. BOUWMEESTER *Angew. Chem. Int. Ed.* **2003**, *42*, 5354.

[10] H. WANG, C. TABLET, A. FELDHOFF, J. CARO, *J. Membr. Sci.* **2005**, *262*, 20.

[11] H. WANG, C. TABLET, W. YANG, J. CARO, *Mater. Lett.* **2005**, *59*, 3750.

[12] J. CARO, H. WANG, C. TABLET, A. KLEINERT, A. FELDHOFF, T.SCHIESTEL, M. KILGUS, P. KÖLSCH, S. WERTH, *Catal. Today* **2006**, *118*, 128.

[13] J.D. GALE, A.L. ROHL, *Mol. Simul.* **2003**, *29*, 291.

[14] B. DICK, A. OVERHAUSER, *Phys. Rev.* **1958**, *112*, 90.

[15] C.R.A. CATLOW in *Solid State Chemistry – Techniques* (Eds. A.K. CHEETHAM, P. DAY), Clarendon Press, Oxford, **1987**.

[16] A. FELDHOFF, J. MARTYNCZUK, M. ARNOLD, M. MYNDYK, I. BERGMANN, V. SEPALAK, W. GRUNER, U. VOGT, A. HÄHNEL, J. WOLTERSDORF, *J. Solid State Chem.* **2009**, *182*, 2961.

[17] C.A.J. FISCHER, M.S. ISLAM, R.J. BROOK, *J. Solid State Chem.* **1997**, *128*, 137.

[18] S.M. WOODLEY, P.D. BATTLE, J.D. GALE, C.R.A. CATLOW, *Phys. Chem. Chem. Phys.* **1999**, *1*, 2535.

[19] M. CHERRY, M.S. ISLAM, C.R.A. CATLOW, *J. Solid State Chem.* **1995**, *118*, 125.

[20] L. GE, W. ZHOU, R. RAN, S.S. LIU, Z. SHAO, W. JIN, N. XU, *J. Membr. Sci.* **2007**, *306*, 318.

[21] S. ISLAM, *J. Mater. Chem.* **2000**, *10*, 1027.

Appendix B

Formulas

Listed below are the formulas on which the calculation of educt conversion as well as product selectivities and product yields are based on. The total flow rates of the effluents at the outlet $F_{\mathrm{total}}^{\mathrm{out}}$ were determined by using Ne as an internal standard. It is assumed that Ne does not take part in the reactions.

$$F_{\mathrm{total}}^{in}\, c_{\mathrm{Ne}}^{\mathrm{in}} = F_{total}^{\mathrm{out}}\, c_{\mathrm{Ne}}^{\mathrm{out}} \tag{6.1}$$

F_{total}^{in} is the total flow rate of the inlet, $c_{\mathrm{Ne}}^{\mathrm{in}}$ and $c_{\mathrm{Ne}}^{\mathrm{out}}$ equal the concentrations of Ne at the inlet and outlet, respectively. The conversion defines the percentage of educt A which has been converted to product B by using eqn. 6.2. $F(\mathrm{A})_{\mathrm{out}}$ and $F(\mathrm{A})_{\mathrm{in}}$ correspond to the flow rates of A at the outlet and inlet, respectively.

$$X(\mathrm{A}) = \left(1 - \frac{F(\mathrm{A})_{\mathrm{out}}}{F(\mathrm{A})_{\mathrm{in}}}\right) \tag{6.2}$$

The selectivity S equals the ratio between the formed product B and the amount of reacted educt A (eqn. 6.3). $F(\mathrm{B})_{\mathrm{out}}$ is the flow rate of product B at the outlet and ν_{i} is the corresponding stoichiometric factor in the reaction.

$$S(\mathrm{B}) = \frac{F(\mathrm{B})_{\mathrm{out}} - F(\mathrm{B})_{\mathrm{in}}}{F(\mathrm{A})_{\mathrm{in}} - F(\mathrm{A})_{\mathrm{out}}} \frac{|\nu_{\mathrm{A}}|}{\nu_{\mathrm{B}}} \tag{6.3}$$

The resulting yield of product B from a selectivity towards B obtained at a certain conversion of educt A can be described by using eqn. 6.4.

$$Y(\mathrm{B}) = X(\mathrm{A}) \cdot S(\mathrm{B}) \tag{6.4}$$

Publications and Contributions to Conferences

Publications included in this work (in chronological order)

(i) Olefin Production by a Multistep Oxidative Dehydrogenation in a Perovskite Hollow-Fiber Membrane Reactor
OLIVER CZUPRAT, STEFFEN WERTH, STEFFEN SCHIRRMEISTER, THOMAS SCHIESTEL, JÜRGEN CARO
ChemCatChem **2009**, *1*, 401.

(ii) Oxidative dehydrogenation of propane in a perovskite membrane reactor with multi-step oxygen insertion
OLIVER CZUPRAT, STEFFEN WERTH, JÜRGEN CARO, THOMAS SCHIESTEL
American Institute of Chemical Engineers Journal **2010**, *56*, 2390.

(iii) Oxidative coupling of methane in a perovskite hollow fiber membrane reactor
OLIVER CZUPRAT, THOMAS SCHIESTEL, HARTWIG VOSS, STEFFEN WERTH, JÜRGEN CARO
Industrial & Engineering Chemistry Research **2010**, *49*, 10230.

(iv) Dehydrogenation of propane with selective hydrogen combustion: A mechanistic study by transient analysis of products
OLIVER CZUPRAT, JÜRGEN CARO, VITA A. KONDRATENKO, EVGENII V. KONDRATENKO
Catalysis Communications **2010**, *11*, 1211.

(v) Influence of CO_2 on the oxygen permeation performance of perovskite-type $BaCo_xFe_yZr_zO_{3-\delta}$ hollow fiber membranes
OLIVER CZUPRAT, MIRKO ARNOLD, STEFFEN SCHIRRMEISTER, THOMAS SCHIESTEL, JÜRGEN CARO
Journal of Membrane Science **2010,** *364*, 132.

(vi) *In-situ* X-ray diffraction study of carbonate formation and decomposition in perovskite-type $BaCo_xFe_yZr_zO_{3-\delta}$

KONSTANTIN EFIMOV, OLIVER CZUPRAT, ARMIN FELDHOFF

Journal of Solid State Chemistry **2010**, *submitted for publication.*

Publications not included in this work (in chronological order)

(vii) MM-Simulation of Alkylammonium Monolayers Intercalated in Clays

ANDREAS M. SCHNEIDER, OLIVER CZUPRAT, SEBASTIAN FESSEL, PETER BEHRENS, JOSEF BREU

Zeitschrift für anorganische und allgemeine Chemie **2008**, *634*, 2077.

(viii) Oxidative Dehydrierung niederer Alkane in einem selektiven Membranreaktor mit gestufter Sauerstoffzugabe und in-situ Wasserstoffoxidation

OLIVER CZUPRAT, STEFFEN WERTH, STEFFEN SCHIRRMEISTER, THOMAS SCHIESTEL, JÜRGEN CARO

Chemie Ingenieur Technik **2009**, *81*, 1591.

(ix) Highly effective NO decomposition by in situ removal of inhibitor oxygen using an oxygen transporting membrane

HEQING JIANG, LEI XING, OLIVER CZUPRAT, HAIHUI WANG, STEFFEN SCHIRRMEISTER, THOMAS SCHIESTEL, JÜRGEN CARO

Chemical Communications **2009**, *44*, 6738.

(x) Improvement of oxygen permeation for hydrogen production from water dissociation in surface-modified $BaCo_xFe_yZr_{1-x-y}O_{3-\delta}$ hollow fiber membrane

HEQING JIANG, FANGYI LIANG, OLIVER CZUPRAT, KONSTANTIN EFIMOV, ARMIN FELDHOFF, STEFFEN SCHIRRMEISTER, THOMAS SCHIESTEL, HAIHUI WANG, JÜRGEN CARO

Chemistry – A European Journal **2010**, *16*, 7898.

Contributions to conferences

(i) Molecular Mechanics study on the interaction at organic-inorganic interfaces: alkylammonium ions in clay minerals
OLIVER CZUPRAT*, ANDREAS M. SCHNEIDER, JOSEF BREU, PETER BEHRENS
20. Deutsche Zeolith-Tagung, Halle/Saale (Germany), 5th-7th of March **2008** (Poster).

(ii) MM-Simulation of Alkylammonium Monolayers Intercalated in Clays
ANDREAS M. SCHNEIDER*, OLIVER CZUPRAT, SEBASTIAN FESSEL, PETER BEHRENS, JOSEF BREU
14. Vortragstagung der GDCh-Fachgruppe Festkörperchemie und Materialforschung, Bayreuth (Germany), 24th-26th of September **2008** (Poster).

(iii) Olefin production by a two-step oxidative dehydrogenation in a novel perovskite hollow fiber membrane reactor
OLIVER CZUPRAT*, STEFFEN WERTH, STEFFEN SCHIRRMEISTER, THOMAS SCHIESTEL, JÜRGEN CARO
42. Jahrestreffen Deutscher Katalytiker, Weimar (Germany), 11th-13th of March **2009** (Poster).

(iv) Olefin production by a multi-step oxidative dehydrogenation in a novel perovskite hollow fiber membrane
OLIVER CZUPRAT*, STEFFEN WERTH, STEFFEN SCHIRRMEISTER, THOMAS SCHIESTEL, JÜRGEN CARO
21st North American Meeting of the North American Catalysis Societey, San Francisco, CA (USA) 7th-12th of June **2009** (Poster).

(v) Olefin production by a multi-step oxidative dehydrogenation in a novel nano-designed perovskite hollow fiber membrane reactor
OLIVER CZUPRAT*, STEFFEN WERTH, STEFFEN SCHIRRMEISTER, THOMAS SCHIESTEL, JÜRGEN CARO
NanoDay 2009 der Leibniz Universität Hannover, Hannover (Germany), 30th of September **2009** (Poster).

(vi) Olefin production by a multi-step oxidative dehydrogenation in a novel perovskite hollow fiber membrane reactor
OLIVER CZUPRAT*, STEFFEN WERTH, STEFFEN SCHIRRMEISTER, THOMAS SCHIESTEL, JÜRGEN CARO
43. Jahrestreffen Deutscher Katalytiker, Weimar (Germany), 10th-12th of March **2010** (Talk).

(vii) Production of light alkenes by a multi-step oxidative dehydrogenation in a novel perovskite hollow fiber membrane reactor
OLIVER CZUPRAT*, STEFFEN WERTH, STEFFEN SCHIRRMEISTER, THOMAS SCHIESTEL, JÜRGEN CARO
21st International Symposium on Chemical Reaction Engineering, Philadelphia, PA (USA), 13th-16th of June **2010** (Talk).

(viii) Phase selectivity in ionothermal zeotype synthesis by using ionic liquids with mixed anions
SVEN JARE LOHMEIER*, OLIVER CZUPRAT, RUSSELL E. MORRIS, PETER BEHRENS
16th International Zeolite Conference, Sorrento (Italy), 4th-9th of July **2010** (Talk).

Erklärung zur Dissertation

Ich erkläre, dass ich die vorliegende Dissertationsschrift selbstständig verfasst und alle benutzten Hilfsmittel sowie zur Hilfeleistung herangezogene Institutionen vollständig angegeben habe.
Diese Dissertation wurde wurde nicht bereits als Diplom- oder ähnliche Prüfungsarbeit verwendet.

Hannover, den 19.10.2010

Curriculum Vitae

Personal data

Name	Oliver Czuprat
Date of birth	6th / January / 1980
Place of birth	Hannover, Germany
Nationality	German
Marital status	unmarried, no children

Languages

German	native language
English	fluent
French	conversation
Latin	intermediate proficiency certificate

Higher Education

10/2010	**Leibniz Universität Hannover**, Naturwissenschaftliche Fakultät, **submission of doctoral thesis:** “Oxidative Activation of Light Hydrocarbons in a Perovskite Hollow Fiber Membrane Reactor”
03/2008-12/2010	**Leibniz Universität Hannover**, Institute of Physical Chemistry and Electrochemistry **Scientific co-worker**, group of Prof. Dr. J. Caro
09/2005-06/2006	**Stanford University, USA,** Department of Organic Chemistry **visiting researcher**, group of Prof. P. Wender, Topic: “Rh(I)-catalyzed [4+2] cyclo-additions”
10/2002-01/2008	**Leibniz Universität Hannover**, Chemistry-Degree: Diplom-Chemiker **Diploma Thesis**, group of Prof. Dr. P. Behrens, Institute of Inorganic Chemistry, “Theoretische Untersuchungen zu Wechselwirkungen an organisch-anorganischen Grenzflächen“
11/2000-09/2002	**Leibniz Universität Hannover**, study courses in „Physics“

Education

1992-1999	**Elsa-Brändström-Schule**, Hannover Degree: Abitur Intensive courses: Mathematics, Physics
1990-1992	**Orientierungsstufe Döhren**, Hannover
1986-1990	**Grundschule Olberstr.**, Hannover

Civilian Service

08/1999-08/2000	**Pflegeheim Dr. med. E.-A. Wilkening**, Hannover

Others

10/2000-12/2004	**Norddeutscher Rundfunk (NDR)**, Landesfunkhaus Hannover, editorial video text journalist